Applicability of 2-D Time-Lapse High-Resolution Seismic Reflection Approach to Image Natural Salt-Dissolution and Subsidence in Central Kansas and Improved Post-Processed Vibroseis Data Characteristics

by

Daniel Rice
B.S., Millsaps College, 2007

Submitted to the Department of Geology
and the Faculty of the Graduate School of the University of Kansas
in partial fulfillment of the requirements for the degree of
Master of Science
2009

Advisory Committee:

Richard D. Miller, Chairman

Ross Black

J. Douglas Walker

Robert H. Goldstein
for the Department

Date Defended: June 15, 2009

The Thesis Committee for Daniel Rice certifies that this
is the approved version of the following thesis:

Applicability of 2-D Time-Lapse High-Resolution Seismic Reflection Approach to Image Natural Salt-Dissolution and Subsidence in Central Kansas and Improved Post-Processed Vibroseis Data Characteristics

Advisory Committee:

Richard D. Miller, Chairman

Ross Black

J. Douglas Walker

Robert H. Goldstein
for the Department

Date Approved: _____June 19, 2009_____

Table of Contents

List of Figures

List of Tables

Abstract

The effectiveness of 2-D time-lapse imaging for monitoring natural dissolution of the Hutchinson Salt in eastern Reno County, Kansas was shown to be restricted when comparing high-resolution seismic reflection data acquired in 2008 with data acquired in 2001 across an active subsidence feature. Seismic reflection data were acquired in both 2001 and 2008 across an active sinkhole at the intersection of U.S. Highway 50 and Victory Road in Hutchinson, KS as part of a comprehensive study by the Kansas Department of Transportation to assess subsidence risk and prediction. Data were collected and processed as identical as possible on both surveys. Processed results concluded that acquisition line separation must be within 15% of the Fresnel Zone radius at the target horizon when imaging natural dissolution features. Due to the rate of vertical and horizontal change and the lack of subsurface symmetry common to these features, apparent changes in geology could be related to survey line separation and not true geologic changes.

The need for higher fidelity vibroseis data has prompted experimentation on the limiting factors; one of those is the accuracy of the groundforce measurement and associated noise threshold and fine sensitivity of source monitoring sensors and wavelet extraction techniques. Vibroseis correlation and deconvolution methods were compared and used to determine the optimal method for processing high frequency vibroseis data taking advantage of groundforce estimates using improved mass and baseplate measurements. The recorded data were correlated and deconvolved with a groundforce calculated using low noise accelerometers located on the mass and baseplate and is superior to traces produced using standard accelerometers and low A/D digital traces commonly used for calculating groundforces. The use of a calculated groundforce from low noise accelerometers for deconvolution provides a preferred alternative to the common approach of cross-correlating vibroseis traces with a generated synthetic sweep.

Introduction

Time-lapse seismic reflection techniques

The effectiveness of time-lapse seismic reflection methods was tested using data acquired to image dissolution of the Hutchinson Salt in central Kansas. Time-lapse seismic reflection methods are routinely used for reservoir monitoring (Wang, 1997). Anthropogenic salt dissolution features have been studied using time-lapse in Kansas (Lambrecht, 2006; Miller et al., 2006). The success of time-lapse surveys depends on repeatability (Bertrand, 2008). Repeatability is affected by source signature (Saunders, 2004), amplitude and frequency (Bisshop, 1994), processing techniques (Lecref, 2004), and near-surface conditions (Yun, 2007).

Techniques have been used in the oil and gas industry to equalize time-lapse seismic data. One such approach involves separating the differences in the data in time, amplitude, phase and frequency in an attempt to analyze non-repeatability factors (Jin, 2004). Other methods include applying match filters to attenuate variations of signal (Hoeber, 2005), using histogram whitening to balance true amplitudes (Luo, 2001), attenuating differences by cross-equalization (Rickett, 2001), and using an inversion algorithm to characterize noise (Routh, 2008).

Sinkhole at Hwy 50 and Victory Road

A sinkhole that formed from natural dissolution of the Hutchinson Salt at the intersection of US 50 and Victory Road approximately 8 miles southeast of Hutchinson, KS (Figures 1 and 2) was first elevation surveyed in 1998 when the bowl shaped depression was 0.3 m below construction grade at its deepest point. Surface

elevation surveys performed by the Kansas Department of Transportation (KDOT) over the next three years documented a 0.9 m maximum change in the highway elevation. In 2001, the sinkhole was centered 30 m northwest of the intersection with a 91 m wide bowl-like shape surface geometry. Seismic surveys in Reno County targeting individual sinkholes have generally focused on the upper 250 m to image any dissolution feature within the Hutchinson Salt (Miller, 2002; Miller, 1993; Nissen, 2002). In its thickest locations, the Hutchinson Salt can be 145 m thick with a basal contact 240 m below ground surface. Past surveys have successfully produced good signal quality and high-resolution images (Miller, 2002).

The Kansas Geological Survey (KGS) acquired seismic reflection data in 2001 for the Kansas Department of Transportation (KDOT) to evaluate the risk of subsidence during scheduled highway maintenance operations at the intersection of US 50 and Victory Road in central Kansas. Data was acquired along the northern edge of US 50 and along eastern ditch of Victory Road. This survey focused on delineating the subsurface expression of the sinkhole, evaluating and identifying any threat to the highway's stability. The data allowed for surface and subsurface growth potential and rates to be predicted (Miller, 2002).

This sinkhole was interpreted from the 2001 seismic survey to be the result of reactivation of natural salt dissolution processes that had over time been responsible for a 457 m wide sinkhole that has filled with sediment. Based on 2001 data, a portion of this paleosinkhole appears to have been dormant since the deposition of the Quaternary Equus beds. Based on sequential bed geometries, subsidence at this site

has been active as recent as 1 million years ago. It seems apparent from seismic data that the change in elevation observed between 1998 and 2001 or since construction is the result of recent re-activation of subsurface subsidence between bedrock and the top of salt. The subsidence area appears to have resulted from reactivated leaching and associated failure that has likely been inactive since pre-Quaternary (Miller, 2002).

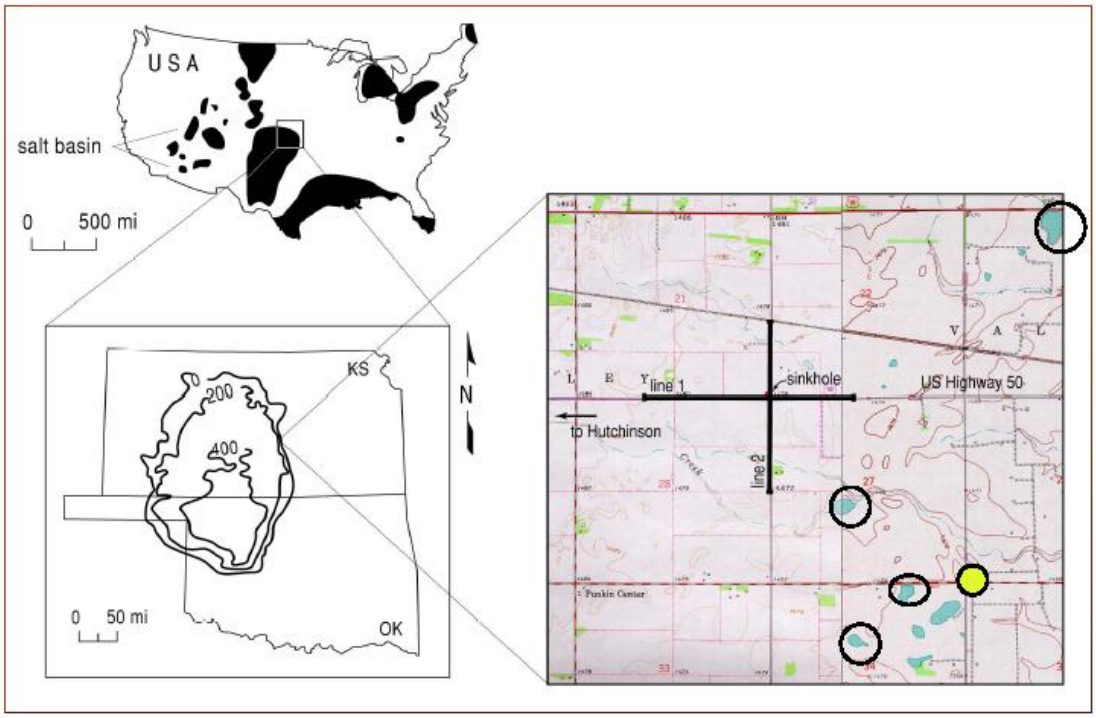

Figure 1. Isopach map of the Hutchinson Salt Member and the location of the study site within Reno County, Kansas (Miller, 2002).

Figure 2. 2001 survey in the north road ditch, 2008 survey in the south road ditch (modified from Williamson, 2008).

Seismic study along Highway 50

The KGS began acquiring seismic data in 2003 to delineate rock layers within and above the Hutchinson Salt Member and attempt to appraise the overall stability of the rock column within the proposed location of a Hwy 50 bypass around Hutchinson. An 8-mile seismic line was acquired along the southern edge of Hwy 50 in 2008 as the second part of a 15-mile profile focused on imaging the salt from just west of the City of Hutchinson, Kansas to the salt dissolution edge around 2 miles east of the intersection of Hwy 50 and Victory Road. Objectives of the project included studying the dissolution patterns within the salt in proximity to subsidence in the overlying sediments and determining geometry and failure potential of any structures associated with dissolution or mining of the salt.

Use of the Highway 50 seismic data

For this study, portions of the 2001 and 2008 data sets were used. Both the 2001 and 2008 surveys imaged the same sinkhole at the intersection of US 50 and Victory Road, so an opportunity was taken to test time-lapse as a method to measure actual subsurface growth. In doing this, it became obvious that the lateral rate of changes common to these dissolution features has a significant impact on when time-lapse comparisons can be applied. A true time-lapse comparison of this type of natural salt dissolution feature cannot be obtained without nearly coincident receiver locations. This criterion was tested with the differencing of 2001 and 2008 surveys, since they were parallel and separated by more than 15 m.

High-frequency vibroseis data processing

Near-surface high-frequency vibroseis processing typically involves cross-correlating the vibroseis signal with a synthetic sweep or filtered groundforce to extract the frequency variable vibroseis source wavelet resulting in a representative zero-phase Klauder wavelet spectrally consistent with the sweep range (Yilmaz, 2001). A synthetic sweep is used for cross-correlation because measurements of the components of true groundforce not having been accurately obtained. The cross-correlation operation can be expressed by

$$x_{cc}(t) = r(t) * s(t) \bigstar s(t) = r(t) * k(t) \text{ (Yilmaz, 2001)}$$

where $x_{cc}(t)$ is the cross-correlation, r(t) is the geological reflectivity, s(t) is the sweep, * is the convolution operator, ★ is the cross-correlation operator, k(t) is the Klauder wavelet, and all values are time dependent. Frequencies can destructively interfere due to system response and earth properties and reduce amplitudes during correlation. Because correlation is time dependent, frequency errors occur with any time spectral variations (Brittle, 2001).

Sweep deconvolution involves the same convolutional model as cross-correlation but is performed in the frequency domain (Ghose, 2002). Convolution in the frequency domain is multiplication; the equation can be written as:

$$X(f) = R(f)S(f)$$

where $X(f)$ is the recorded trace, $R(f)$ is the geological reflectivity, and $S(f)$ is the sweep. This allows the sweep to be removed through division:

$$R(f) = X(f) / S(f)$$

In an ideal noise-free case, assuming accurate measurements, a perfect reflectivity trace can be obtained (Brittle, 2001).

Deconvolution should always produce superior results than cross-correlation with an accurately determined reference signal (van deer Veen et al, 1999). After correlation, the shape of the sweep directly affects the amplitude spectra; whereas for deconvolution, the resulting trace spectra is independent of sweep shape. This is true because deconvolution attempts to equalize or flatten all amplitudes in the frequency domain. Therefore, all the frequencies in the sweep are considered to have identical amplitudes after deconvolution is applied correctly (Bickel, 1982). This effectively boosts the high frequency portion of the post correlated data. Vibroseis whitening is a method commonly applied to vibroseis data prior to cross-correlation with the synthetic sweep to enhance target signals. The upper portion of the usable bandwidth often contains weak signals (Doll and Coruh, 1995). Deconvolution eliminates the need for vibroseis whitening by enhancing the higher frequency portion of the signals.

Groundforce is a measure of the energy input into the ground in vibroseis exploration (Sheriff, 2002). Groundforce is calculated using mass and baseplate accelerometer data. Current groundforce measurements calculated from standard accelerometers contain high levels of noise and do not accurately represent true groundforce. During the 2008 acquisition, in an effort to improve frequencies and

signal-to-noise ratios, optimized sensors, placement and recording were tested. Groundforce can be calculated using a weighted sum formula:

$$F = m_b x_b + m_r x_r, \text{ (Sallas, 1984)}$$

where F is groundforce, m_b is the mass of the baseplate (370 lbs), x_b is the baseplate acceleration, m_r is the mass of the reaction mass (311 lbs), and x_r is the reaction mass acceleration. Cross-correlation and deconvolution methods were evaluated using the groundforce, both individual accelerometer data sets, and the synthetic or ideal sweep. These operations were used to evaluate the potential for improving conventional vibroseis correlation used for most data processing.

Geologic Setting

Reno County, Kansas

Geological events in Kansas during the Permian were predominately influenced by marine transgressions and regressions. Limestone, chert, and shale were deposited as sea levels rose and fell. The Hutchinson Salt was left when seas regressed. During the Cretaceous, seas depositing limestone, sandstone, and chalk covered much of western Kansas. The Tertiary resulted in the deposition of sand, gravel, and porous rock in the western half of the state. The Quaternary began 1.6 million years ago with episodes of erosion. Deposition consisted of sands and gravels (Merriam, 1963). At the Reno County study area, a significant amount of erosion has occurred as evidence by the complete lack of Mesozoic and Tertiary materials.

Groundwater access to Permian units improved following the erosion of Cretaceous rocks. Dissolution of the salt and gypsum along the eastern natural front led to the fracturing, slumping and collapse of the overlying units (shale) within the Wellington Formation. The impermeable shale near the migration front now possessed areas capable of transmitting water. This zone of collapse and vertical fluid movement is referred to as the Wellington Aquifer. Groundwater within the Wellington Aquifer moves in all directions from the potentiometric high east of Hutchinson, KS and moves vertically due to changes in density along the front (Gogel, 1981).

Permian units including the Hutchinson Salt Member (up to 100 m thick near Hutchinson) unconformably underlie Tertiary/Quaternary Equus Beds (Figure 3) at the survey site. The salt dips westward at 6 m/mi from the dissolution front currently 6 miles east of Hutchinson. The eastern margin of the salt unit is being eroded by contact with groundwater through the Wellington aquifer (Watney, 2003). Seismic data from 2001 shows a salt thickness of 40 m within 0.5 mi of the salt front, revealing that 60 m of salt has been removed by dissolution (Miller, 2002).

Well logs from the study area show key Permian units that are readily identified on seismic data collected in Reno County (Miller, 2002). Stratigraphic data from a well northwest of Hutchinson (Nelson #1 well) (Figure 4) shows the top of The Chase Group at 310 m deep, top of the Lower Wellington Shales at 246 m, top of the Hutchinson Salt at 146 m, top of the Upper Wellington Shales at 96 m and the top of the Ninnescah Shale at 18 m (Watney, 2003). At a well southeast of the survey

area (Evans ‘W’ 5), the top of the salt is interpreted at 136 m (Figure 4). The salt becomes increasingly shallower to the east.

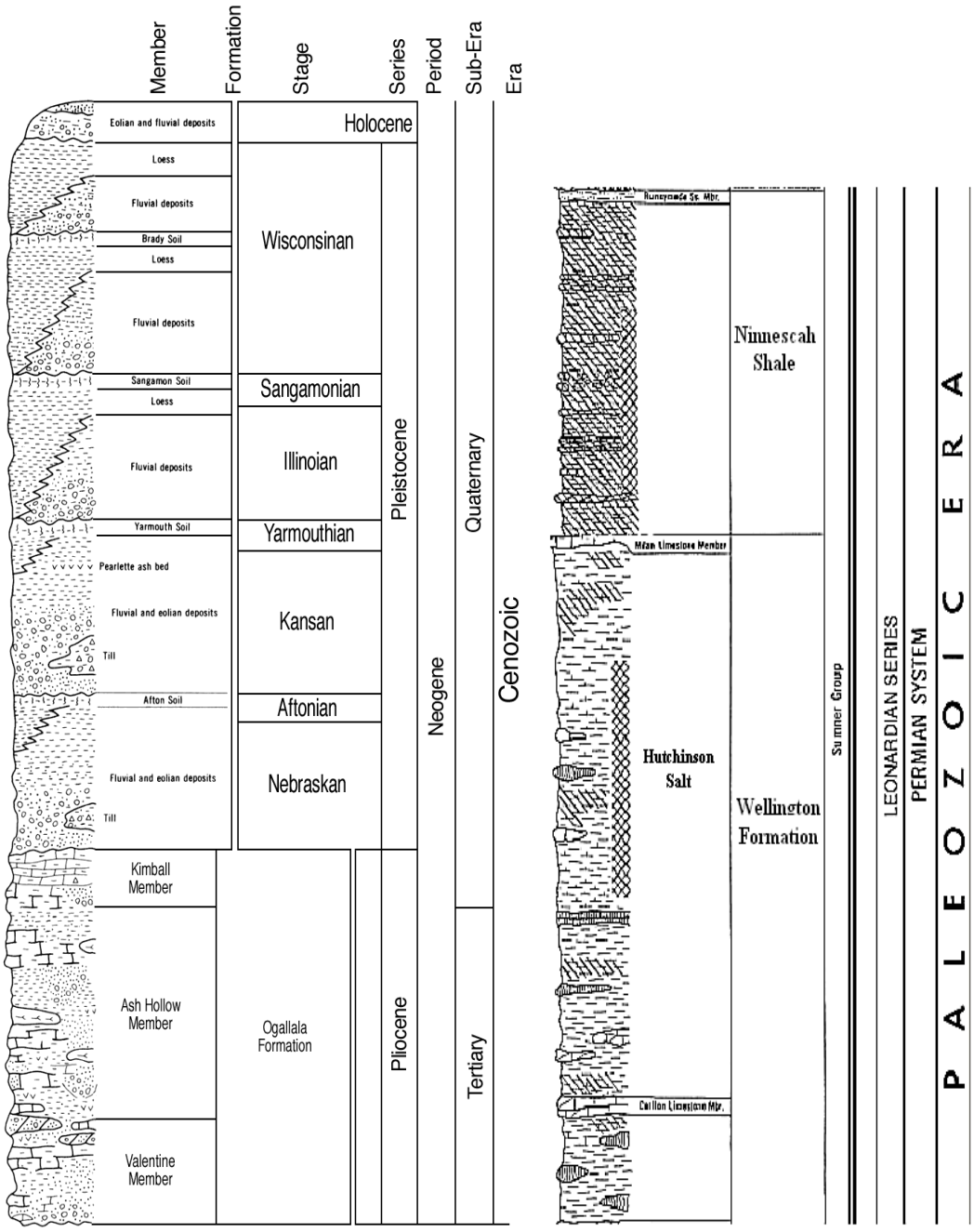

Figure 3. Generalized section of the geologic formations found at the survey site showing Tertiary/Quaternary units overlying Permian units (Kansas Geological Survey).

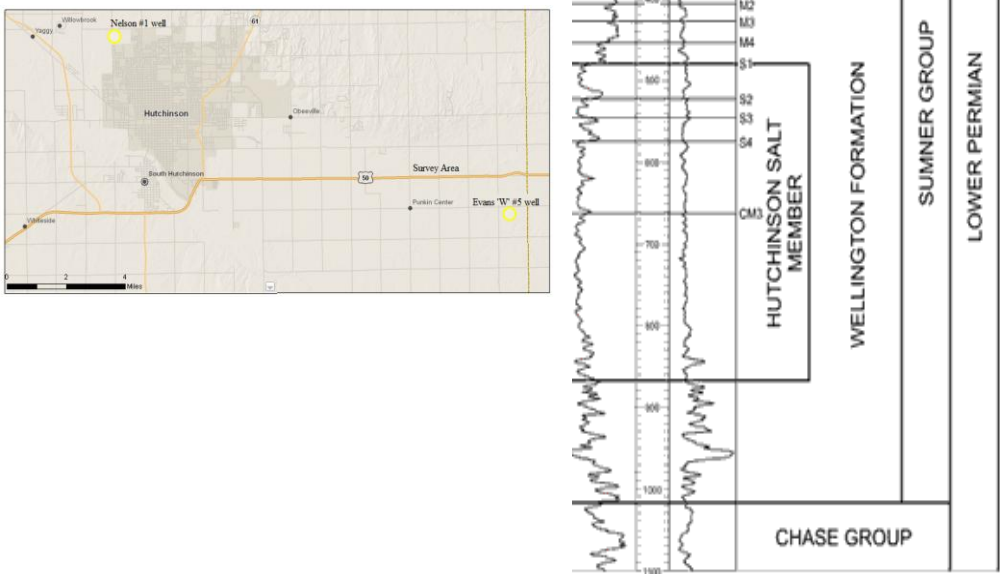

Nelson #1 well

Figure 4. Location of well logs near Hutchinson, Kansas (Whatney, 2003; Kansas Geological Survey).

Natural Dissolution vs Anthropogenic Dissolution

The subsidence at this site is strongly influenced by the availability of unsaturated brine to the Hutchinson Salt Member and overburden. The salt unit is prone to dissolution along the eastern edge in central Kansas where contact with meteoric ground water has been possible since removal of the Cretaceous units and where numerous sinkholes have formed (Watney, 2003). Sinkholes formed from natural dissolution grow at discontinuous rates that correlate to periods of active dissolution, dormancy, and then re-activation (Abelson et al., 2003).

Sinkholes in this area form when voids produced by dissolution migrate through redbed evaporates and Quaternary sediments that make up the salt overburden. Groundwater continues gaining access to the salt through natural pathways created as the salt front moves west and overburden subsidence results in highly altered zones identified within the Wellington Aquifer (Gogel, 1981). Pore space is created as salt is removed. The pore space continues to expand, eventually leading to failure and subsidence once the strength of the roof rock is exceeded. Gradual surface subsidence is related to brittle deformation allowing both vertical and horizontal sinkhole growth. The result of this form of subsidence is an enlarging bowl-shaped depression with bed geometries and offsets constrained by normal fault geometries (Miller, 2002).

Anthropogenic-induced dissolution can more likely lead to catastrophic sinkholes than natural dissolution. Salt is mined in the Hutchinson area by pumping freshwater down a well into the salt unit, dissolving the salt and creating brine.

Modern processes involve monitoring the size and shape of the subsurface cavern being created and leaving the upper units of the rock salt undisturbed. Improperly plugged oil wells provide pathways for freshwater to flow from overlying aquifers into the salt. This can result in sudden or gradual surface collapse. With anthropogenic dissolution, voids will generally migrate more vertically as compared to horizontal migration seen in natural dissolution features (Walters, 1978).

S*urface expression and associated problem at US 50 and Victory Road*

GPS data collected by KDOT from October 1998 to October 2000 show a drop in the elevation of the centerline of US 50 of 0.12 m (Figures 5 and 6). A more severe drop in elevations is observed/measured along the north edge of the highway in comparison to the south edge (Figures 7 and 8). With the dissolution front of the Hutchinson Salt to the east, both the northern and eastern margins of the sinkhole should be the most active. Elevations increased above the original construction elevation to the west. At most location points on the October 2000 data, elevations increased due to resurfacing the highway. GPS data collected in 2008 were not comparable to previous data. Data were collected at non-uniform intervals and did not measure surface elevations directly on the highway. However, data did show a drop in surface elevations of 1.0 m when approaching the area of interest from either west or east.

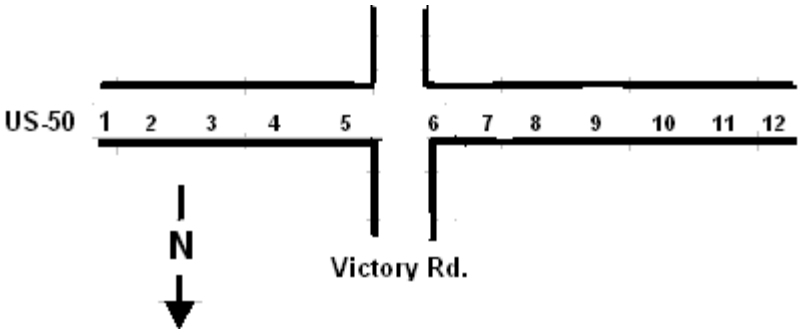

Figure 5. Map showing the surface locations at which elevations were measured from 1998 to 2000.

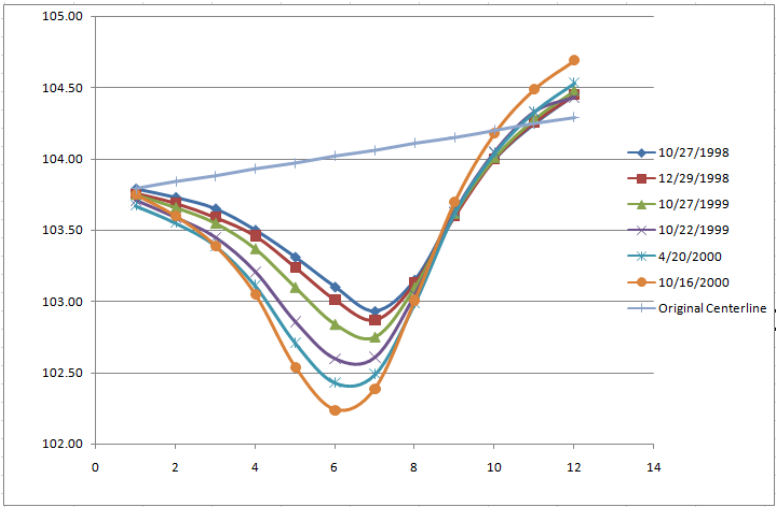

Figure 6. Changes in centerline elevations from construction to 2000.

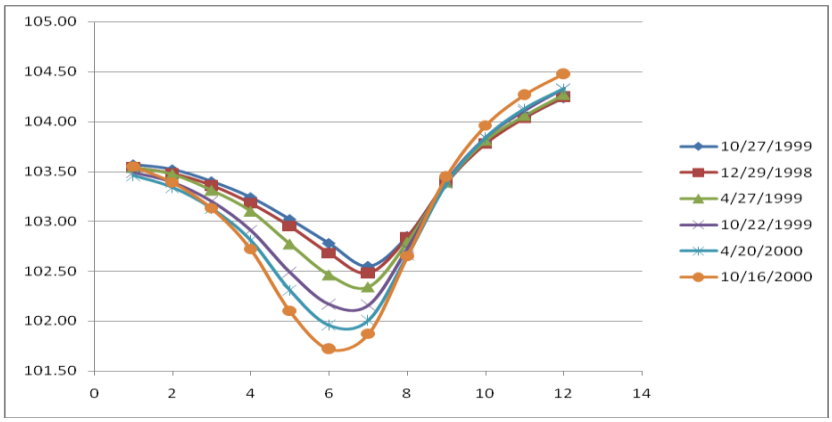

Figure 7. Changes in north edge elevations from 1998 to 2000.

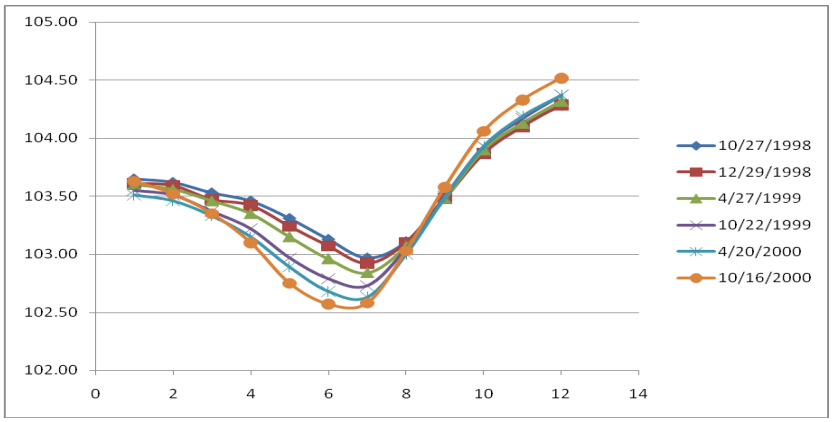

Figure 8. Changes in south edge elevations from 1998 to 2000.

Acquisition

The Kansas Geological Survey (KGS) acquired seismic data in 2001 and 2008. Acquisition in late August 2001 consisted of 2 one-mile intersecting lines (Figure 1), one along the north side of US 50 and a second down Victory Road. The 2001 survey was acquired to evaluate the risk of subsidence during scheduled highway maintenance operations at the intersection of US 50 and Victory Road. An 8-mile survey was acquired in mid-June 2008 along the south side of US 50 to image and study the migrating dissolution front of the Hutchinson Salt. The two lines were not acquired coincident along US 50 due to distinctly different project objectives. The 2008 project was not intended to be part of a time-lapse study of the Victory Road sinkhole when the 15-mile profile was started back in 2003. Therefore the data were acquired on the opposite side of the road and the stations are not exactly coincident.

The 2001 acquisition geometry and equipment focused around a 240-channel rolling fixed spread source/receiver geometry (Figure 9), with 2.5 m receiver station spacing, two 40 Hz geophones at each station (Figure 10), and a source station spacing of 5.0 m. The east-west line was recorded with receivers in the road ditch (Figure 11) along the north side of Highway 50 approximately centered on Victory Road. An IVI Minivib 1 (located on the highway shoulder, Figures 12 and 13) provided three 10-second linear up-sweeps from 25-250 Hz at each shot location (Miller, 2002).

Data acquired in 2008 were recorded with a 240-channel rolling fixed spread (Figure 9), 2.5 m receiver station spacing with two 40 Hz geophones per station placed in the south road ditch (Figure 10) and a 5.0 m source station spacing located on the south road shoulder of Highway 50 and approximately centered on Victory Road (Figure 2). The same IVI Minivib 1 (located on the highway shoulder) as used in 2001 was used to deliver three 10 second linear up-sweeps from 25-300 Hz at each station location.

Seismic data were acquired with four 60-channel Geometrics StrataView seismographs (24-bit) networked to allow simultaneous recording of 240 data channels. The calculated groundforce pilot for each sweep was telemetried from the vibrator to the seismograph and recorded as the first trace of each shot record. To optimize the potential of pre-correlation processing, each shot record was stored uncorrelated in the field (Lambrecht, 2006; Miller, 2002).

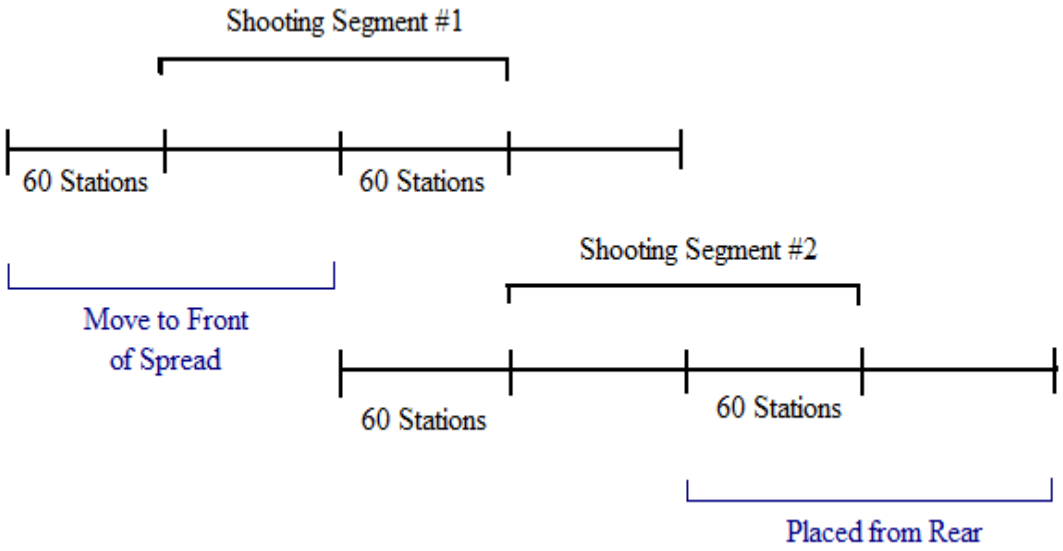

Figure 9. Diagram of the survey parameters used in the 2001 and 2008 data acquisition; 240-channel rolling fixed spread with shot stations at every 5.0 m and receivers at 2.5 m intervals.

Figure 10. Two 40 Hz geophones planted at each receiver location.

Figure 11. Geophones planted in the road side ditch.

Figure 12. IVI Minivib along along the shoulder of US 50.

Figure 13. IVI Minivib the shoulder of US 50.

Previous experiments with low noise accelerometer and tuned placements were expanded to a full field trial on this survey as part of continued attempts to boost resolution and signal-to-noise ratio (Rademacker, 2006). Two types of accelerometers were used for recording (one pair on the mass and one pair on the baseplate) during the 2008 acquisition. The Dytran 3184 model accelerometer with a sensitivity level of 25 mV/g is referred to as the factory accelerometer, since it is standard equipment for IVI Minivib models. The Endevco 7703A-1000 accelerometer with a sensitivity level of 20 mV/g is the model currently being tested by the KGS. Noise from the sensor, recording system, and cable/telemetry are important considerations when using baseplate and mass accelerometers to calculate groundforce. In previous experiments, background noise was recorded at the reaction mass and baseplate (Figure 14). The Endevco accelerometer on the baseplate was used to determine what percentage of noise at a given frequency within a sweep could be attributed to engine noise (Figure 15) (Rademacker, 2006). Noise measurements are important when comparing accelerometer data and processing methods in this system.

One of each accelerometer type was placed on the mass (Figures 16) and then a pair was installed on the baseplate of the IVI Minivib (Figure 17) (Rademacker, 2006). There are two systems recording data from the two types of accelerometers. The onboard computer running the factory controller software and hardware records data from the factory accelerometers response and calculates groundforce. A

Geometrics geode seismograph records data from the KGS installed accelerometers that are run through specially designed pre-amplifiers.

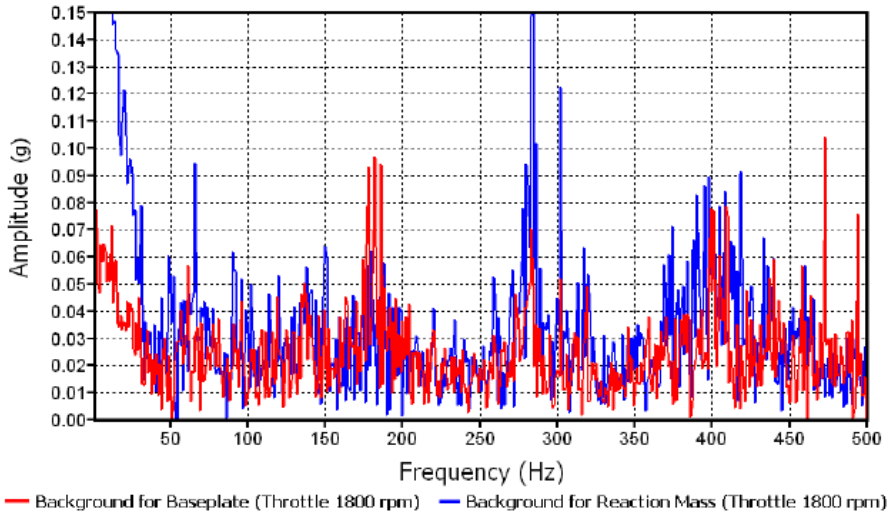

Figure 14 . Background noise recorded at the baseplate and reaction mass. A low amplitude, 10 s linear up-sweep between 0.1 – 1.0 Hz was generated to record amplitudes up to 500 Hz. For this reason any values 1 Hz and below are omitted. The values are generally similar. The engine throttle is constant at 1800 rpm, which is a standard setting when acquiring data. (Rademacker, 2006)

Endevco 7703A-1000			
Frequency (Hz)	**Throttle 1800 rpm**	**Throttle 0 rpm (Engine off)**	**%**
35	0.033	0.004	86.7
65	0.019	0.009	55.2
105	0.073	0.006	92.1
155	0.047	0.006	87.5
250	0.023	0.014	40.2
300	0.036	0.011	68.7
350	0.081	0.011	85.9
400	0.107	0.032	70.6
450	0.031	0.006	80.5

Figure 15. Comparison of accelerometer measurements with the engine throttle set to 1800 rpm and with the engine off. It is revealed that for most frequencies the majority of noise is due to engine noise. (Rademacker, 2006)

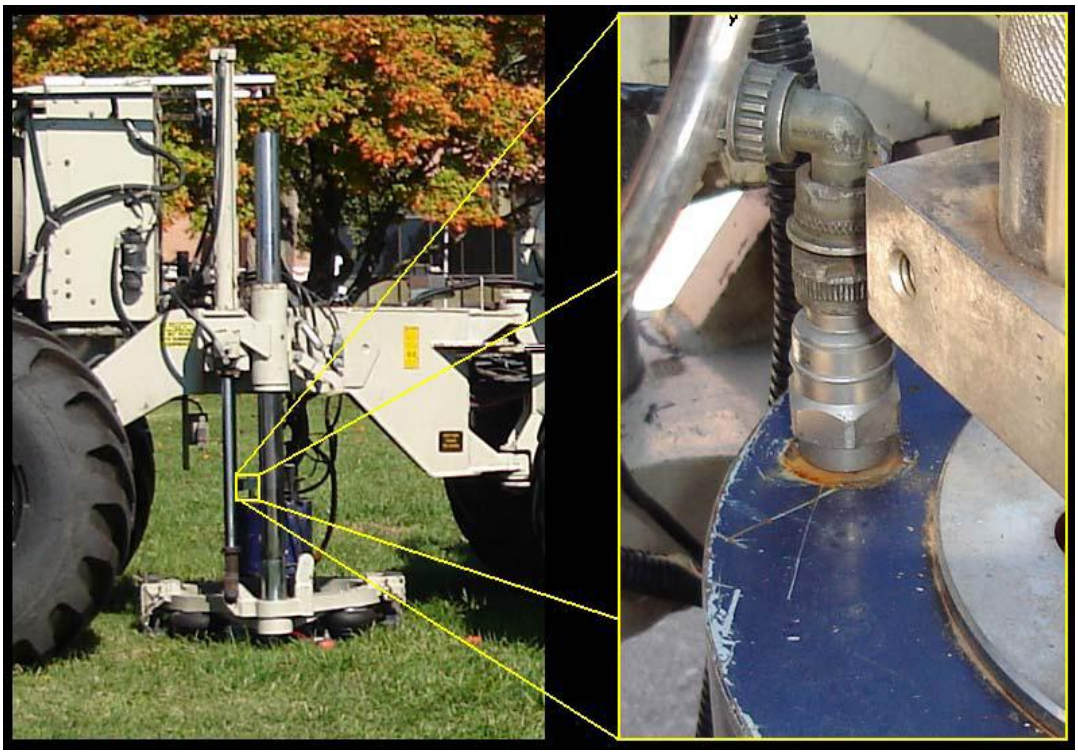

Figure 16. Location of the Dytran Accelerometer on the reaction mass. The Endevco accelerometer was also mounted on the reaction mass.

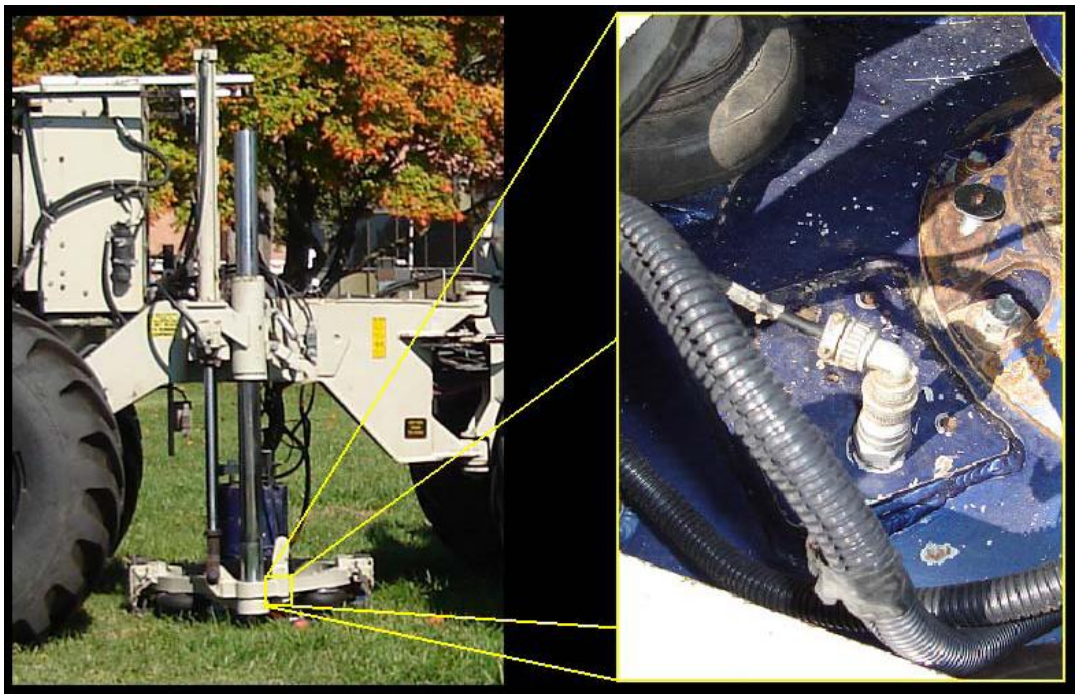

Figure 17. Location of the Dytran Accelerometer on the baseplate. The Endevco accelerometer was also mounted on the baseplate.

Seismic Data Processing

Victory Road Sinkhole

Both seismic data sets were processed using a common-midpoint (CMP) approach consistent with 2-D high-resolution vibroseis data (Figure 18) (Lambrecht, 2006; Steeples and Miller, 1994; Miller et al., 2002; Miller et al., 2008; Miller et al., 2006; Miller et al., 1993). Processing software (WinSeis) developed at the KGS was used for all processing. Processing steps were kept as simple as possible in an effort to accurately compare the 2001 and 2008 data sets. Data-specific operations were avoided to eliminate any processing induced changes. Basic processing (filtering, muting, NMO correction) was performed to ensure any changes seen in the data were directly related to geology. Outside the topographic depression (approximately 90 m) associated with the sinkhole, the surface topography was relatively flat for both surveys (+/- 1 m variation). Static problems are common in reflection data collected in areas where near-surface layers are disturbed by subsidence, resulting in lateral velocity variations (Frei, 1995). Event arrival times can be altered several milliseconds at this site by changes in velocities and distorted rock layers in the upper 30 m (Miller, 2002).

Vibroseis whitening was applied to the uncorrelated data in an attempt to improve the signal-to-noise ratio. This method involves applying automatic gain control (AGC) prior to cross-correlation to reduce the variance of noise (Coruh and Costain, 1983). Common to near-surface high-resolution reflection data is high ambient noise and low signal levels within the high frequency portion of the sweep

(Doll and Coruh, 1995). Vibroseis whitening increases the resolution of near-surface reflections (Klemperer, 1987).

Since telemetried groundforce was recorded as channel 1 during acquisition, the pilot for these data was created during processing to posses the appropriate frequency range and tapers for the different data sets. The equipment used for controlling the vibrator includes a Radio Trigger System (RTS) designed to communicate between the vibrator and the remote seismograph. The RTS transmits a trigger to the vibrator and receives the reference signal at the seismograph. Mechanical vibrator energy is recorded by the mass and baseplate accelerometers and saved to the vibrator's controller computer. The RTS sends the selected pilot data to the seismograph in analog form, and is saved as a pilot trace (groundforce) (Rademacker, 2006).

For processing, synthetic sweeps were created to match the vibrator's drive signal for each survey. A sweep is an oscillating signal with time-variant amplitude and a frequency that varies monotonically with time (Goupillaud, 1976). The sweeps were cross-correlated with the recorded vibroseis signal traces to produce a reflectivity series (Figures 19 and 20 are shot gathers from equivalent surface locations). Cross-correlation using a synthetic sweep to represent the vibrator's open loop drive signal (Cunningham, 1979) is a common process used in processing for single source vibroseis data (Yilmaz, 2001).

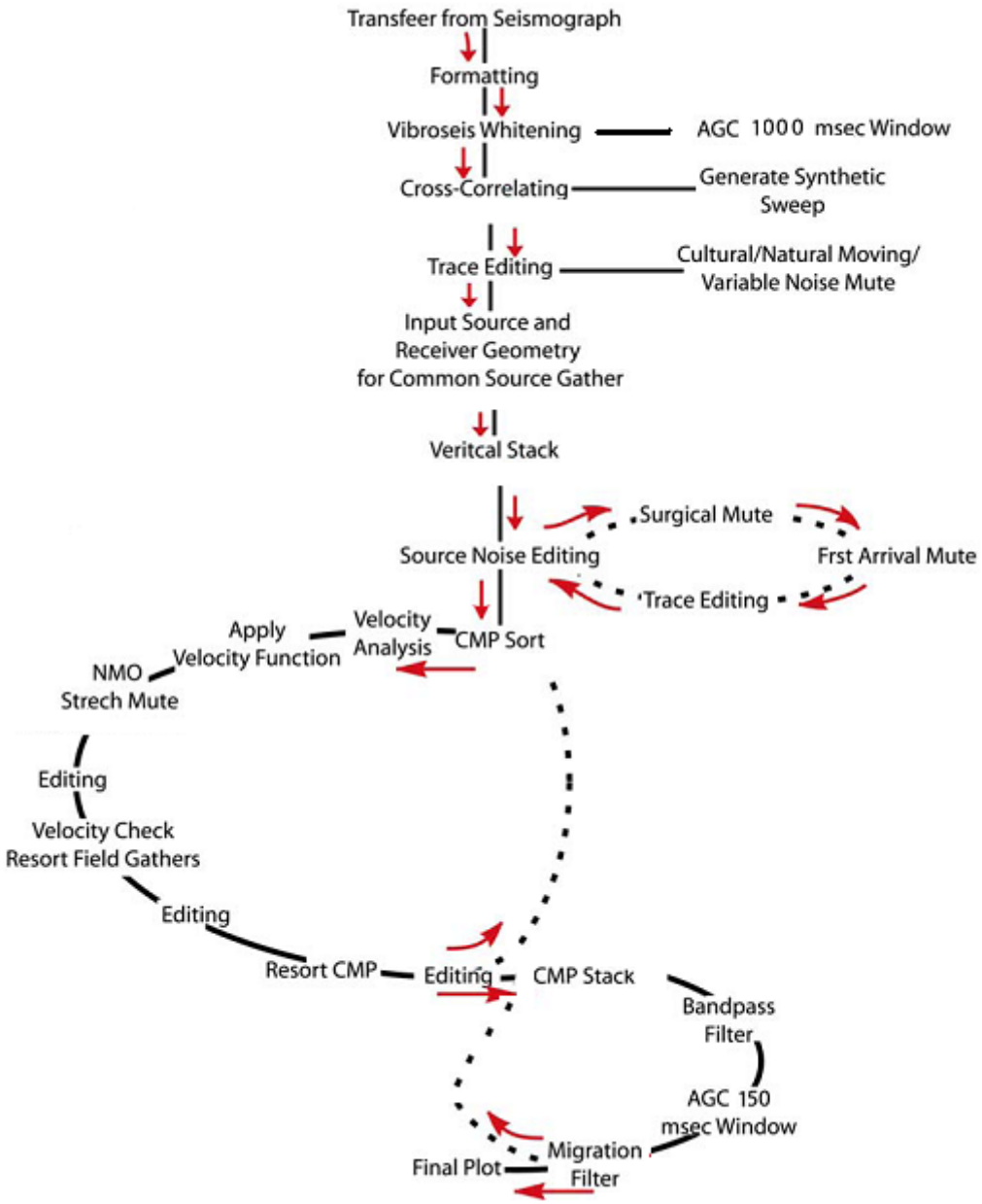

Figure 18. Common 2-D high-resolution near-surface seismic-reflection processing flow (modified from Lambrecht, 2006).

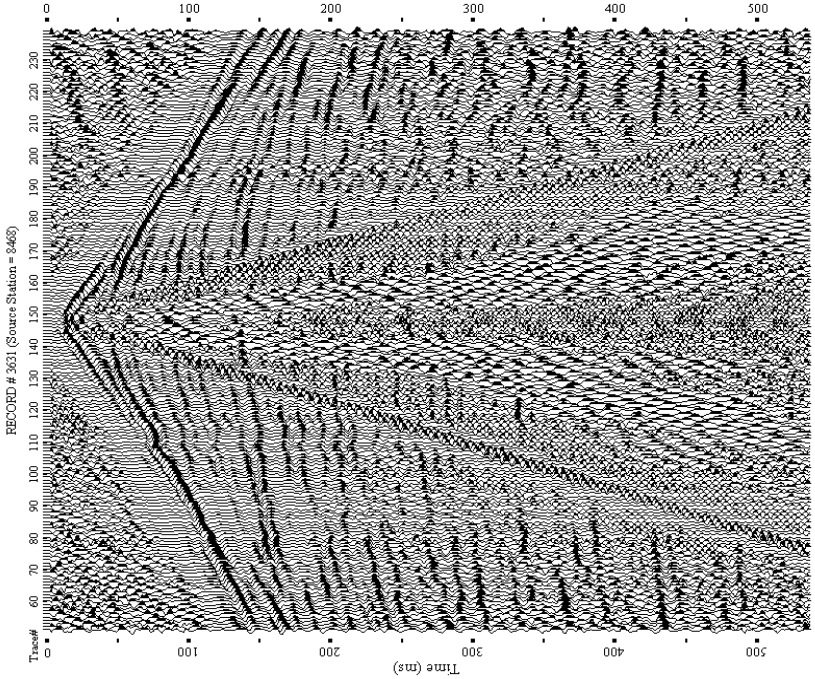

Figure 20. Shot gather from 2008 data with a 50 ms gain applied (2008 Shot 3631 equivalent to 2001 Shot 1576)

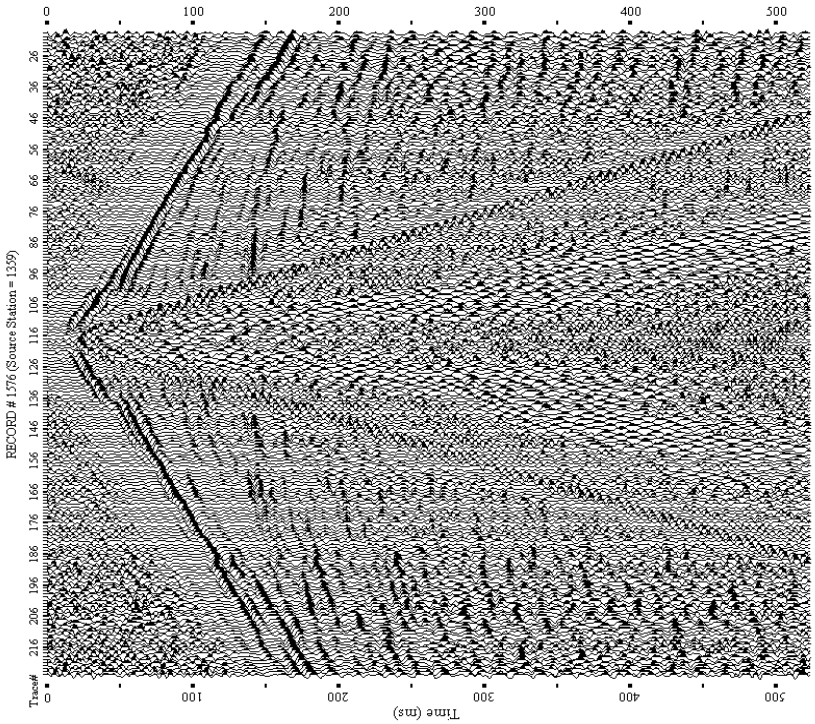

Figure 19. Shot gather from 2001 data with a 50 ms gain applied (2001 Shot 1576 equivalent to 2008 Shot 3631)

Muting and filtering improved signal-to-noise ratios. Dead and/or noisy traces were muted for individual shot gathers. Each of the three shot gathers recorded at each shot point were vertically stacked. This allows for all inconsistent events on the shot gathers to attenuate while enhancing all coherent events (Klemperer, 1987) . First arrival muting was applied to remove refractions, direct wave, and pre-signal noise on a shot by shot basis (Figures 21 and 22). An inside mute was used to remove all energy arriving later in time than the air-coupled wave (Figures 23 and 24). Energy arriving later in time than the air-coupled wave was saturated with noise and possessed minimum reflection data. With detailed filtering, reflections can be enhanced within the 'noise cone'. However, airwave frequencies still remain and often mix with reflection frequencies. The reflections that can be saved are of much lower S/N ratios and simply not worth the added processing time (Baker, 1998).

Velocity analysis was undertaken and normal moveout (NMO) corrections were applied after the data were sorted into CMP gathers. Groups of 20 and 50 CMPs were used for picking velocities with up to nine vertically defined control velocities ranging from 1500 m/s to 3750 m/s. Emphasis was placed on velocity estimates in the upper 200 ms. Near-surface seismic data collected in subsidence areas will be prone to asymmetry of reflection hyperbolae on shot gathers caused by lateral velocity changes and dipping geologic units (Miller, 2002). Choosing appropriate NMO velocities can be affected by the asymmetry. CMP gathers with muting and NMO corrections applied can be seen in Figures 25 and 26. Scaling and

bandpass filtering followed CMP stacking on both data sets to enhance interpretability (Figures 27 and 28).

Migration was applied in an attempt to correct for geometric distortion caused by the complicated near-surface (collapse structures). F-k migration using a single velocity function is a quick process commonly used for deeper surveys (Margrave, 2001). A highly variable shallow velocity function prohibits the effectiveness of this method. Lateral coherency and the signal-to-noise ratios were increased with migration, but resolution was reduced due to spatial aliasing. At early times/depths, velocities are slow and reflection moveout can be large; this leads to spatial aliasing of higher frequencies (Li, 1991). Low stacking velocities found in the near-surface lowers the effectiveness of migration (Black et al., 1994). Reflections arriving later than 200 ms that were difficult to locate in the un-migrated sections are more coherent post migration. However, reflections directly beneath the sinkhole are still incoherent due to improper migration. Migration allowed for a better understanding of the deeper reflections, but provided minimum benefits when interpreting the upper units. In general, the closer reflections are to the source, the less need there is for migration (Black et al., 1994).

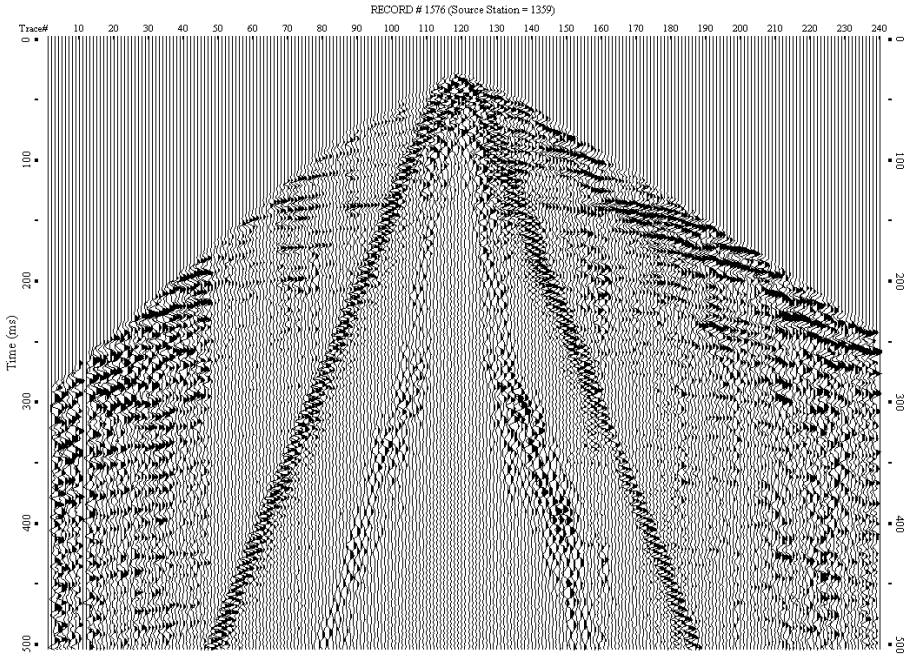

Figure 21. Shot gather from the 2001 data set with First Arrival Muting applied (Shot 1576).

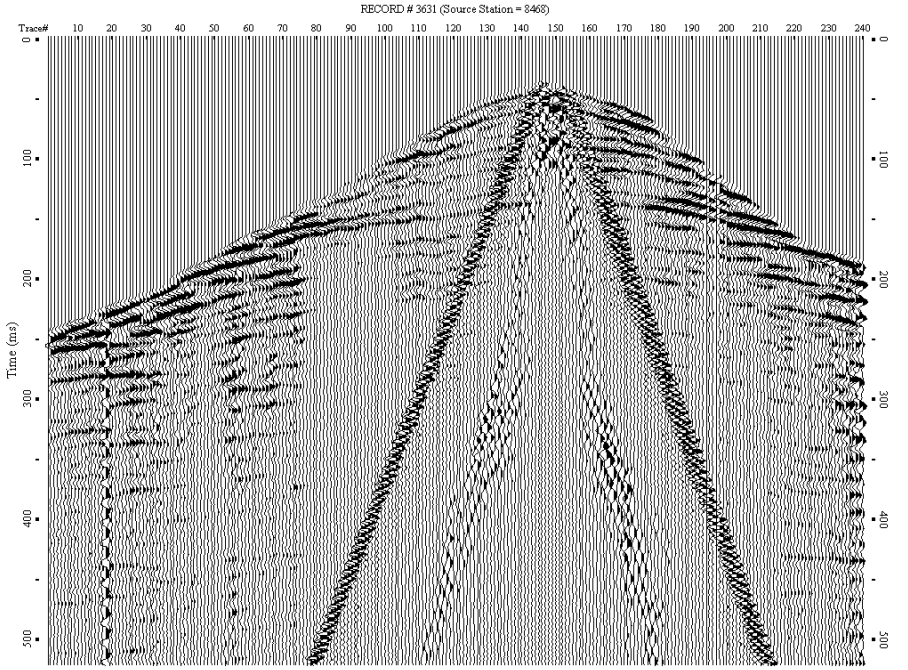

Figure 22. Shot gather from the 2008 data set with First Arrival Muting applied (Shot 3631).

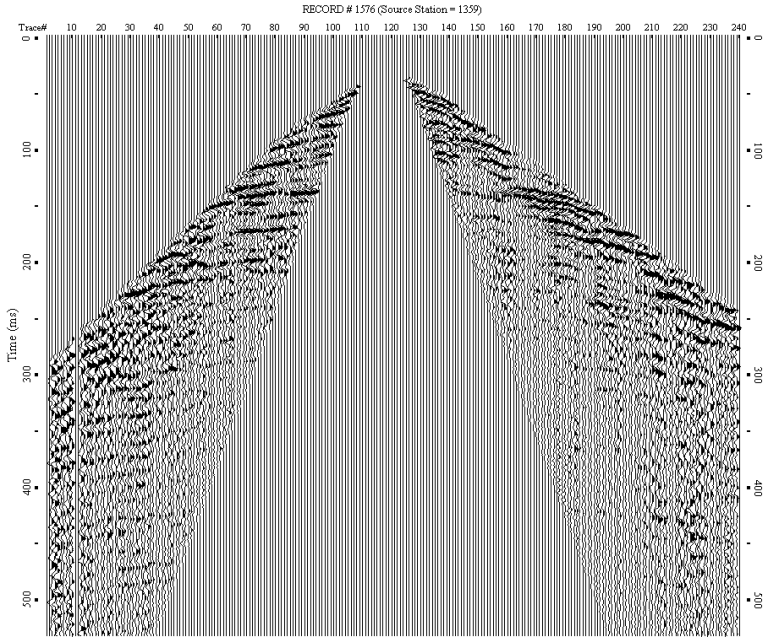

Figure 23.Shot gather from the 2001 data set with a Inside Mute applied (Shot 1576).

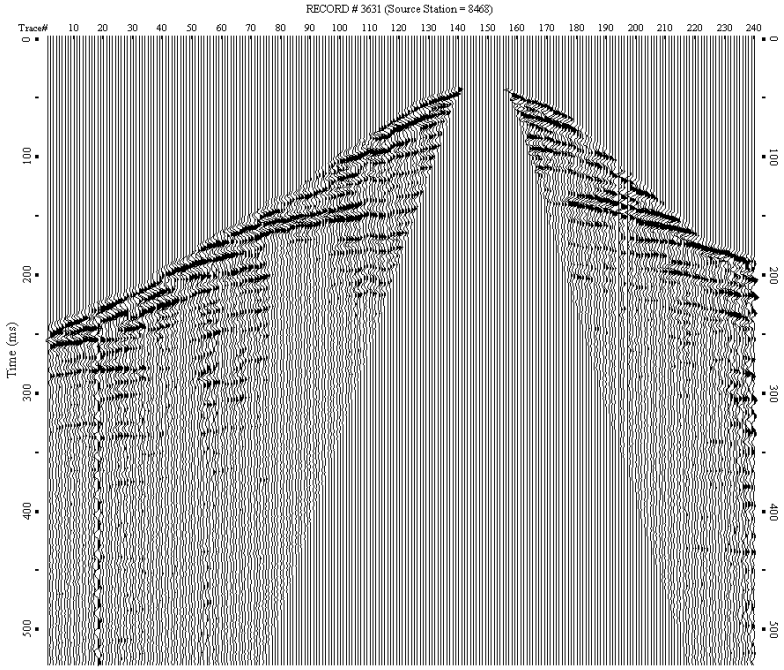

Figure 24. Shot gather from the 2008 data set with a Inside Mute applied (Shot 3631).

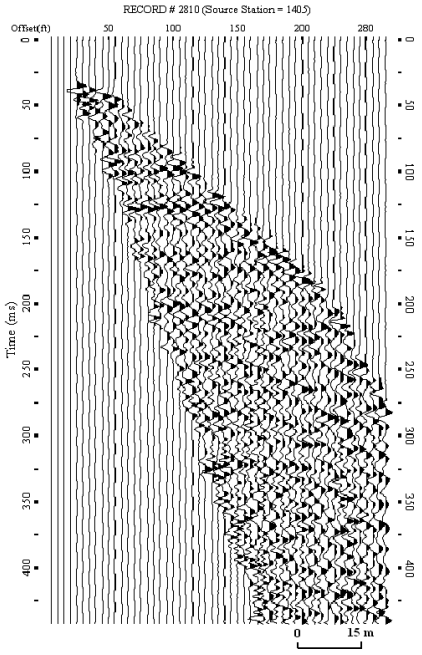

Figure 25. Fully processed CMP gather from the 2001 data set (CMP Gather 2810, equivalent to 2008 CMP Gather 16818).

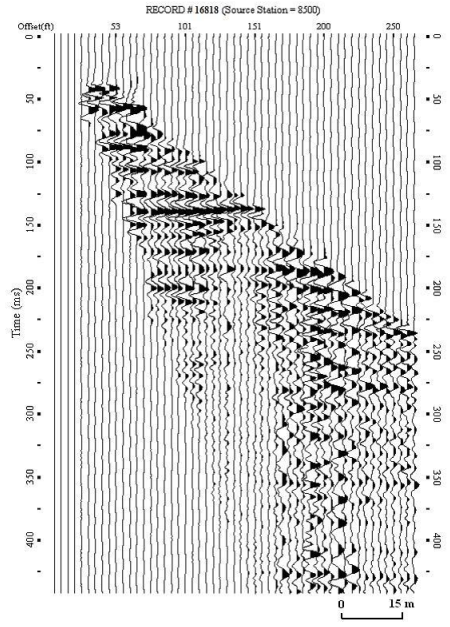

Figure 26. Fully processed CMP gather from the 2008 data set (CMP Gather 16818, equivalent to 2001 CMP Gather 2810).

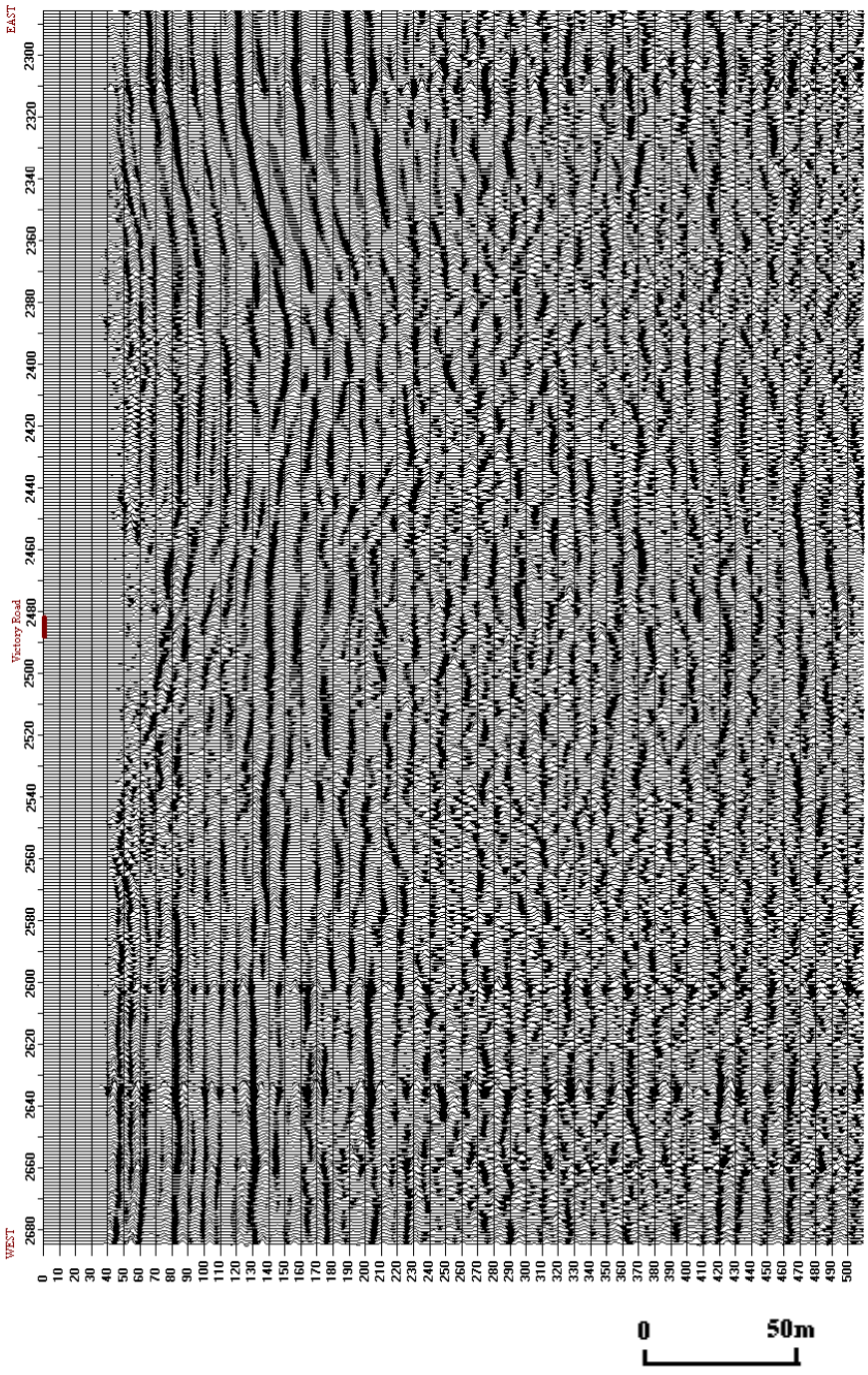

Figure 27. CMP stacked section of the 2001 data set.
The sinkhole is centered around CMP 2486.

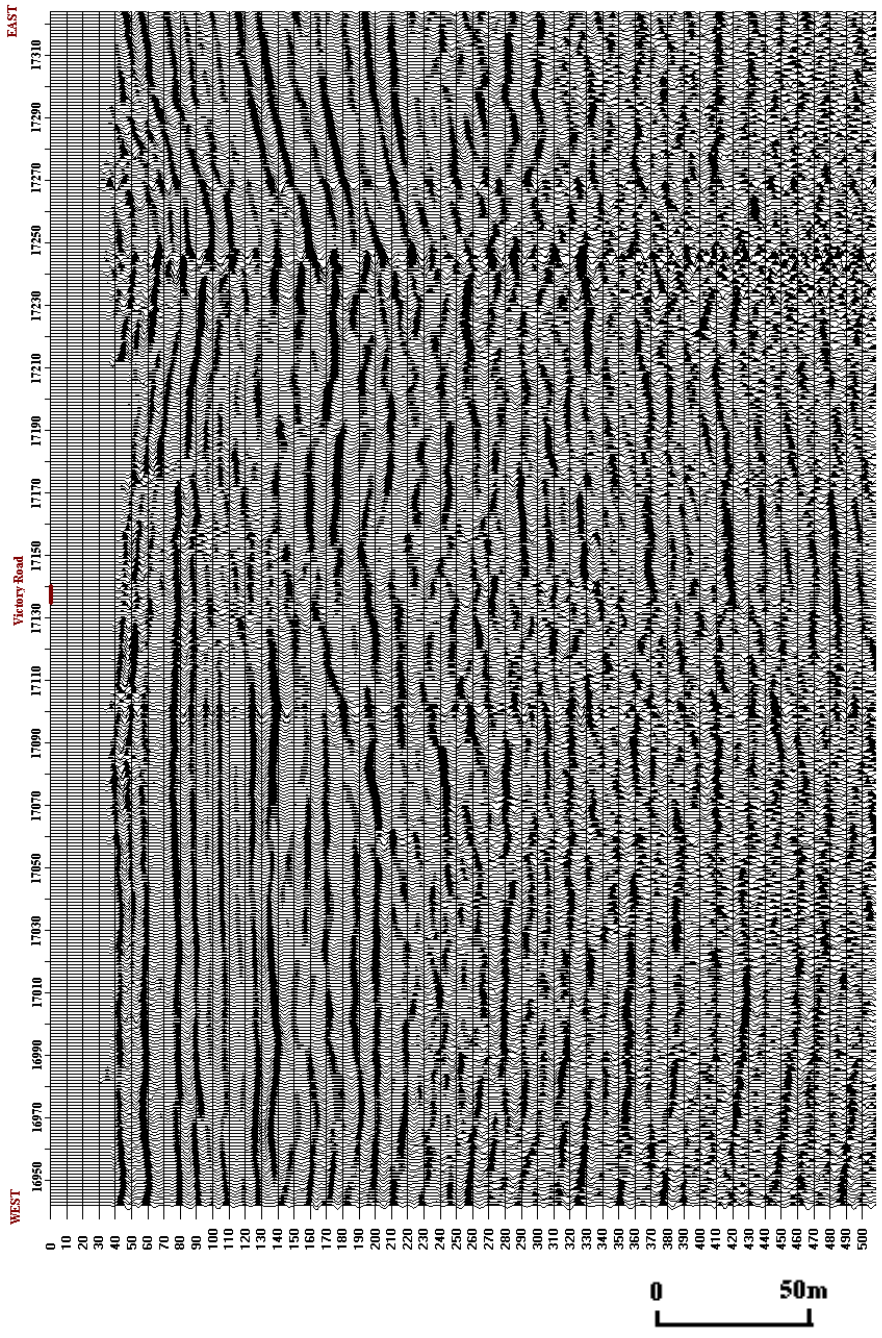

Figure 28. CMP stacked section of the 2008 data set.
The sinkhole is centered around CMP 17142.

Optimization of Correlation / Deconvolution Operation

An experimental mass/baseplate recording system was implemented in 2008 to test different approaches to source wavelet compression. Cross-correlation and deconvolution were performed on all accelerometer data from the reaction mass and baseplate (Figure 29), calculated groundforces (Figure 30), and the created synthetic sweep (Figure 31). A total of seven data pilot traces were used for cross-correlation and deconvolution (Table 1). Appropriate filtering was applied consistently to properly compare processing results. Note the similarity in high amplitude frequency peaks between the baseplate traces and the differences in amplitude values of the reaction mass traces (Figure 32).

With both mass accelerometer traces and both baseplate accelerometer traces appearing almost identical (Figure 29), calculated groundforce from each set were expected to be similar. The calculated groundforce traces are different (Figure 30). A correlation coefficient (0.701) was used to quantify this observed difference in wiggle trace display (Figure 33). Cross-correlation between both mass accelerometer traces and baseplate accelerometer traces would have produced a single spike if they were identical. Cross-correlation determines the linear similarity between two traces (Sheriff, 2002).

Cross-correlation and deconvolution were used on pre-processed vibroseis data. Vibroseis whitening on the raw recorded vibroseis traces was facilitated by using an automatic gain control window of 1000 ms. A synthetic sweep was created to match the frequency range of the vibrator drive signal (25-300 Hz) (Figure 31).

Each raw shot gather was cross-correlated with the synthetic sweep. The raw vibroseis data were correlated with the Dytran reaction mass and baseplate accelerometer traces individually (Figure 29), Endevco reaction mass and baseplate accelerometer traces individually (Figure 29), groundforce calculated using the Dytran accelerometer traces (Figure 30 (b)), and the groundforce calculated using the Endevco accelerometer traces (Figure 30 (c)).

Reference Signal	Cross-correlation	Deconvolution
Synthetic Sweep	Yes	Yes
Telemetried Groundforce Pilot	No	Yes
Dytran Reaction Mass Accelerometer	Yes	Yes
Dytran Baseplate Accelerometer	Yes	Yes
Endevco Reaction Mass Accelerometer	Yes	Yes
Endevco Baseplate Accelerometer	Yes	Yes
Calculated Groundforce from the Dytran Accelerometers	Yes	Yes
Calculated Groundforce from the Endevco Accelerometers	Yes	Yes

Table 1. Seven possible reference signals were used for processing comparisons.

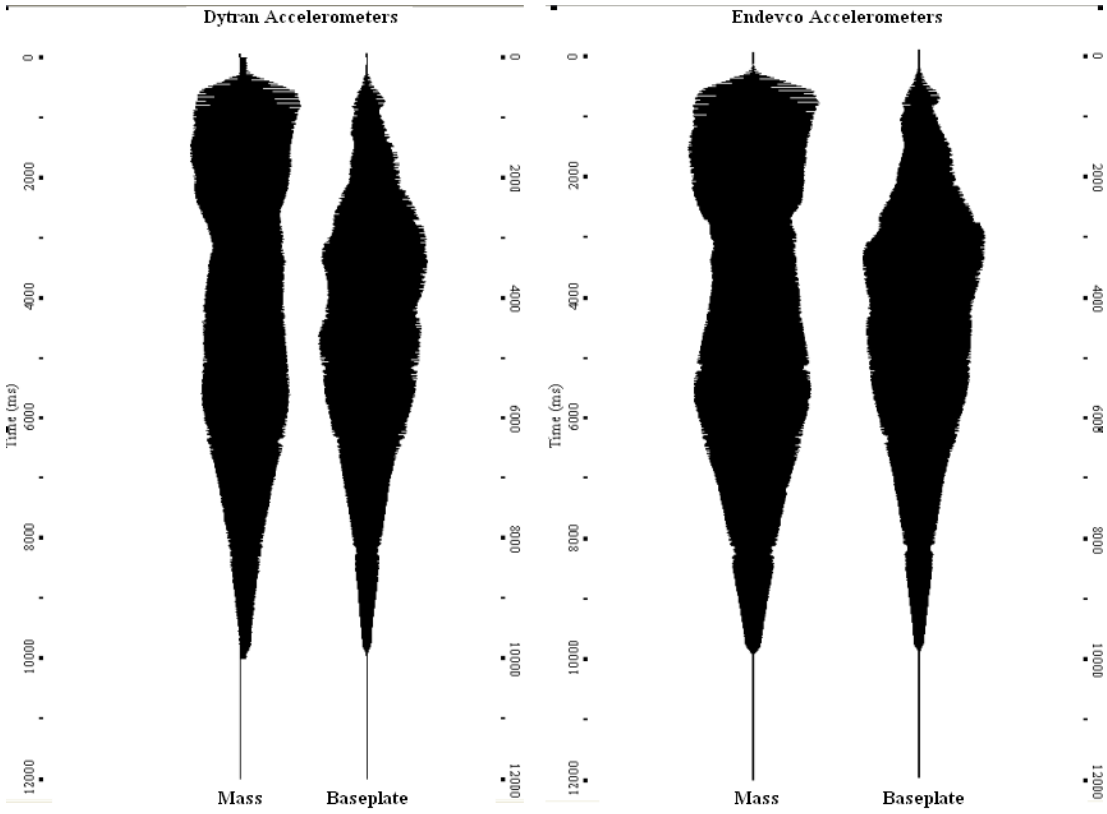

Figure 29. Sweep shape comparison of the Dytran and Endevco accelerometer traces with normalized amplitudes.

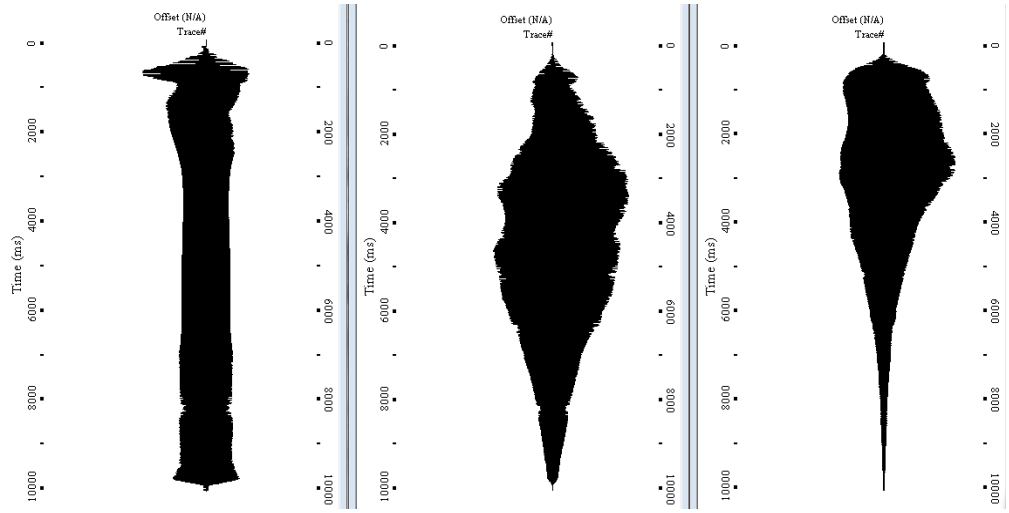

(a) (b) (c)

Figure 30. (a) Telemetried Groundforce pilot of the raw data, (b) Dytran Groundforce, (c) Endevco Groundforce.

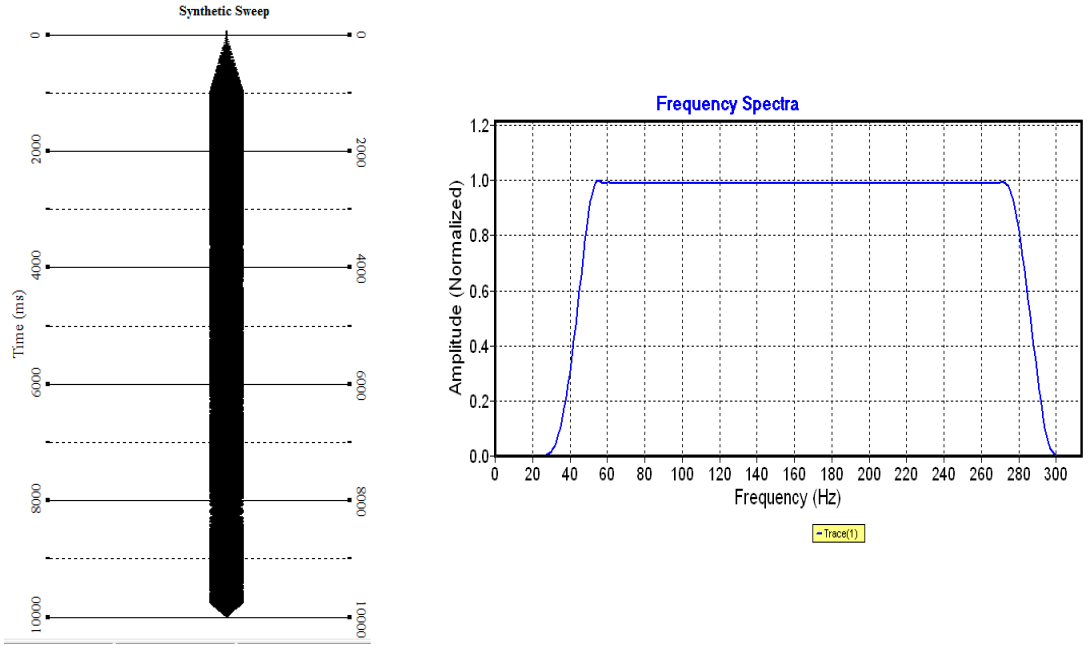

Figure 31. 25-300 Hz synthetic sweep with the associated frequency vs amplitude spectra generated during processing.

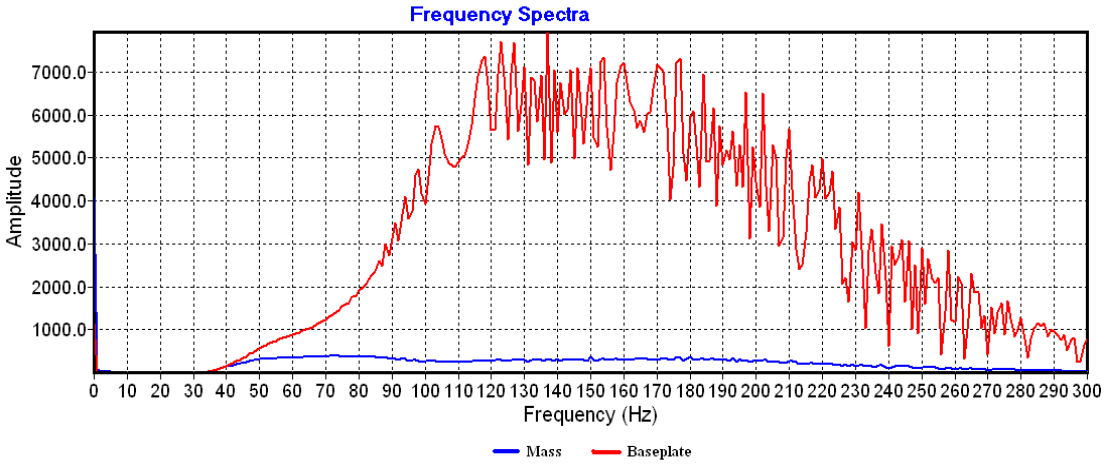

(A)Frequency vs Amplitude spectra for the Dytran Accelerometers (Shot 3901)

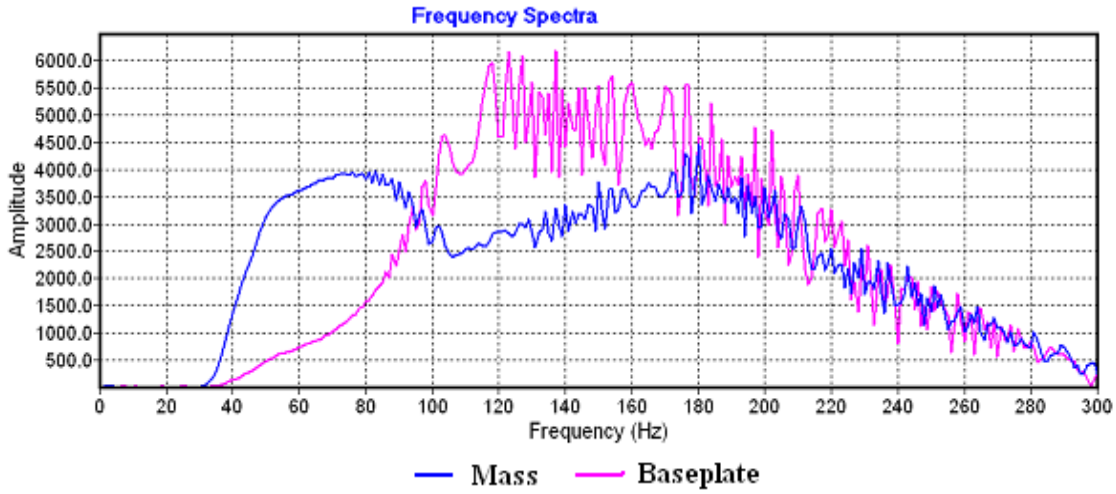

(B)Frequency vs Amplitude spectra for the Endevco Accelerometers (Shot 3901)

Figure 32. Amplitude comparisons for both baseplate and reaction mass accelerometer traces.

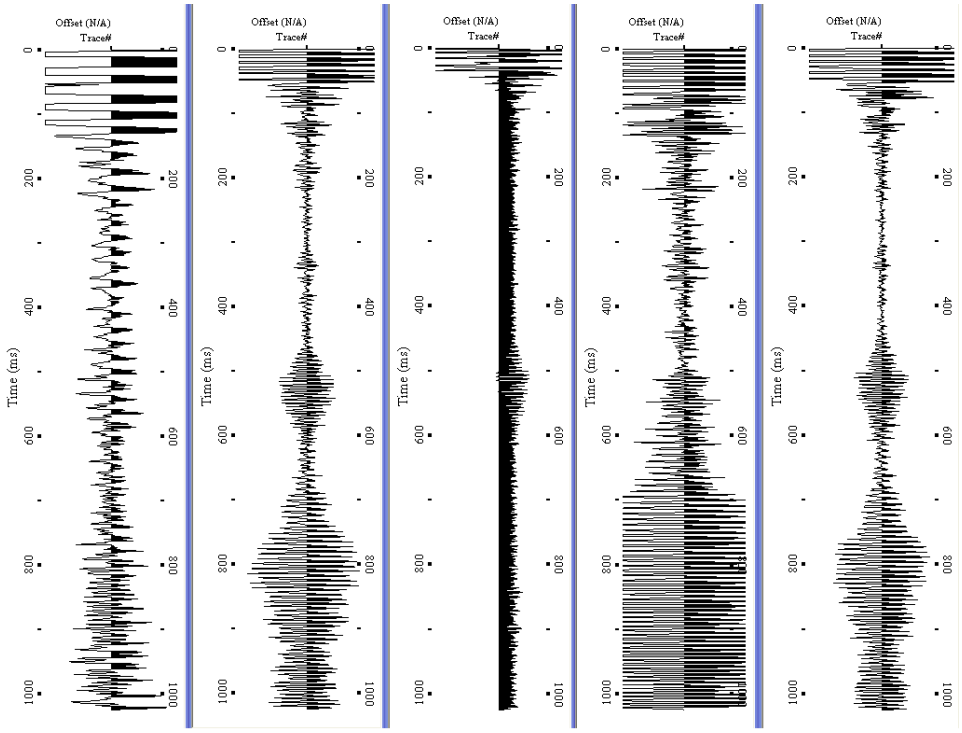

(a) (b) (c) (d) (e)

Figure 33. (a) Correlation of mass traces with correlation coefficient 0.852, (b) baseplate traces with correlation coefficient 0.991, (c) Dytran traces with correlation coefficient –0.194, (d) Endevco traces with correlation coefficient –0.493, (e) Groundforces with correlation coefficient 0.701.

Spectral whitening (band-limited deconvolution) was applied using the synthetic sweep, telemetried groundforce pilot, Dytran reaction mass and baseplate accelerometer traces, Endevco reaction mass and baseplate accelerometer traces, calculated groundforce using the Dytran accelerometers and the calculated groundforce using the Endevco accelerometers as the pilot trace. A frequency range of 30 Hz to 295 Hz was used for deconvolution. The recording sweep during acquisition was 25-300 Hz; accelerometers recorded frequencies well above 300 Hz. A bandwidth within the generated sweep was used for deconvolution.

The effect of noise must be considered for deconvolution and cross-correlation operations. Deconvolution amplifies noise (van der Baan, 2008). Therefore, deconvolution will produce the best results when frequencies outside the sweep are attenuated with a band pass filter and instrument noise is minimized. When cross-correlating with a synthetic sweep, the noise in a recorded trace is cross-correlated with the sweep and effectively filtered consistent with the sweep shape. This results in the removal of the noise outside the sweep's frequency range. Electronic noise caused by inefficiency in the operation shows minimum effect on the cross-correlation results (Brittle, 2001).

Non-rigid motion (structural flexing) of the baseplate can cause errors in using the weighted sum formula (Sallas, 1984) to calculate groundforce (Schrodt, 1987). Each baseplate accelerometer measures the acceleration of the baseplate at one single location and uses that to estimate acceleration across the entire plate. It has been shown that at high frequencies, there can be significant phase differences across the

baseplate during a sweep (Brook et al, 1991). Avoiding decoupling of the baseplate with the ground is critical in calculating an accurate groundforce. Amplitude control between the reaction mass and baseplate during a sweep is used to prevent decoupling (Schrodt, 1987).

van der Veen et al. (1999) discuss the validity of using the weighted sum method to calculate groundforce. A portable vibrator with a permanent magnet (66 kg) acting as a reaction mass connected to a baseplate of 3.5 kg via a spring was used for the experiment. The use of the weighted sum method accurately represents true groundforce up to 900 Hz. Authors of this paper compared deconvolution using groundforce measured by three load cells placed below a portable vibrator and groundforce calculated using the weighted sum method. Results revealed an accurate estimation of groundforce within the main frequency range of interest for shallow reflection surveys (~30-500 Hz) with a peak output force of 112 pounds. In relation, the vibrator used in the 2008 survey has a sweep frequency range of 15 – 500 Hz with a peak output force of 6,000 pounds.

Results

Seismic Interpretation of the Victory Road Sinkhole

Primary reflection events in the upper 200 ms can easily be identified and correlated on shot gathers from both data sets (Figure 34). Shot gathers from each data set possess consistency in reflections zero-offset arrival times and character for interpreted horizons. The bedrock surface is the top of the Ninnescah Shale and is represented by reflection events on both gathers arriving at approximately 40 ms. The reflection from the top of the Hutchison Salt arrives at approximately 125 ms on both gathers. Consistency in these arrival times and their wavelet characteristics are important for accurately processing and comparing the two data sets. Data collected in 2008 has a higher signal-to-noise ratio than 2001 data (Figure 34). Improved signal-to-noise ratios in 2008 can be seen in the CMP stacked sections (Figures 27 and 28). Lateral velocity irregularities due to structural and material changes lead to the irregular reflection patterns observed on shot gathers. Reflections interpreted on the shot gathers correlated well with reflections interpreted on the CMP stacked sections.

Vertical resolution was sufficient to interpret units located within the paleosinkhole located to the east of Victory Road (Figures 27 and 28). The bedrock reflection from the top of the Ninnescah Shale varies in time across both seismic lines, but generally arrives at approximately 40 ms (or around 33 m deep) in areas outside the interpreted subsidence zones. The top of the Upper Wellington Shale reflection arrives at approximately 80 ms (or around 63 m deep). The relative high

amplitude, low frequency reflection at 130 ms (or around 122 m deep) is the top of the Hutchinson Salt. The salt reflection arrives much later in time within the paleosinkhole due to dissolution. The Lower Wellington Shale reflection can be seen at approximately 200 ms (or around 190 m deep). These key reflection events could be consistently correlated across both seismic lines.

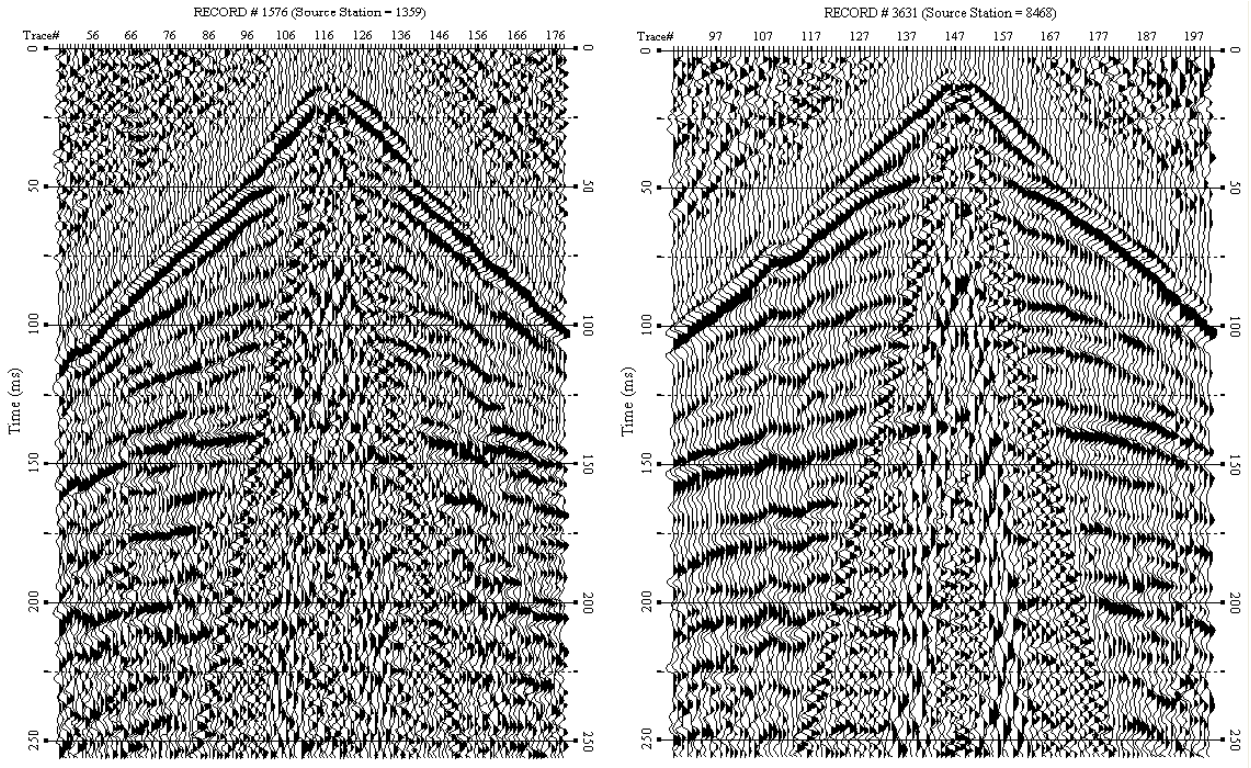

Figure 34. Shot gathers showing key reflection events from 2001 (left) and 2008 (right). Shot gathers are from equivalent surface locations.

Both seismic lines show a synform or 'bowl-shaped' depression near the sinkhole area. Units appear to be gently dipping or sagging into the center of the paleosinkhole on the data. The horizontal resolution is not small enough to accurately image the faulting caused by the brittle deformation. Changes in surface elevations (Figures 5-7) correlate to the subsurface sag seen in the 2001 line between CMPs 2460 and 2500 (Figure 35) and the 2008 line between CMPs 17120 and 17160 (Figure 36). As the elevations indicate, more subsidence has occurred along the northern edge of Hwy 50. The 2008 data (Figure 36) show more coherency in the shallow reflections than the 2001 data (Figure 35). Less disturbed reflections can be seen to the west in the lines (Figures 35 and 36). The slumping or collapsing of the rocks above the salt is obvious in both lines. Interpretations of the lines support the idea of the overburden rocks collapsing into a void within the salt unit caused by the natural removal of salt.

Deeper reflections (greater than 200 ms) beneath the subsidence feature are present in the stacked sections (Figures 27 and 28), but possess less potential resolution. These reflections appear to still suffer from static issues compared to the shallow reflections. These static issues can be seen on both shot gathers in reflections later than 200 ms (between traces 100 and 117 at 210 ms) (Figure 34). Time delays (pull downs) and geometric distortions are expected when imaging beneath subsidence features (Anderson et al., 1995) (Figure 37). Time delays are caused by decreases in material velocities caused by changes in compaction structures and material bulk properties within the synform (Figure 37 (b)). Diffractions and

distorted reflection arrivals are due to the small radius of curvature of the synform and the associated velocity structure (Figure 37 (c)). These effects were considered when interpreting seismic data in a subsidence zone.

The sequence and timing of subsidence in 2001 can be determined by the location and dip of the disturbed layers. At least two episodes of subsidence prior to the current surface subsidence can be interpreted. The Ninnescah Shale and Upper Wellington units fill the synform flatly (CMPs 2360-2445, 50 – 100 ms) (Figure 38). This area represents the original subsidence episode, prior to deposition of the Equus beds, which formed after a strain release in a brittle manner. Secondary subsidence is evident by the faulting of the Ninnescah Shale and Upper Wellington units (CMPs 2300 – 2360 and CMPs 2445 – 2520, 35 – 85 ms). This episode was the result of low-stress release forming the synform. The current surface sinkhole at Victory Road (intersection of Hwy 50 and Victory Road centered at CMP 2486) is the result of the reactivation of the paleosinkhole centered about CMP 2390. The top of the salt beneath CMP 2390 dips downward more severely than the overlying units. The unit directly overlying the salt at 130 ms is flat, revealing bridging caused by current dissolution.

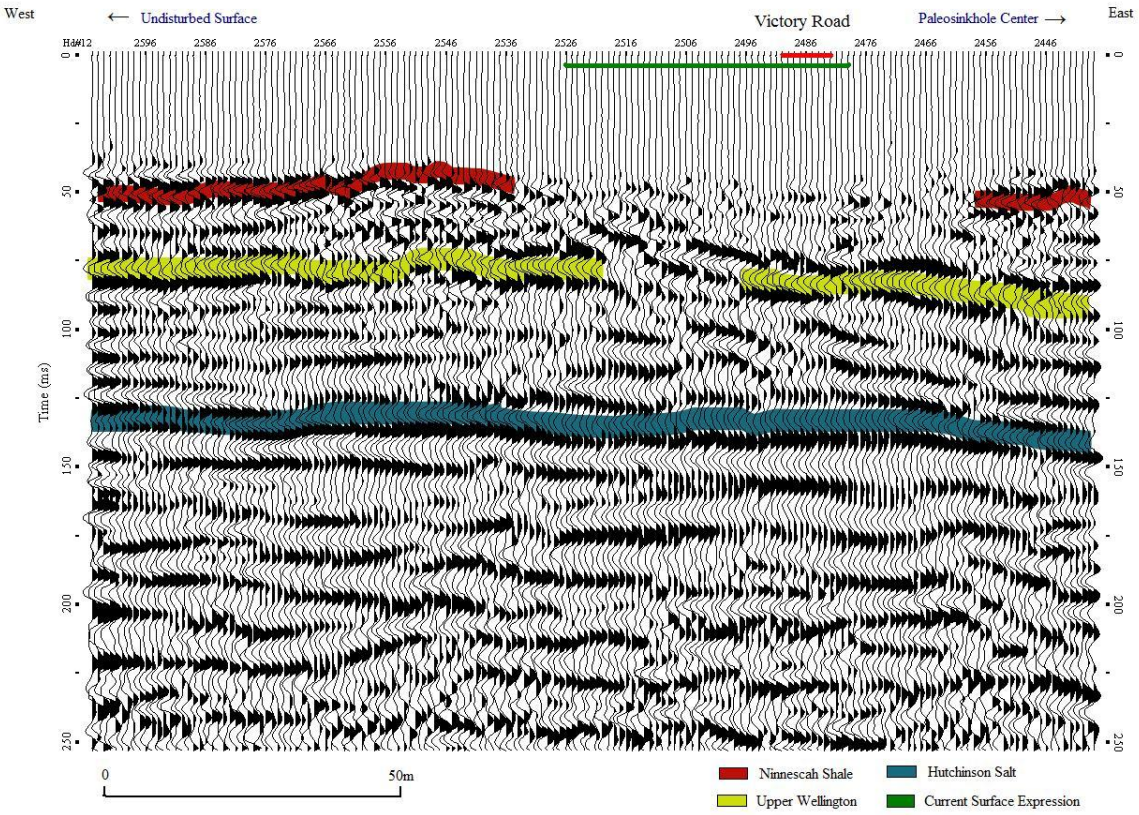

Figure 35. 2001 data set showing the disturbed units beneath the current surface expression. This is the active portion of the subsidence feature. Victory Road is centered around CMP 2486.

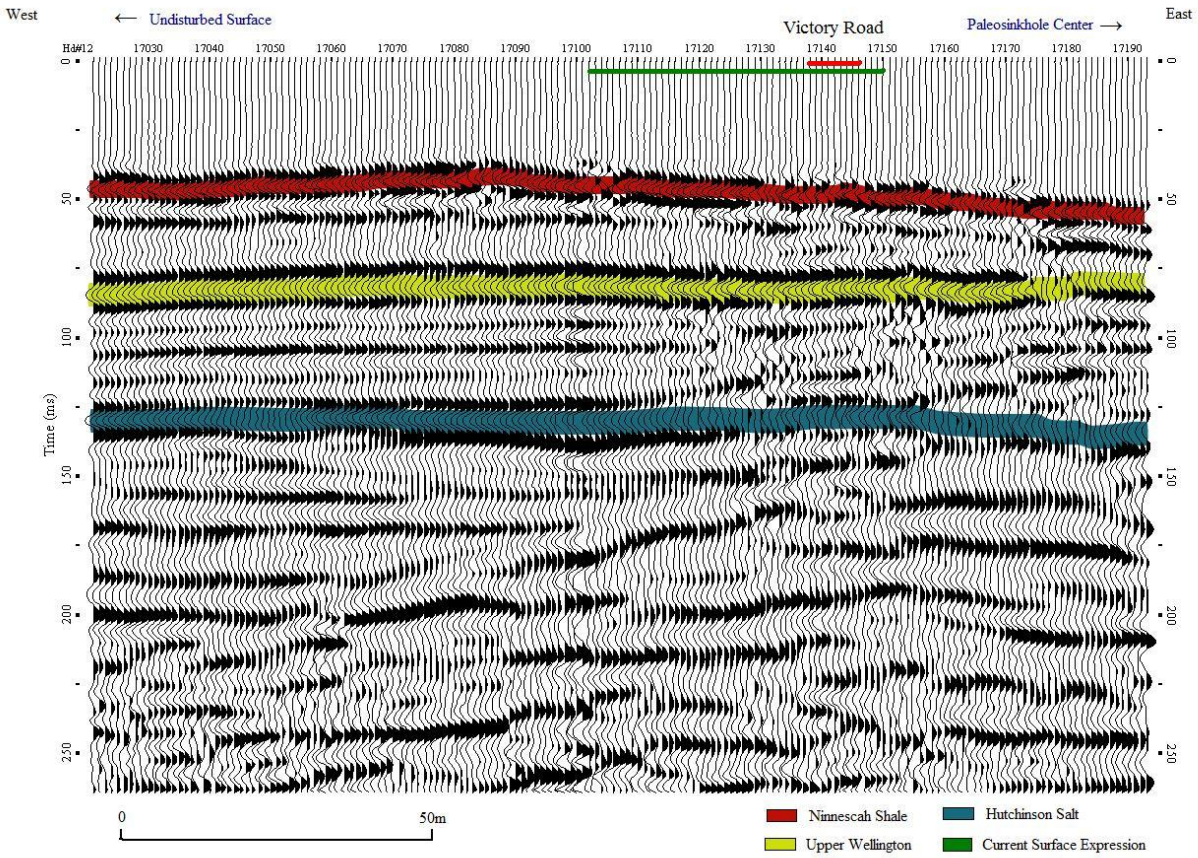

Figure 36. 2008 data set showing the disturbed units beneath the current surface expression. This is the active portion of the subsidence feature. Victory Road is centered around CMP 17142.

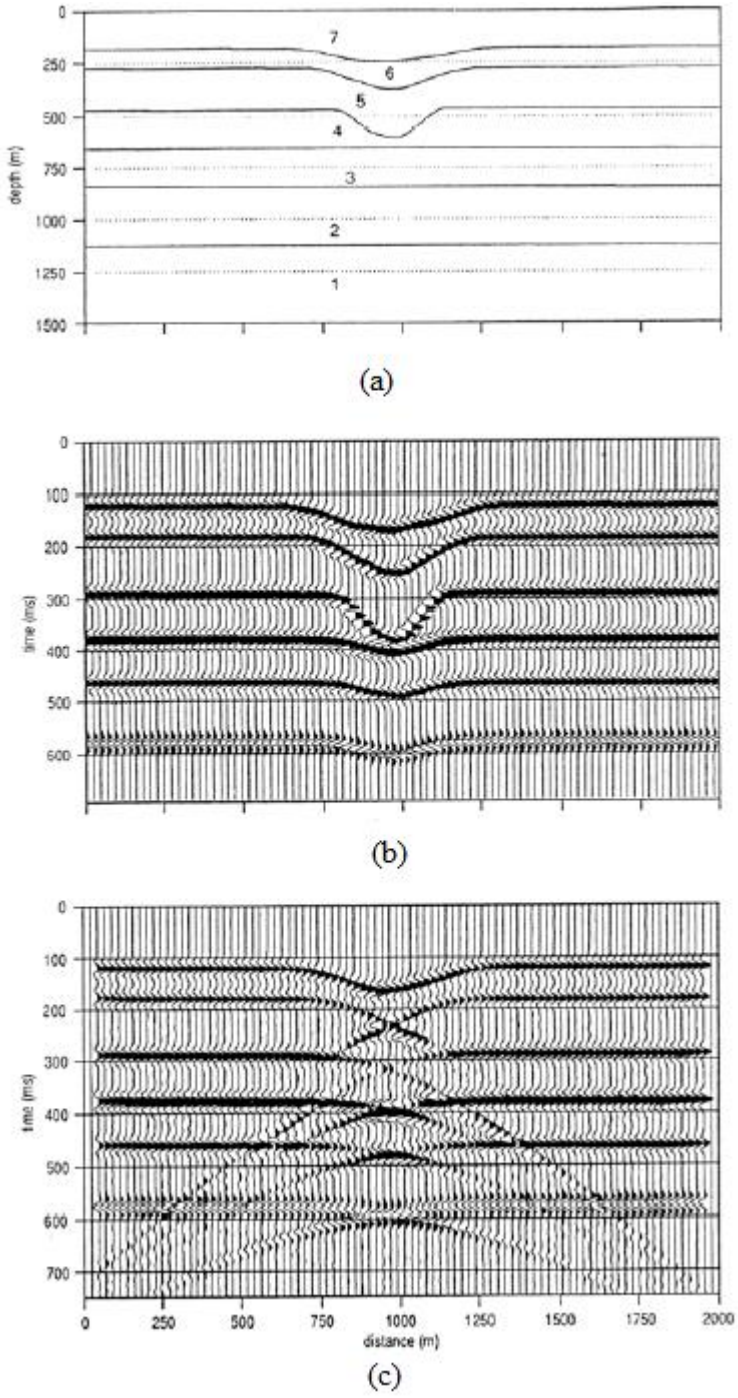

Figure 37. (a) Cross-section of a common dissolution feature with units 1-3 flat beneath the synform; (b) synthetic seismogram with time delays observed beneath the synform; (c) synthetic seismogram with observable diffractions (Anderson, 1995).

Time-Lapse Interpretation

Signal-to-noise ratios were better on 2008 data. Data were collected in late August 2001 and mid-June 2008. Near-surface soil-moisture conditions were much higher during the 2008 acquisition. Wetter conditions improve coupling, also leading to increased signal-to-noise ratios (Jefferson, 1998; Jefferson 1995). Collecting data on opposite sides of the highway (approximately 15 m) can account for differences seen between the data sets. With the amount of lateral variation that can be expected within a subsidence zone, the 2008 survey could be imaging a completely different structural condition.

Interpretation of the current dissolution episode causing the surface expression west of Victory Road showed no significant change in the subsurface structure. There is better coherency within the reflections less than 100 ms on the 2008 data (Figure 36) compared to the 2001 data (Figure 35). Directly beneath the surface expression on the 2008 line are irregularities in the Ninnescah Shale reflection at 45 ms (CMPs 17130 to 17142) (Figure 36). This is the active subsidence zone causing the surface change. To the east of this episode at 50 ms (CMPs 17162 to 17170) is a possible future subsidence zone. There are prominent changes in coherency in the Ninnescah Shale and the Upper Wellington from 80 ms to 90 ms (CMPs 17170 to 17180).

Interpretation of the Ninnescah Shale on the 2008 section shows a gradual dip from west to east (CMPs 17100 to 17180) (Figure 39). Surface elevation data collected in October of 2000 in the south lane showed a gradual drop in elevations

from west to east, mimicking the reflection from the top of the Ninnescah Shale. Surface elevations will continue to drop as gradual deformation continues within the underlying salt.

Changes in geology cannot be interpreted with complete assurance due to the offset between the surveys. Interpretations must account for the 15 m lateral offset of the surveys. Subsidence structures can abruptly change laterally and be unpredictable in shape. Therefore it is critical that receivers be as close to the same location as possible when performing a time-lapse study. Successful time-lapse seismic imaging of salt dissolution features (Miller, 2008; Lambrecht, 2006) have focused on acquiring data as close to the original locations as possible.

Evaluation of the feasibility of time-lapse seismic was aided by imaging the paleosinkhole. It was apparent through interpretation of the stacked sections that each line was imaging a different portion of the paleosinkhole. The flat units within the synform on the 2001 extend approximately 100 m in width. Assuming symmetry within the sinkhole, the center of the feature would have a 100 m diameter. If the 2001 survey intersected the center of the sinkhole, then the flat lying units would extend some 50 m to the south. If true, the 2008 survey would have revealed flat lying units above the salt. Since there were no flat units, the center of the sinkhole must be a minimum of 34 m north of the north road ditch with a radius of approximately 225 m. Faulted units, similar to those seen between CMPs 2310 and 2350 on the 2001 data are being imaged on the 2008 line. The 2008 line imaged

faulted units south of the paleosinkhole center while the 2001 line imaged the southern portion of the paleosinkhole center (Figure 40).

Resolution affects the effectiveness of 2-D time-lapse surveys. The Fresnel zone radius determines horizontal resolution. The Fresnel zone is dependent upon depth, frequency, and velocity (Sheriff, 2002). With a depth of 122 m and frequency of approximately 100 Hz, the Fresnel zone radius at the top of the Hutchinson Salt is 33 m. A structure at this depth must be at least 33 m in size in order to be uniquely imaged. Vertical resolution is often assumed to be ¼ of the wavelength (Sheriff, 2002). A more realistic assumption is ½ of the wavelength. At the top of the salt, the vertical resolution is approximately 8 m to 10 m. These resolution limits are too large to image lateral changes in this natural dissolution feature.

The importance of considering lateral variations within subsidence features can easily be visualized on the 2001 stacked section (Figure 27). North/south cross-sections through the data set, separated by only 10 to 15 m, can be entirely different. For example, a 2D cross-section through CMP 2355 will show faulted units above the salt. A 2-D cross-section through CMP 2365 will show flat lying units and bridging above the salt. For a true time-lapse study of this paleosinkhole, a maximum line offset of 5 m must be acknowledged.

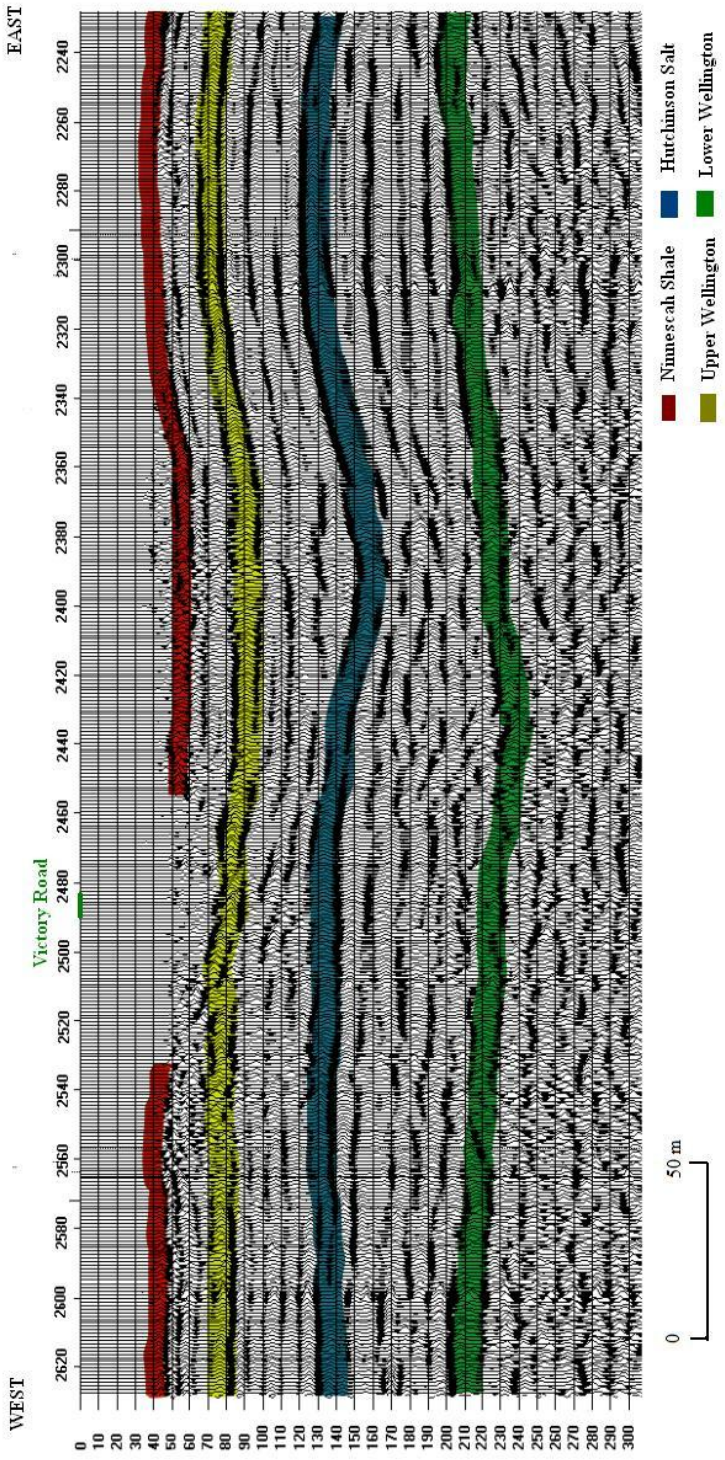

Figure 38. Interpreted 2001 CMP stacked section.

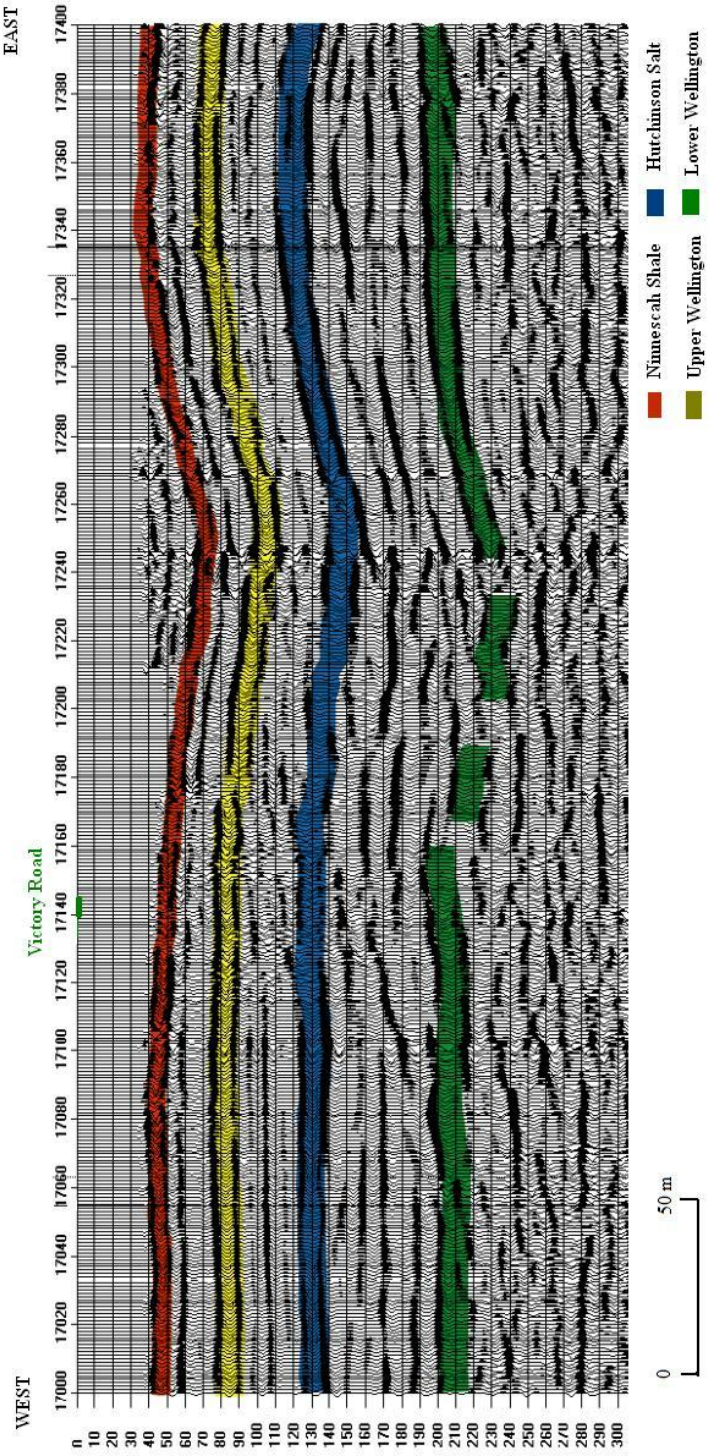

Figure 39. Interpreted 2008 CMP stacked section.

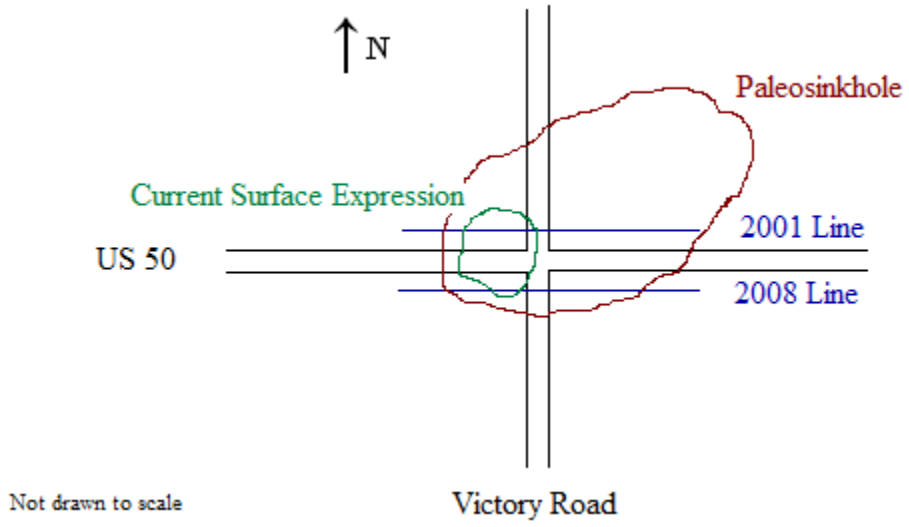

Figure 40. Illustration showing the location of the current surface expression and the interpreted orientation of the paleosinkhole centered northeast of the US 50 and Victory Road intersection. The 2001 seismic line imaged a portion of the center of the paleosinkhole. The 2008 seismic line imaged a portion of the faulted edges of the paleosinkhole.

Correlation / Deconvolution Comparisons

The purpose of any seismic data processing method is to enhance the signal-to-noise ratio and/or resolution. Using accelerometer data deconvolving with an accurate measure of groundforce allows for a more representative reference signal (other than a synthetic signal) to be used for removing the vibroseis source signature during data processing. Comparisons between correlation and deconvolution of the various groundforce calculations, accelerometer data, and the synthetic sweep are part of this research project to evaluate a new sensor system used during acquisition of the US 50 seismic data ranged from very qualitative observation through quantitative wavelet analysis. The objective of the analysis is to extend the resolution of the method further based on the theory that predicts significant gains are possible using an accurately calculated groundforce deconvolution is used to remove the vibroseis wavelet regardless of setting and target.

Cross-correlation with the synthetic sweep (Figure 41) was used as an objective result to compare all the following processing results. Shot gathers with approximately 120 traces and 400 ms of data were selected for analysis (a more extensive set of shot gathers for each processing method are presented in Appendix A). Differences are evident between the cross-correlation of reaction mass accelerometer data (Figures 42 and 43) and baseplate accelerometer data (Figures 43 and 44). Cross-correlation of the raw data with reaction mass accelerometer traces produced shot gathers visually similar to cross-correlation with the synthetic sweep. Low frequency (<50 Hz) events arriving later than the air-coupled wave are more

dominant in the shot gathers produced from cross-correlating with reaction mass accelerometer traces compared to cross-correlating with the baseplate accelerometer traces.

Cross-correlation with the baseplate accelerometer trace results in reflection events with a narrowband (ringing) appearance (Figures 44 and 45). This effect is most noticeable from traces 30 to 55 and 75 ms to 200 ms on both shot gathers. Cross-correlation does not remove the source wavelet; which for vibroseis, will be a zero phase Klauder wavelet with a shape that is dependent on the sweep and how efficiently the entire energy spectra is transmitted to the ground. Large and cyclic side-lobes of the source wavelet give the ringing effect and are the result of narrow bandwidth of recorded data (Ghose, 2002).

Based on visual inspection, there is minimum difference between the data from the Dytran accelerometers and the Endevco accelerometers (Figures 42 - 45). Differences can be observed between using reaction mass accelerometer data and baseplate accelerometer data for cross-correlation. Amplitude spectra were used to quantify these observations. Cross-correlated traces from each type of accelerometer and from both mass and baseplate possess nearly identical spectra (Figures 47 - 50). Frequencies below 100 Hz have higher relative amplitude for traces correlated with the reaction mass accelerometer. At frequencies greater than 100 Hz, traces correlated from the mass and baseplate accelerometers possess similar spectra.

.

.

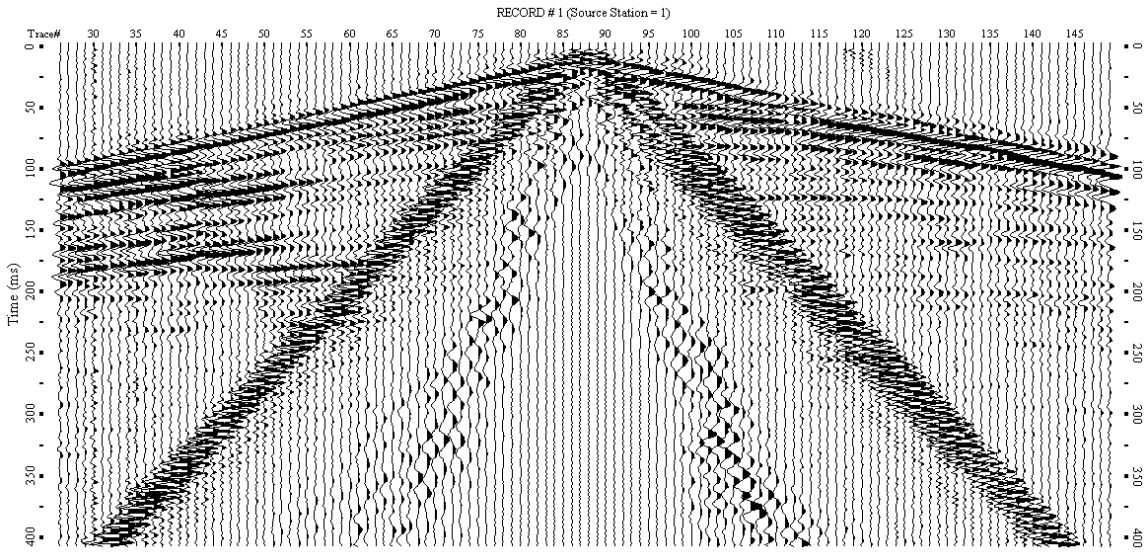

Figure 41. Cross-correlation with the Synthetic Sweep (Shot 3901) representing the standard and baseline for comparisons in this study.

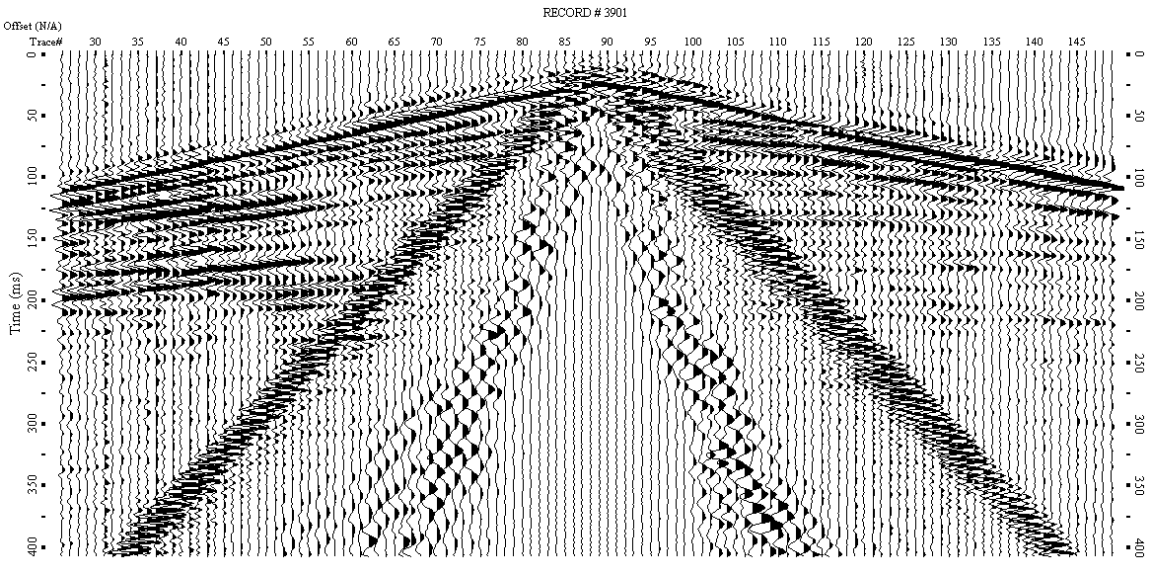

Figure 42. Cross-correlation with the Dytran Accelerometer on the Reaction Mass (Shot 3901).

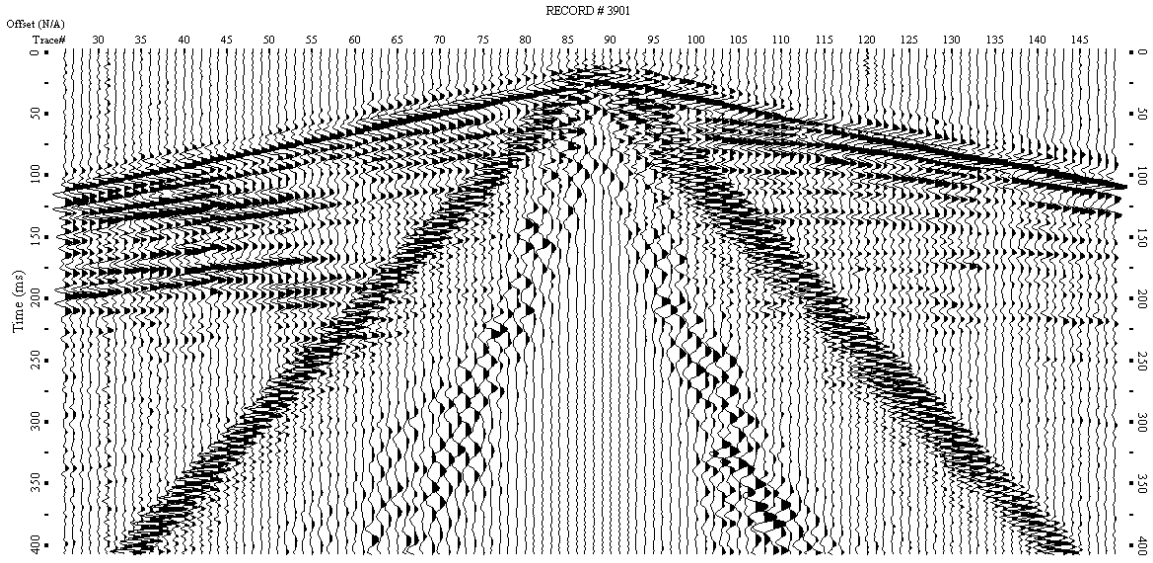

Figure 43. Cross-correlation with the Endevco Accelerometer on the Reaction Mass (Shot 3901).

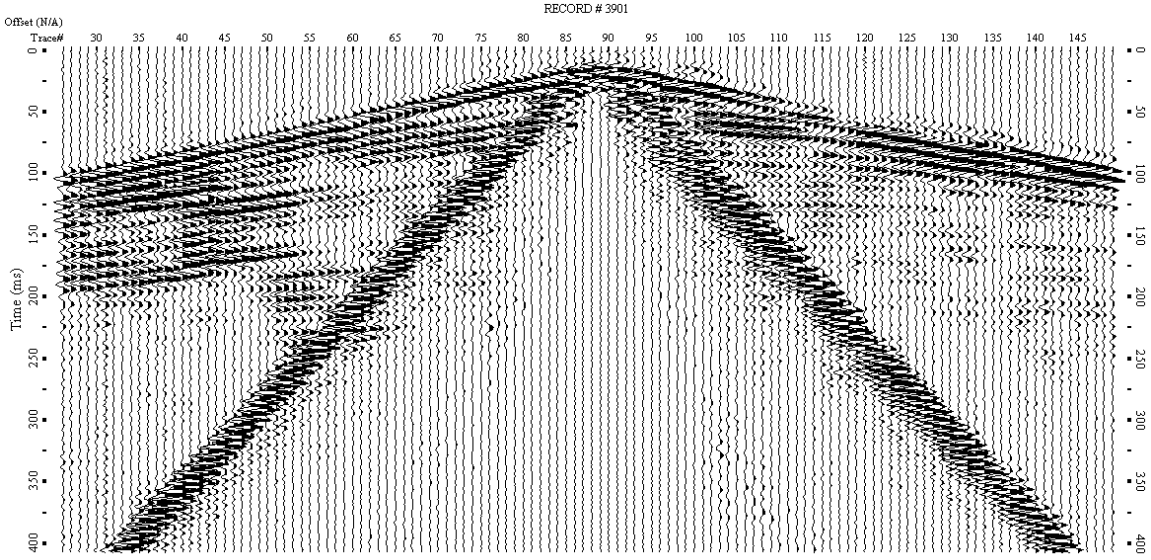

Figure 44. Cross-correlation with the Dytran Accelerometer on the Baseplate (Shot 3901).

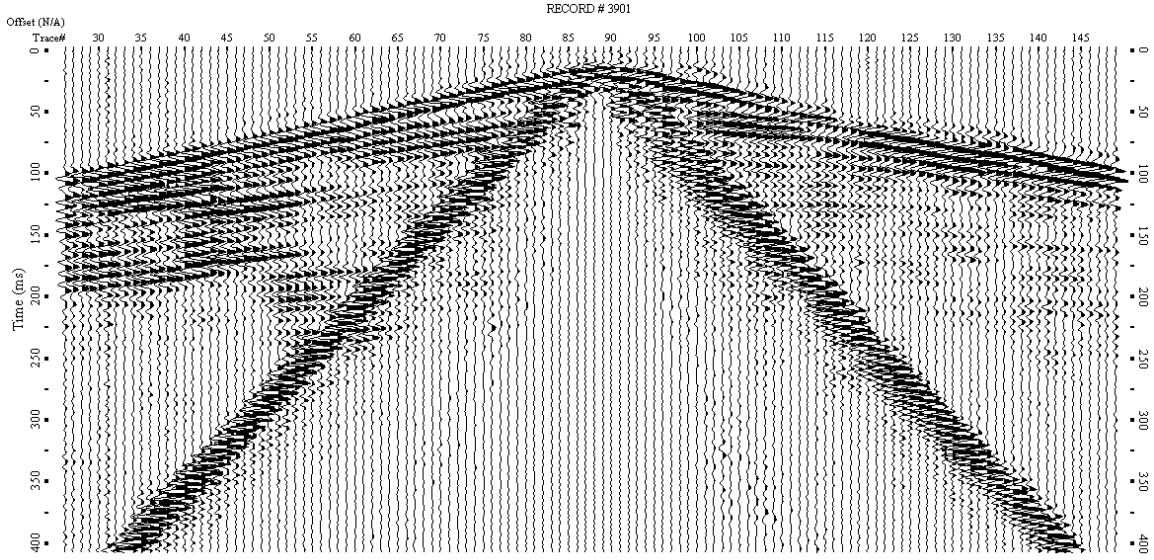

Figure 45. Cross-correlation with the Endevco Accelerometer on the Baseplate (Shot 3901).

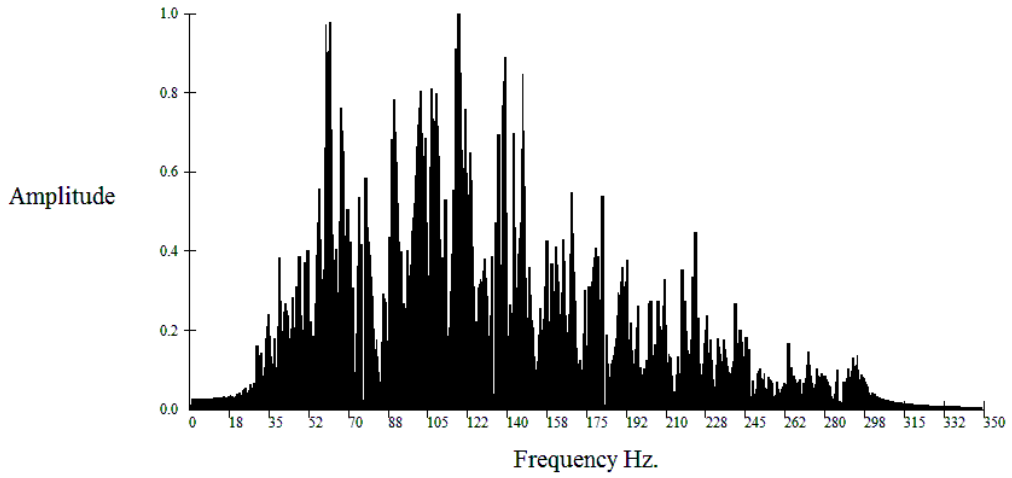

Figure 46. Cross-correlation with the Synthetic Sweep (Shot 3901).

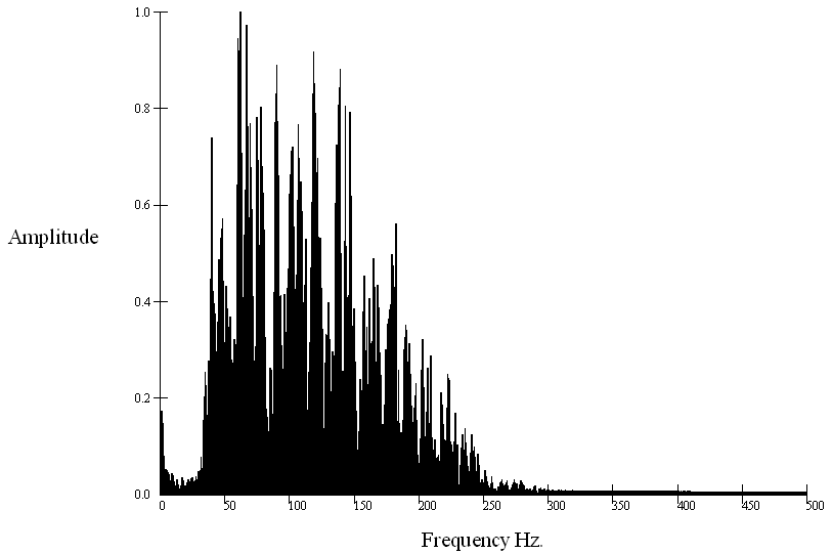

Figure 47. Cross-correlation with the Dytran Accelerometer on the Reaction Mass (Shot 3901).

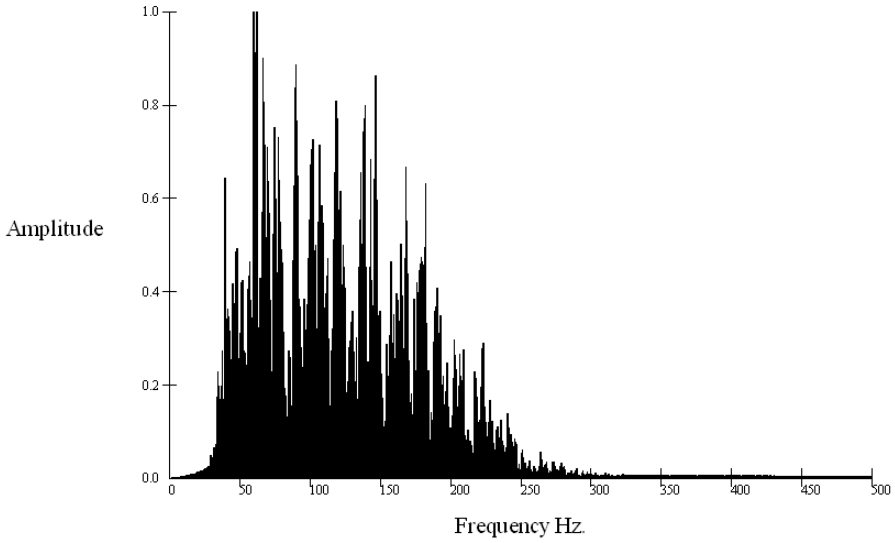

Figure 48. Cross-correlation with the Endevco Accelerometer on the Reaction Mass (Shot 3901).

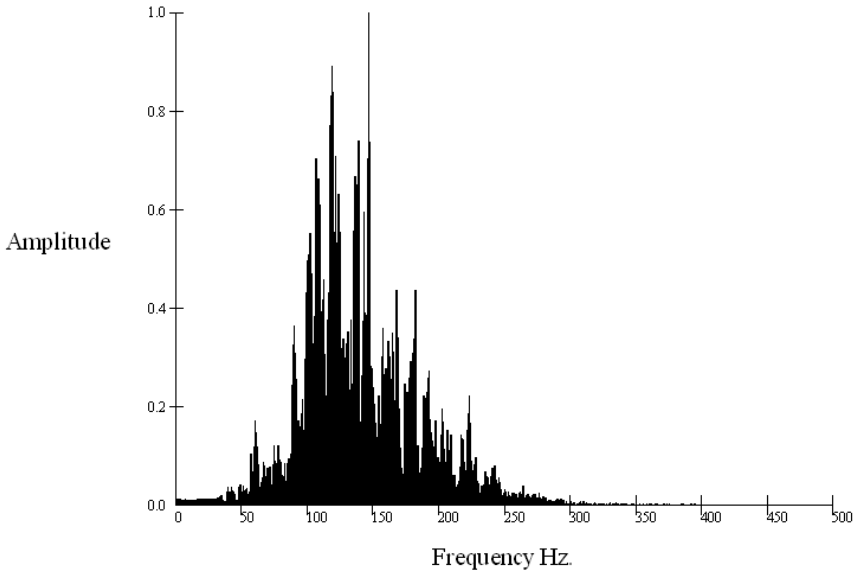

Figure 49. Cross-correlation with the Dytran Accelerometer on the Baseplate (Shot 3901).

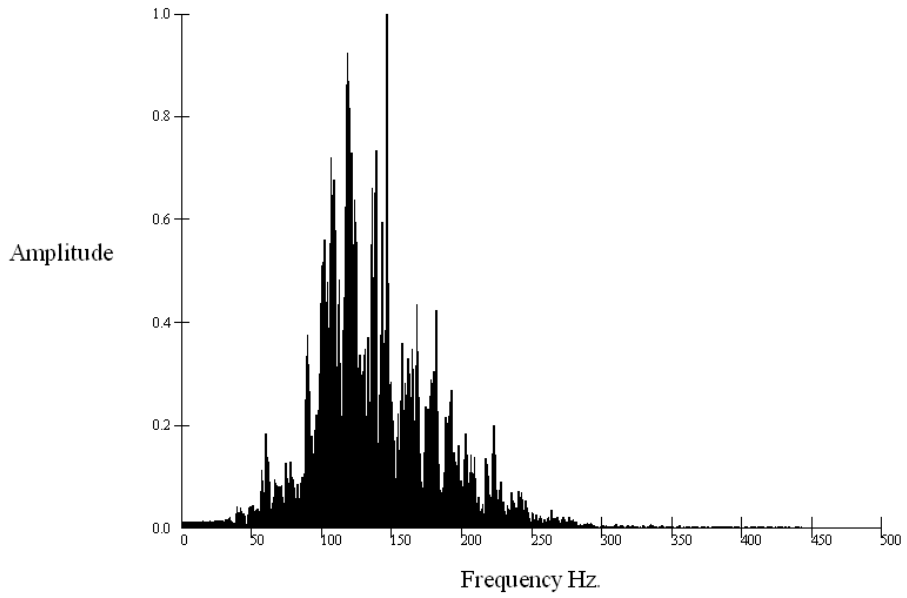

Figure 50. Cross-correlation with the Endevco Accelerometer on the Baseplate (Shot 3901).

There are noticeable differences between the cross-correlation with the two calculated groundforce data sets (Figures 51 and 52). Low frequency ground roll is higher amplitude when the Endevco accelerometers are used as the pilot. Later reflection events (>175 ms) are of higher amplitude when the groundforce calculated using the Endevco accelerometers are used compared to when the Dytran accelerometers are used. Both methods produced relatively narrowband (ringing) reflection events compared to cross-correlation with the synthetic sweep. Correlation with groundforce that contains harmonic energy will result in ghost arrivals, regardless of the accuracy in which the harmonic distortion is preserved in the ground force (van deer Veen et al., 1999). Harmonic distortion will appear as oscillations about the fundamental frequency (Schrodt, 1987). Ghost arrivals can be avoided by using deconvolution with an accurately calculated groundforce (van deer Veen et al, 1999).

Cross-correlation of the raw data with the calculated groundforces show different amplitude spectra (Figures 53 and 54). The spectrum from cross-correlation with the calculated groundforce using the Dytran accelerometers resembles the baseplate spectrum using Dytran accelerometers where frequencies below 100 Hz are low amplitude. The spectrum from cross-correlation using the groundforce calculated from the Endevco accelerometers appears to most closely resemble a combination of the mass and baseplate spectra of each Endevco accelerometer. The spectrum has an increase in amplitudes for the frequencies below 100 Hz with a dominant frequency around 120 Hz. This observation is consistent with the suggestion that the Endevco

accelerometers provide a more accurate measure of true groundforce. True groundforce measurements should be a combination of mass and baseplate movements.

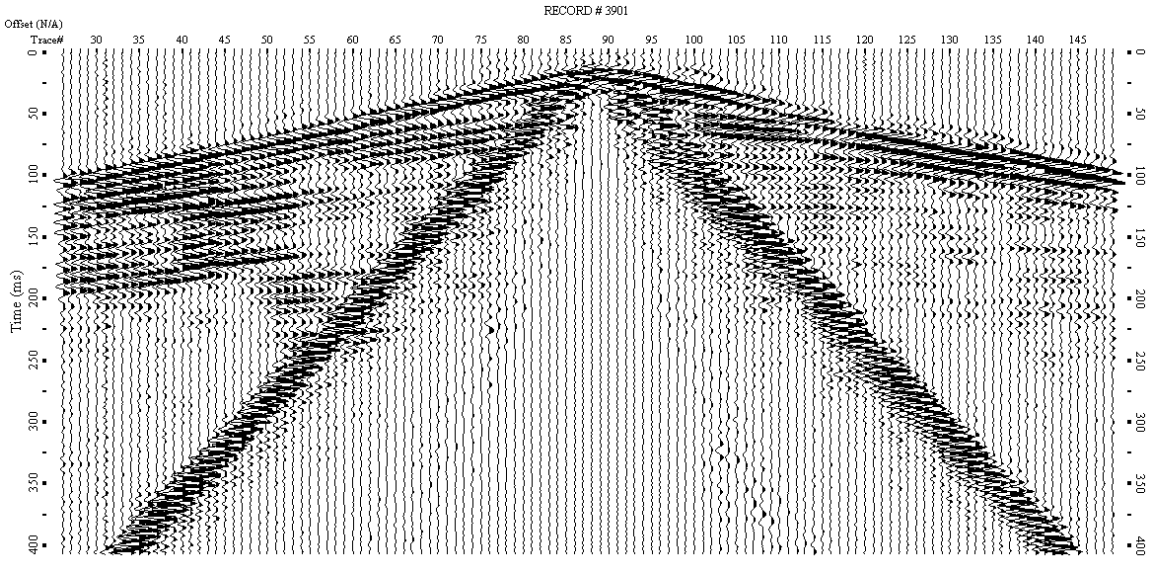

Figure 51. Cross-correlation with the Groundforce calculated from the Dytran Accelerometers (Shot 3901).

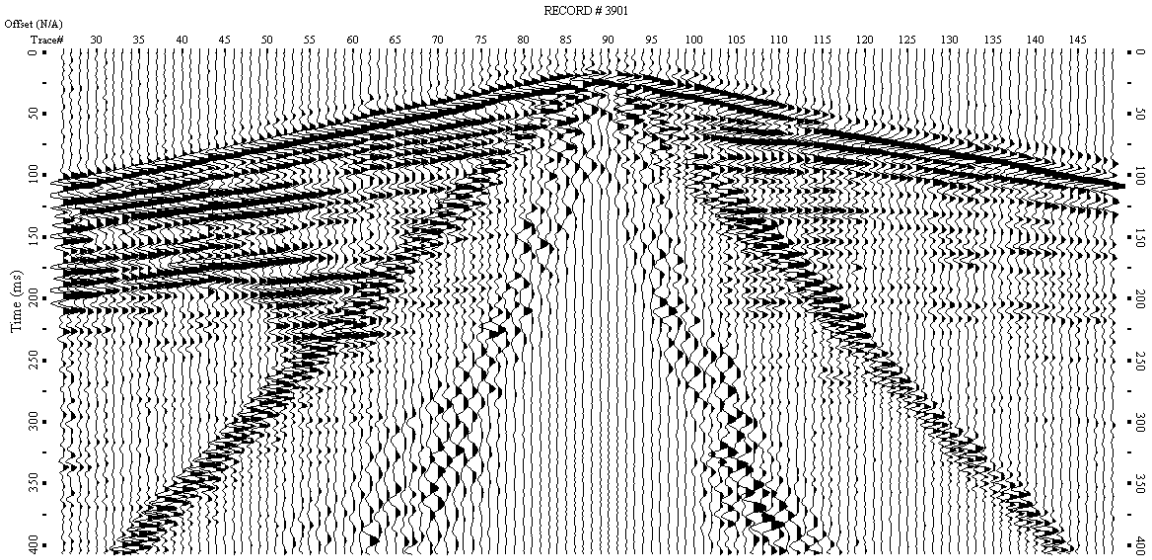

Figure 52. Cross-correlation with the Groundforce calculated from the Endevco Accelerometers (Shot 3901).

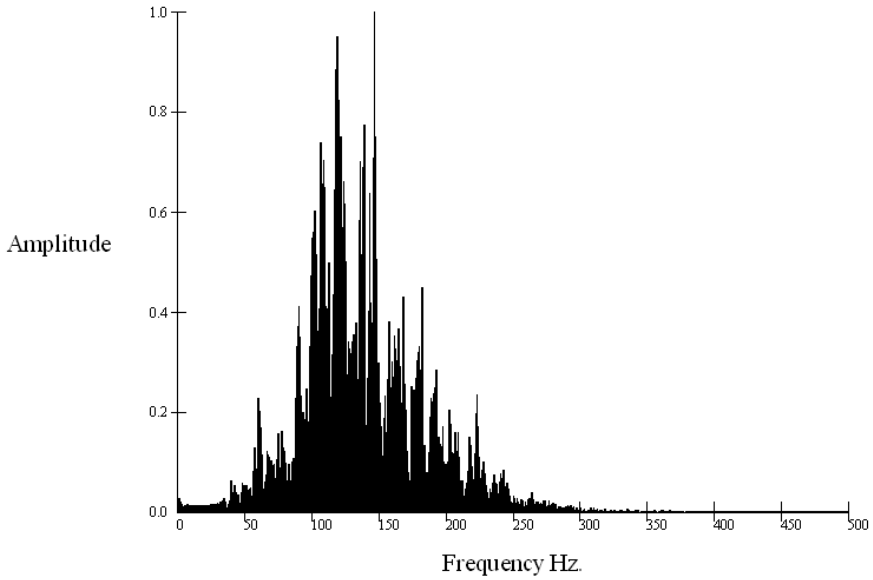

Figure 53. Cross-correlation with the calculated Groundforce using the Dytran Accelerometers (Shot 3901).

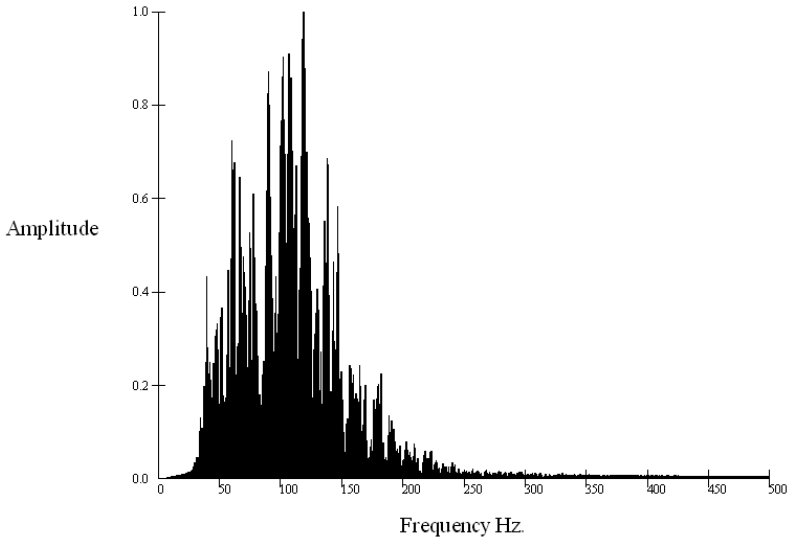

Figure 54. Cross-correlation with the calculated Groundforce using the Endevco Accelerometers (Shot 3901).

By using the synthetic sweep as a reference signal for deconvolution, it produced a shot gather (Figure 55) similar to cross-correlation with the synthetic sweep (Figure 41). Reflections appear to possess similar relative amplitudes and frequencies (80 – 125 Hz). Groundroll is present more in the deconvolution results. Deconvolution will boost all coherent events including groundroll (Bekara, 2008). The shot gather produced from deconvolution with the groundforce pilot of the raw data (Figure 56) shows a record with chatter because of the embedded telemetry noise. However, amplitude spectra for both deconvolution results are almost identical (Figures 57 and 58).

Amplitude spectra comparison of the deconvolution results and the cross-correlation results (Figure 46) reveal differing amplitude peaks. The spectrum resulting from cross-correlation shows dominant peaks from 55 Hz to 145 Hz. The spectra produced from deconvolution shows a narrower band of frequencies, 105 Hz to 145 Hz, with dominant peaks. This shows that deconvolution reduces the amplitude of the lower frequencies (< 70 Hz). Near-surface high-resolution seismic surveys often target frequencies at 80 Hz and above; thus, deconvolution is increasing the signal-to-noise ratio. Key reflections within this data set range from 80 Hz to 130 Hz.

Deconvolution with either accelerometer type produced very similar shot gathers (Figures 59 - 62). Shot gathers generated by deconvolution of baseplate accelerometers with the raw data are contaminated by 35 Hz noise. The source of the

35 Hz noise could be baseplate decoupling or the vibrator's resonant frequency (Schrodt, 1987). After applying a bandpass filter to remove the 35 Hz noise, shot gathers using baseplate accelerometers as the pilot for deconvolution are similar (Figures 63 and 64). No advantages are evident in selecting one type of accelerometer over the other when using either baseplate or reaction mass mounted accelerometers for deconvolution. Deconvolution of the filtered baseplate gathers do provide comparable results to cross-correlation with the synthetic ideal sweep (Figure 41). Resolution (7 m and 6 m respectively) and relative amplitudes of the reflections are comparable between the cross-correlation with the synthetic sweep and deconvolution using the baseplate accelerometer traces.

Spectral analysis of the various combinations of vibrator accelerometers using the deconvolution method provided quantitative results that matched qualitative observations. Spectra for deconvolution of either type of accelerometer are almost identical (Figures 65 - 68). Looking at individual accelerometer data, deconvolution with the reaction mass accelerometers (Figures 65 and 66) resulted in amplitude spectra that most closely match that seen from cross-correlating raw data with the synthetic sweep. This creates the theory that poor baseplate measurements are inhibiting accurate groundforce calculations. The low frequency event (~35 Hz) evident on shot gathers from the baseplate deconvolution (Figures 67 and 68) dominates the spectra. Frequencies above 40 Hz are very low amplitude.

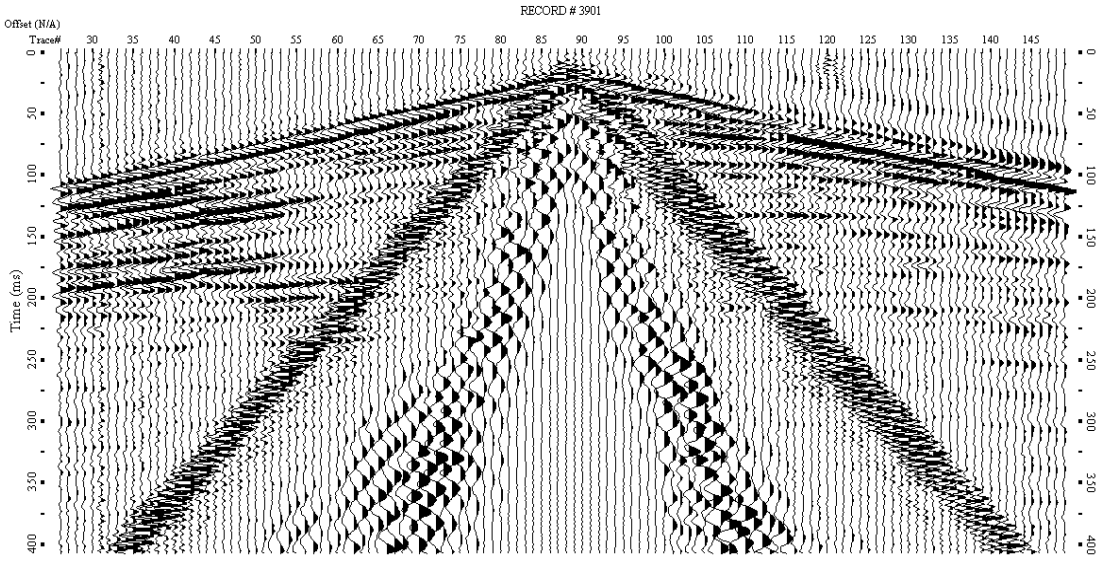

Figure 55. Deconvolution with the Synthetic Sweep (Shot 3901).

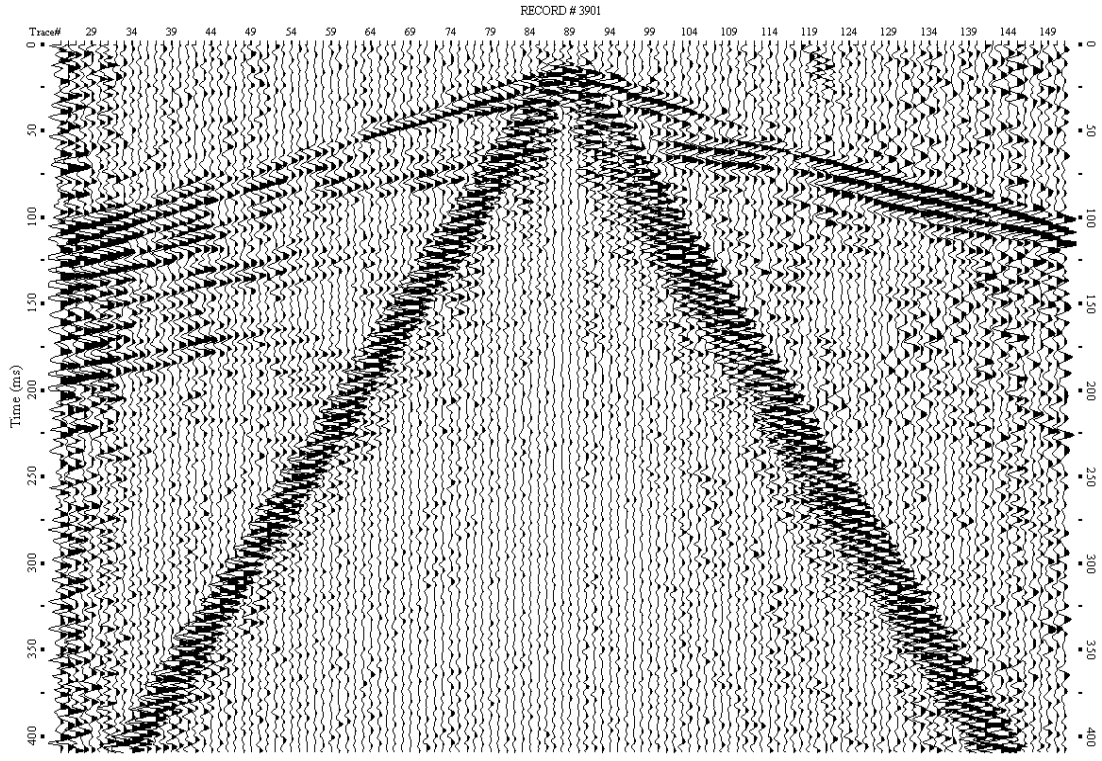

Figure 56. Deconvolution with the groundforce pilot of the uncorrelated data (Shot 3901).

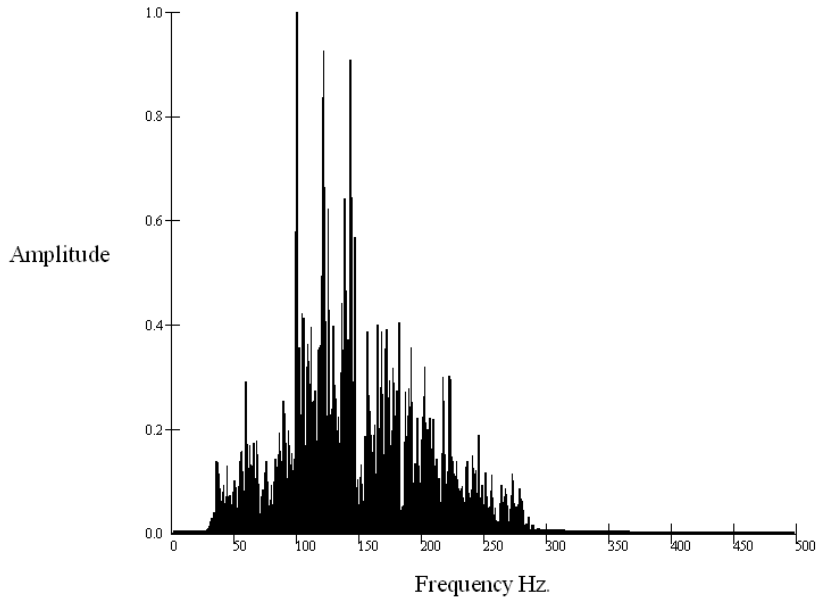

Figure 57. Deconvolution with the Synthetic Sweep (Shot 3901).

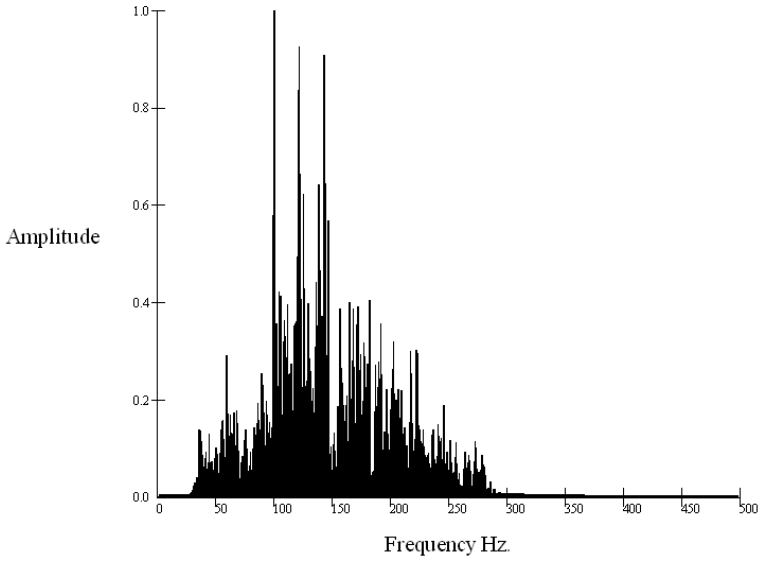

Figure 58. Deconvolution with the groundforce pilot of the uncorrelated data (Shot 3901).

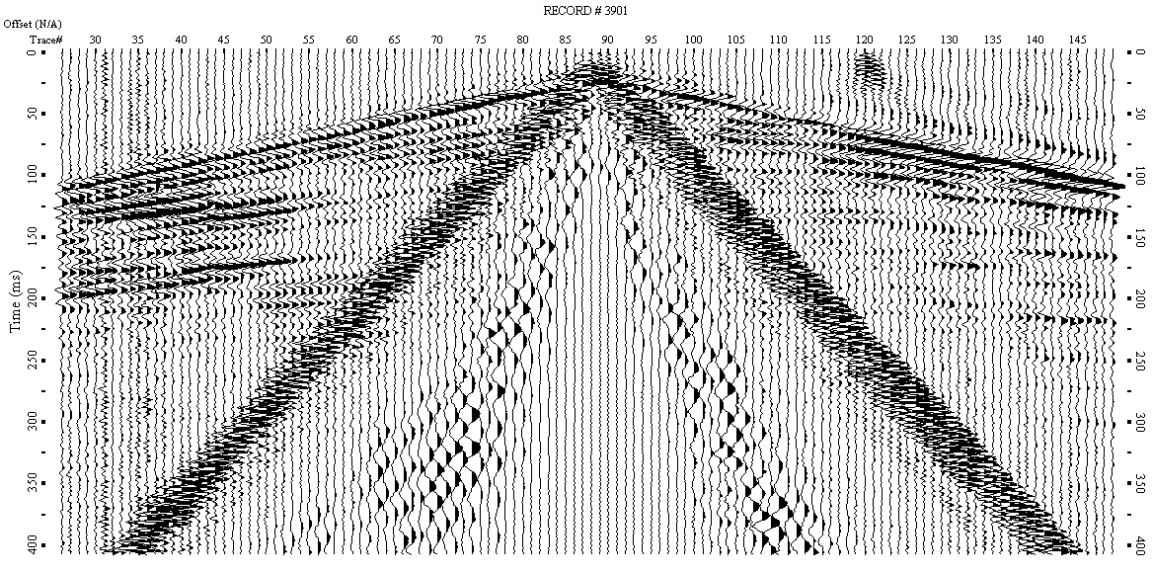

Figure 59. Deconvolution with the Dytran Accelerometer on the Reaction Mass (Shot 3901).

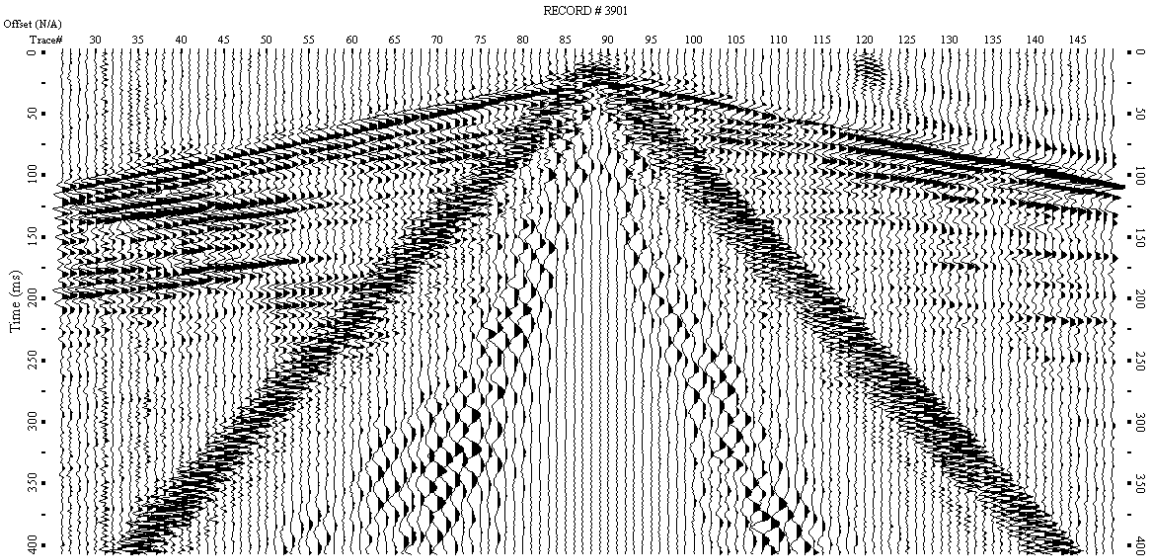

Figure 60. Deconvolution with the Endevco Accelerometer on the Reaction Mass (Shot 3901).

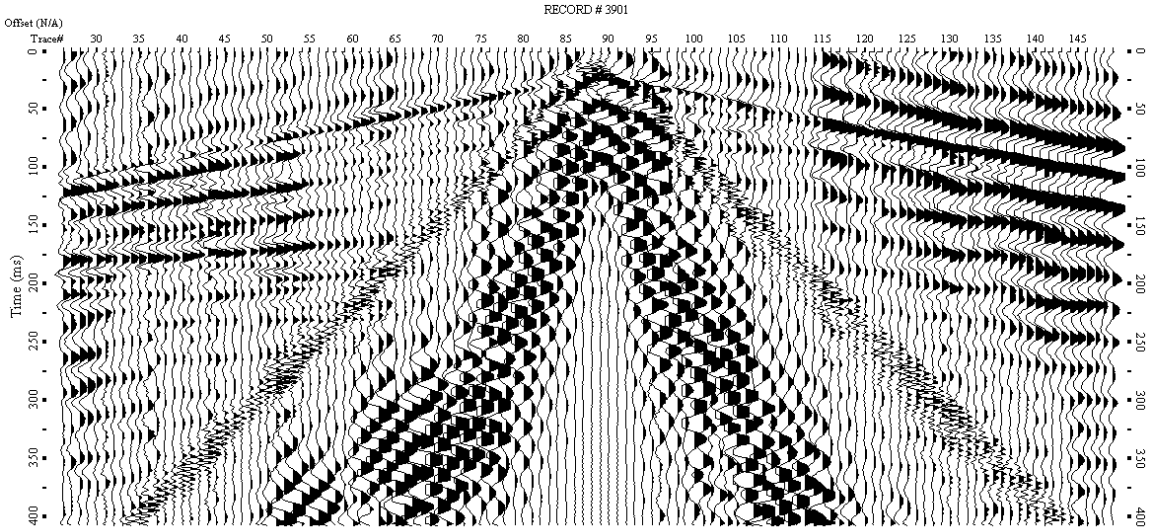

Figure 61. Deconvolution with the Dytran Accelerometer on the Baseplate (Shot 3901).

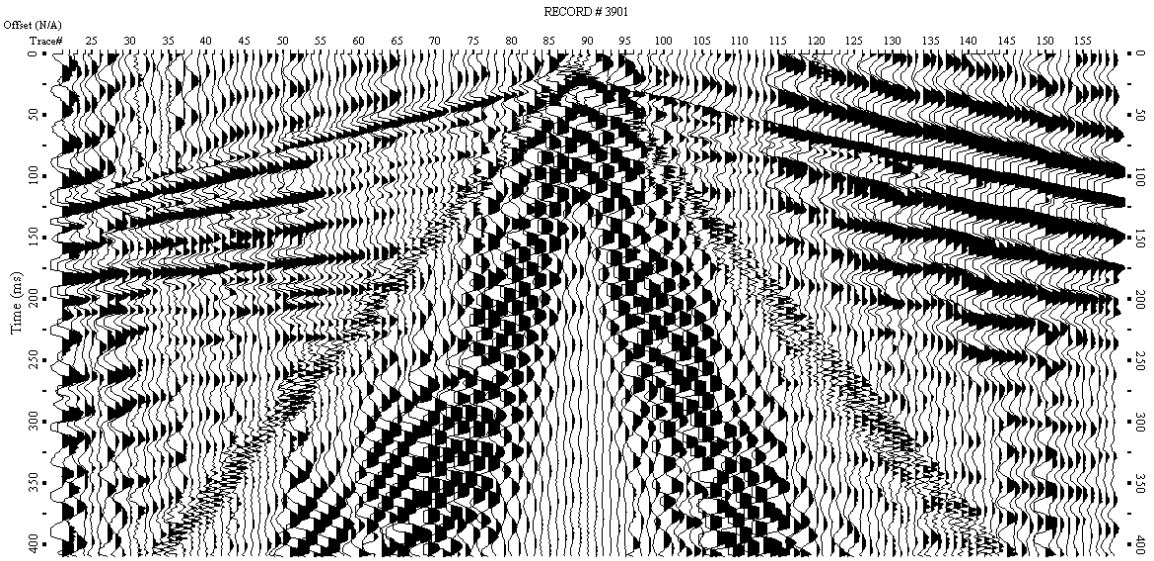

Figure 62. Deconvolution with the Endevco Accelerometer on the Baseplate (Shot 3901).

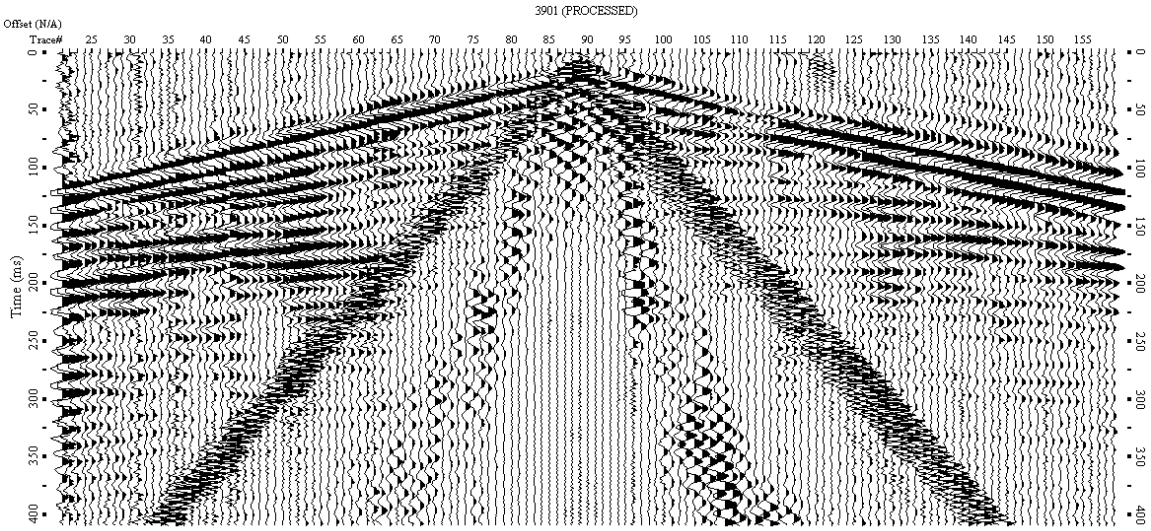

Figure 63. Deconvolution with the Dytran Accelerometer on the Baseplate (Shot 3901), filtered.

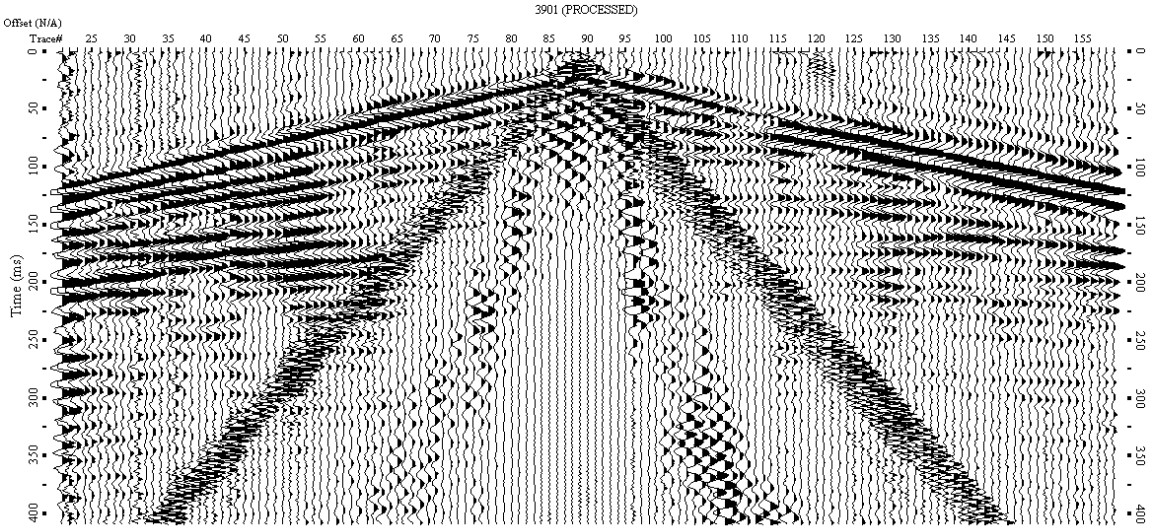

Figure 64. Deconvolution with the Endevco Accelerometer on the Baseplate (Shot 3901), filtered.

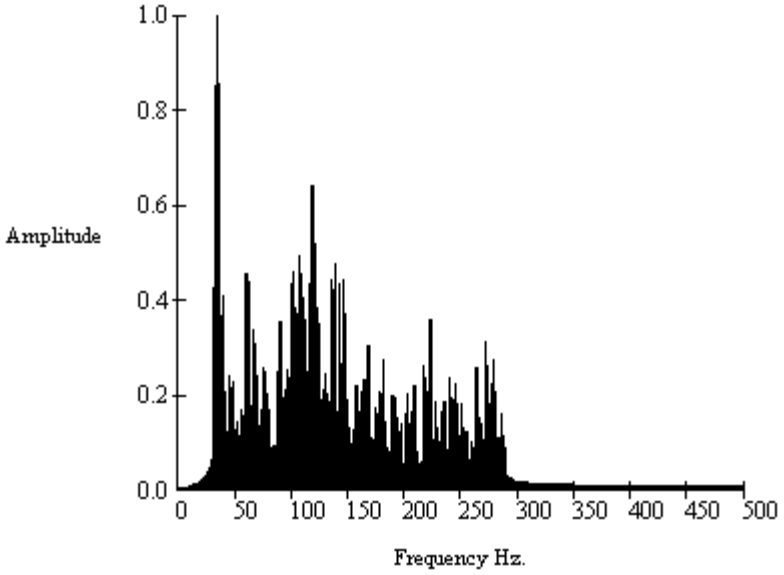

Figure 65. Deconvolution with the Dytran Accelerometer on the Reaction Mass (Shot 3901).

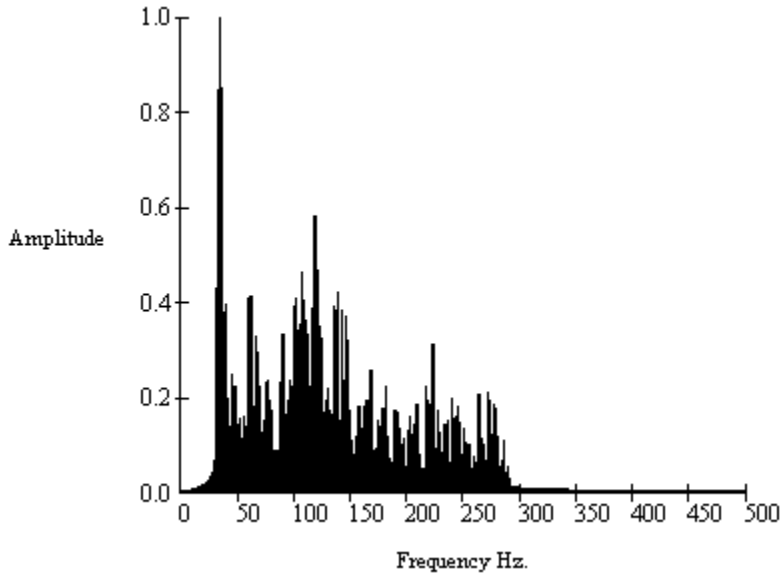

Figure 66. Deconvolution with the Endevco Accelerometer on the Reaction Mass (Shot 3901).

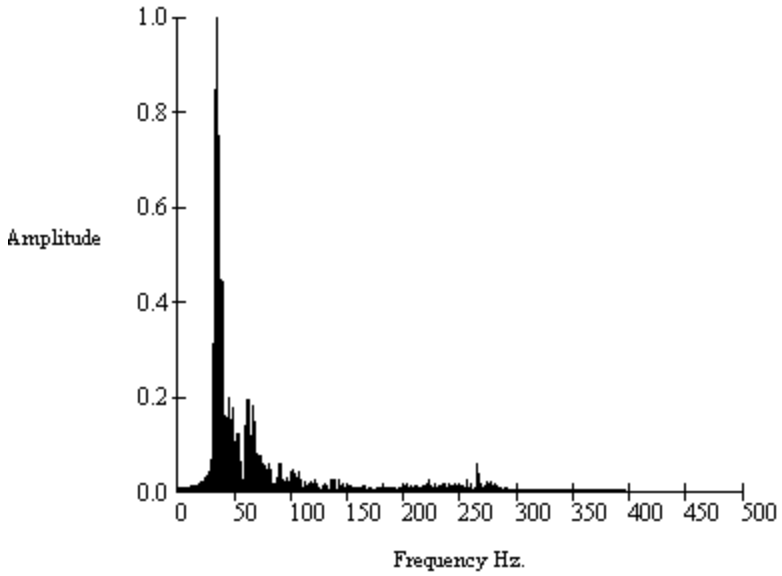

Figure 67. Deconvolution with the Dytran Accelerometer on the Baseplate (Shot 3901).

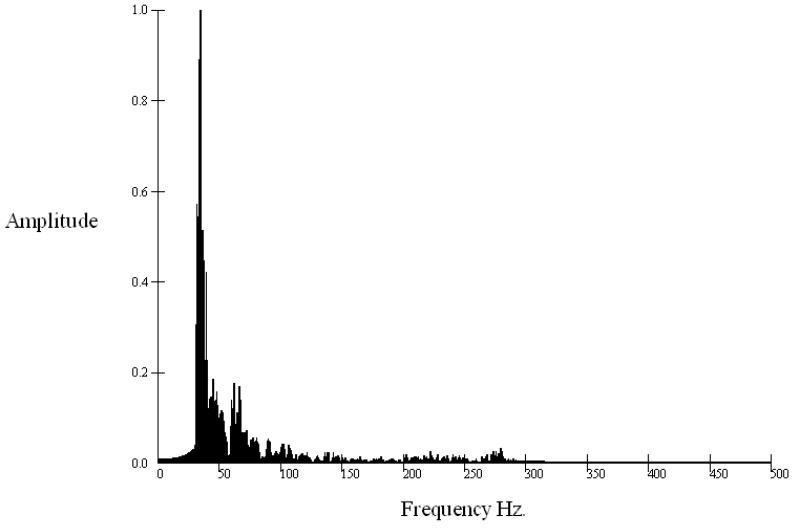

Figure 68. Deconvolution with the Endevco Accelerometer on the Baseplate (Shot 3901).

Deconvolution using the calculated groundforces produced contrasting gathers. What is being recorded by the Endevco accelerometers is different than what is being transmitted by the Dytran accelerometers. The same low frequency noise evident on shot gathers from baseplate only deconvolution (Figures 61 and 62) is obvious when groundforce calculated from the Dytran accelerometers is used for deconvolution (Figure 69). Deconvolution using the groundforce calculated from the Endevco accelerometers produced both low (35 Hz) and high (270 Hz) frequency noise on shot gathers (Figure 70).

The similarities between deconvolution using the Dytran baseplate accelerometer data (Figure 61) and deconvolution using the groundforce calculated from the Dytran accelerometers (Figure 69) indicates that groundforce calculated using the Dytran accelerometers poorly represents the signal going into the ground. By using only the baseplate Dytran accelerometer, it produces the same results as the ground force calculated from mass and baseplate Dytran accelerometers. Deconvolution using individual mass and baseplate accelerometers using the Dytran and Endevco models resulted in near identical shot gathers. Deconvolution using the groundforces produced contrasting gathers; therefore, the process of calculating the two groundforces is prone to errors. Deconvolution using the two groundforces should produce the same amplitude spectra since the individual mass and baseplate spectra are almost identical.

Groundforce deconvolution results were filtered using bandpass filters to remove noise (Figures 71 and 72). Deconvolution with the groundforce calculated

using the Endevco accelerometers (Figure 72) is extremely comparable to the cross-correlation with the synthetic sweep. Groundforce calculated using mass and baseplate Endevco accelerometers produced results of higher resolution (vertical resolution of approximately 7 m in the upper 200 ms) from all previous deconvolution methods (vertical resolutions ranging from 8 m to 12 m in the upper 200 ms); giving rise to the idea that the Endevco accelerometers provide a more accurate calculation of true groundforce. Increased resolution can be seen on the shot gather from deconvolution with the calculated groundforce from the Endevco accelerometers (Figure 72) on traces 24 to 38 at 180 ms where two reflections can be identified (vertical resolution of 7 m). On the shot gather from deconvolution with the calculated groundforce from the Dytran accelerometer (Figure 71), there appears to be only one reflection at 180 ms from traces 24 to 38 (vertical resolution of 12 m). The same observation can be made from traces 100 to 112 at 75 ms.

Deconvolution with the accurately calculated groundforce will produce results that most accurately represent an ideal impulsive seismogram (Yilmaz, 2001). Cross-correlation with the synthetic sweep results in data with the most appealing reflection characteristic (high frequency with high resolution) for most near-surface seismic surveys. Frequency spectra (Figures 73 and 74) from groundforce deconvolution data display low frequencies (<40 Hz) with high amplitudes evident on shot gathers. Higher frequency (>200 Hz) amplitude peaks (Figure 74) match peaks seen in Figure 71, only of higher amplitudes. A narrower bandpass filter was applied to the Endevco groundforce to remove the higher frequencies. The spectra after filtering (Figures 75

and 76) possess more balanced amplitudes when the Endevco accelerometers are used to calculate groundforce for deconvolution compared to the use of the Dytran accelerometers.

Although the resulting frequency range is smaller compared to the filtered Dytran groundforce frequency range, the reflection frequencies (100 – 130 Hz) of interest are of higher amplitudes. Amplitudes of the lower frequency (< 40 Hz) energy are not as dominating as they are in the spectrum from the unfiltered gather (Figure 74). The idea of any processing method is to maximize reflection amplitudes and frequency while minimizing noise. Comparing the spectrum of the cross-correlation with the synthetic sweep (Figure 46) to the spectrum of using the calculated groundforce from the Endevco accelerometers for deconvolution (Figure 76) shows the similarities between the two spectra between 50 Hz and 200 Hz. Frequencies above 150 Hz in Figure 76 are of higher amplitudes (by as much as 50% at 175 Hz). The two spectra are comparable enough to suggest that using the Endevco accelerometers to calculate groundforce and perform deconvolution yields similar results to cross-correlation with the synthetic sweep.

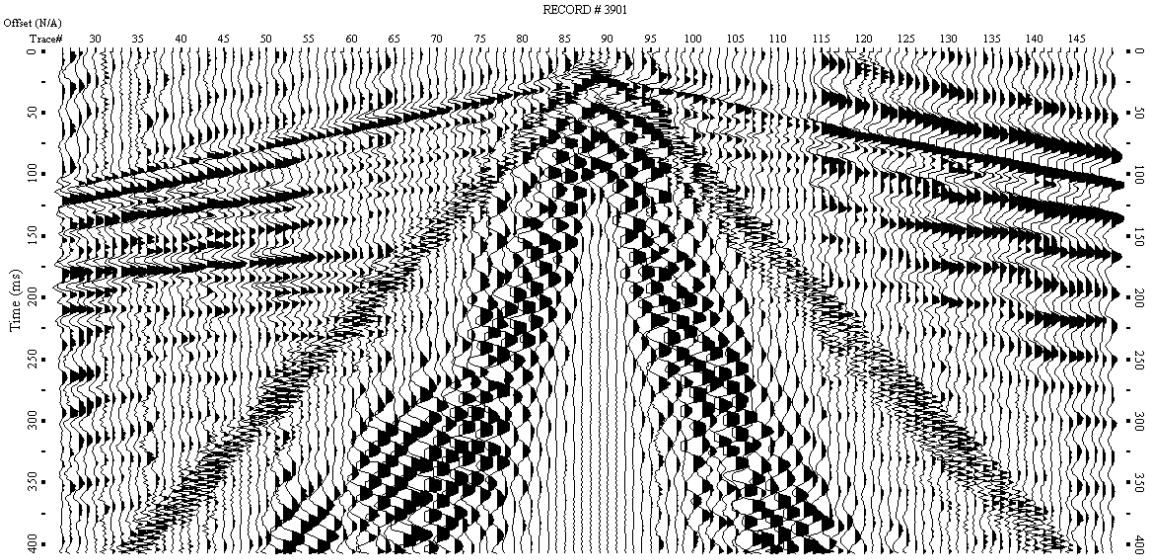

Figure 69. Deconvolution with the Groundforce calculated from the Dytran Accelerometers (Shot 3901), unfiltered.

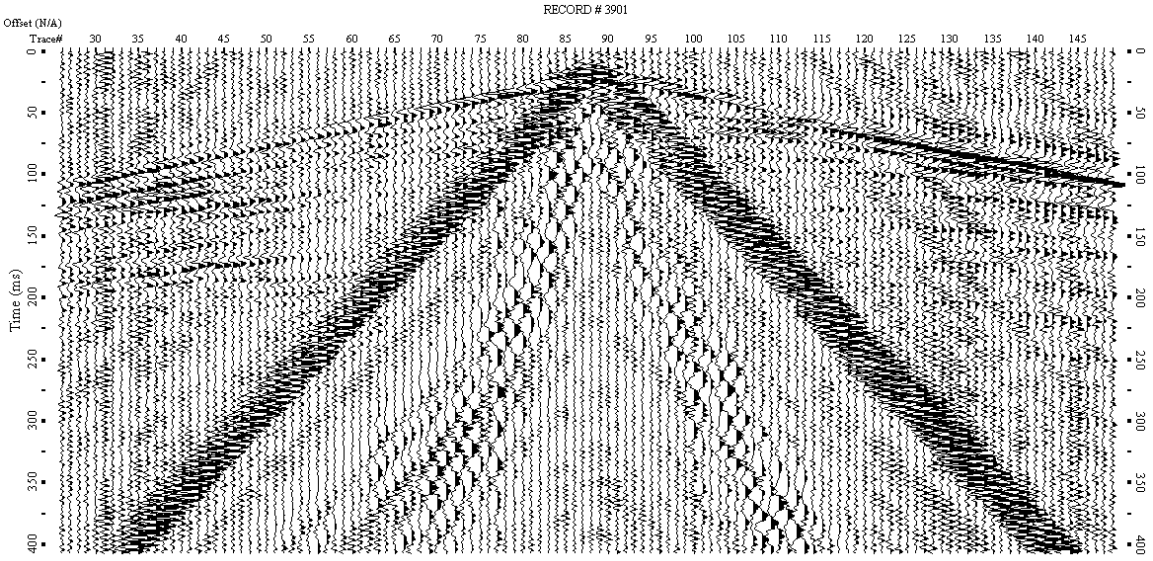

Figure 70. Deconvolution with the Groundforce calculated from the Endevco Accelerometers (Shot 3901), unfiltered.

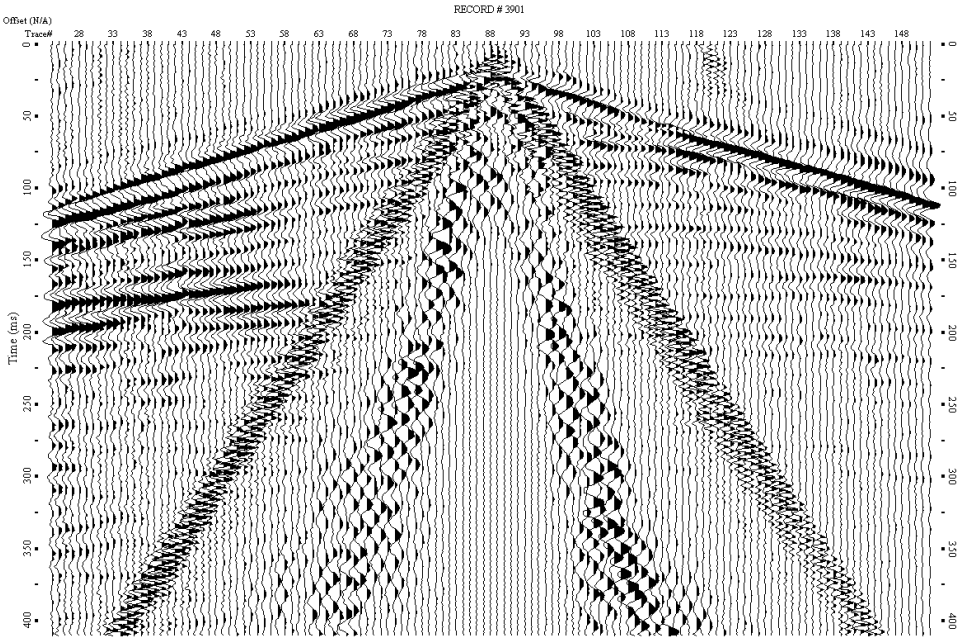

Figure 71. Deconvolution with the Groundforce calculated from the Dytran Accelerometers (Shot 3901), filtered using a bandpass filter (40-50 Hz, 290-300Hz).

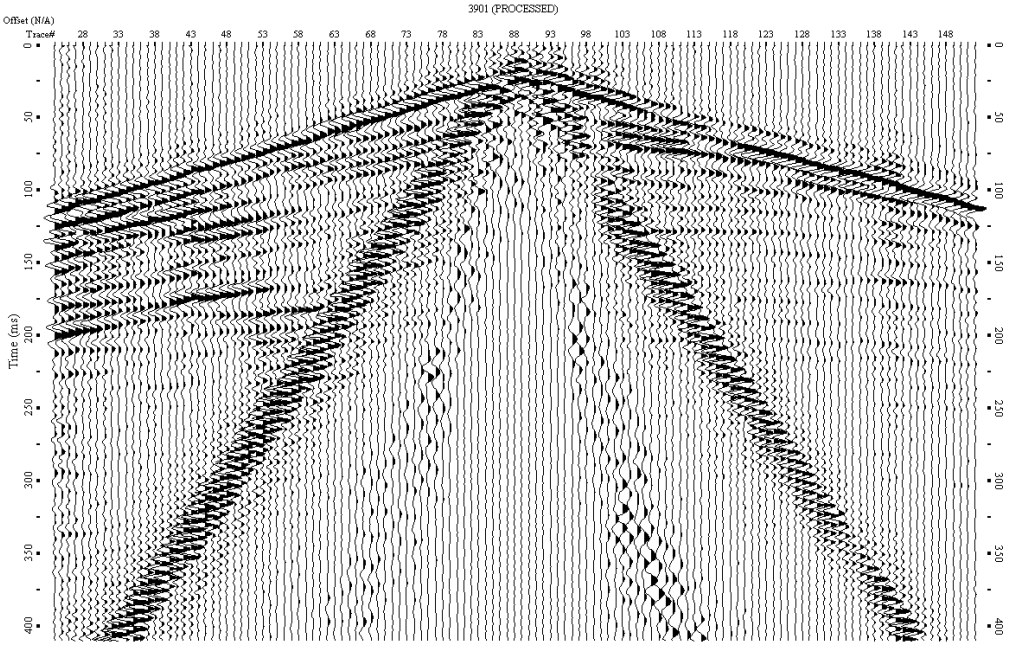

Figure 72. Deconvolution with the Groundforce calculated from the Endevco Accelerometers (Shot 3901), filtered using a bandpass filter (40-50 Hz, 170-180 Hz).

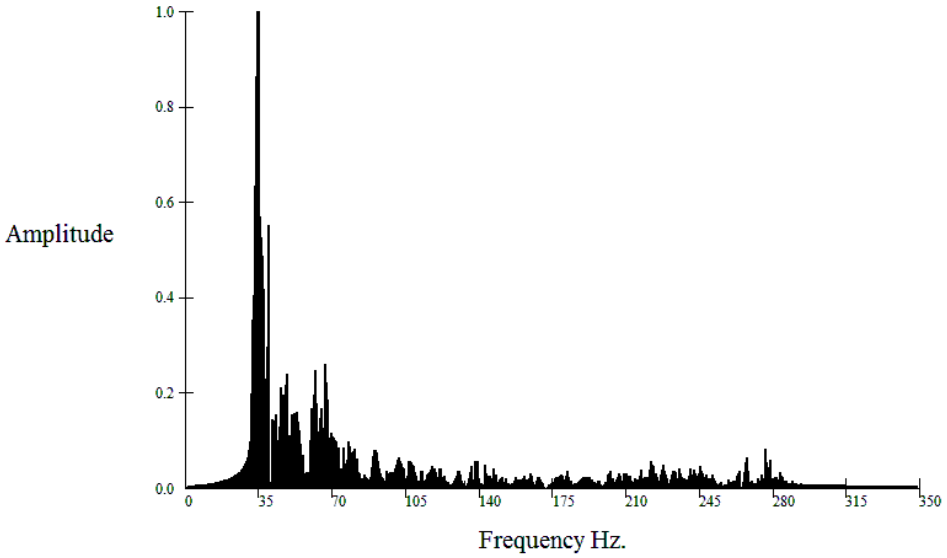

Figure 73. Deconvolution with the calculated Groundforce from the Dytran Accelerometers (Shot 3901), unfiltered.

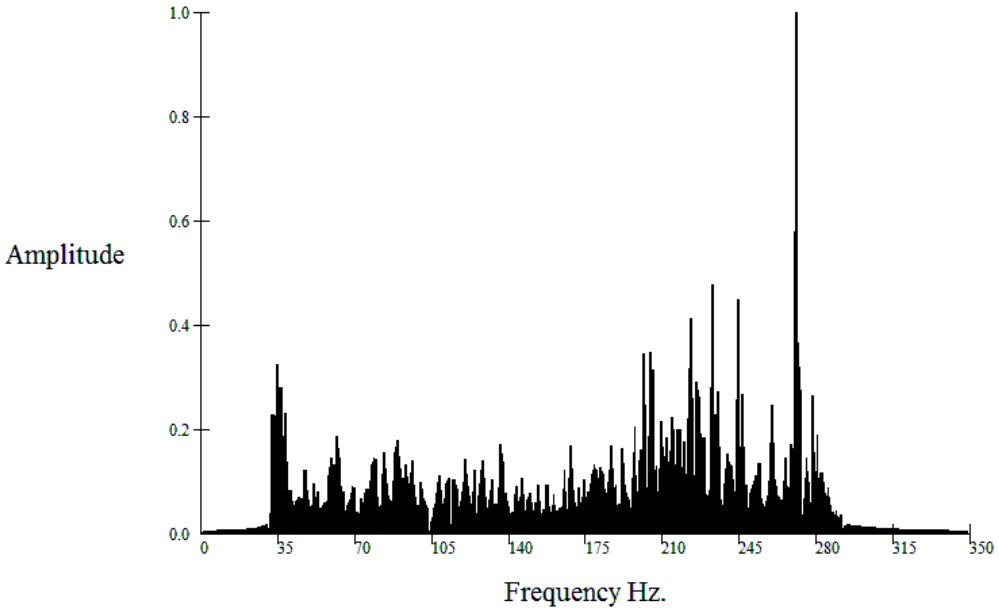

Figure 74. Deconvolution with the calculated Groundforce From the Endevco Accelerometers (Shot 3901), unfiltered.

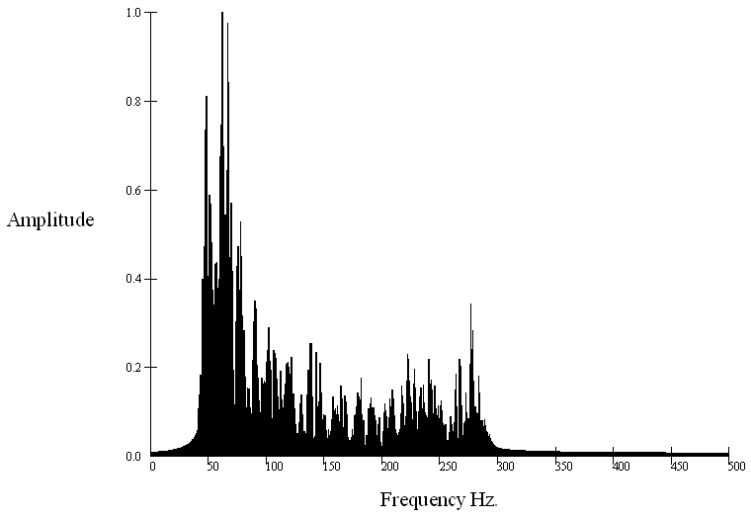

Figure 75. Deconvolution with the calculated Groundforce from the Dytran Accelerometers (Shot 3901), filtered.

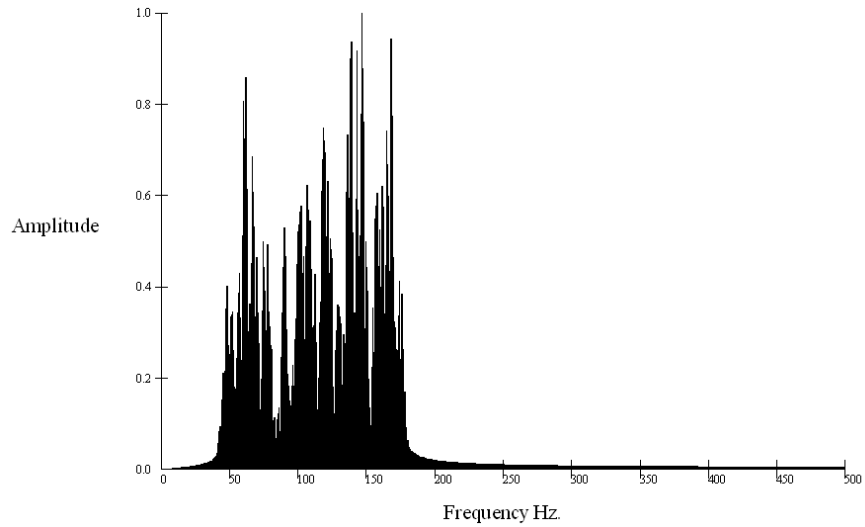

Figure 76. Deconvolution with the calculated Groundforce from the Endevco Accelerometers (Shot 3901), filtered.

Through qualitative analysis of resolution, dominant frequencies, noise, and amplitude analysis, deconvolution with the calculated groundforces provided the most comparable results to cross-correlation with the synthetic ideal sweep. A time window was chosen (~80-200 ms) on ten traces to compare reflection events on all three shot gathers. Amplitude spectra were used to compare these time sections (Figures 77 - 79).

Each of the gathers show differences in reflection wavelet shapes. One of the most noticeable differences in reflection wavelet shape is the high amplitude coherent event (70 Hz, vertical resolution of approximately 12 m) at 155 ms at trace 50 and 162 ms at trace 40 across all ten traces in the shot gather produced from deconvolution using the groundforce calculated from the Dytran accelerometers (Figure 78 (a)). This 160 ms event is less coherent in the other two shot gathers (Figures 77 (a) and 79 (a)). The coherent event on traces 48-50 at 160 ms (100 Hz, vertical resolution of approximately 8 m) begins to diverge between traces 40-47 in Figure 77 (a). In Figure 79 (a), there is separation in this event (100 Hz and 125 Hz, vertical resolution of 8 m and 7 m) throughout all ten traces, producing higher resolution of reflection events. There is more separation between the reflections seen in the Endevco accelerometer gather when compared to the Dytran accelerometer gather; evidence of increased resolution.

The amplitude spectra of deconvolution with both calculated groundforces and cross-correlation with the synthetic sweep show similarities and differences. Shot gathers from cross-correlation with the synthetic sweep possess high amplitude

spikes at 85, 100, and 120 Hz (Figure 77 (b)). Shot gathers from deconvolution with the groundforce calculated from the Dytran accelerometers possess a single dominant spike at 85 Hz (Figure 78 (b)). Shot gathers from deconvolution with the groundforce calculated from the Endevco accelerometers include spikes at 85, 100, 120, 150, and 170 Hz (Figure 79 (b)). Cross-correlation and deconvolution with the Endevco groundforce produce similar results, with the later having peaks at higher frequencies (>120 Hz). True amplitude analysis was used to compare cross-correlation with the synthetic sweep (Figure 80) and deconvolution with the calculated groundforce using the Endevco accelerometers (Figure 81). Amplitudes above 140 Hz are higher (up to double at 165 Hz) when the calculated groundforce using the Endevco accelerometers are used compared to cross-correlation with the synthetic sweep.

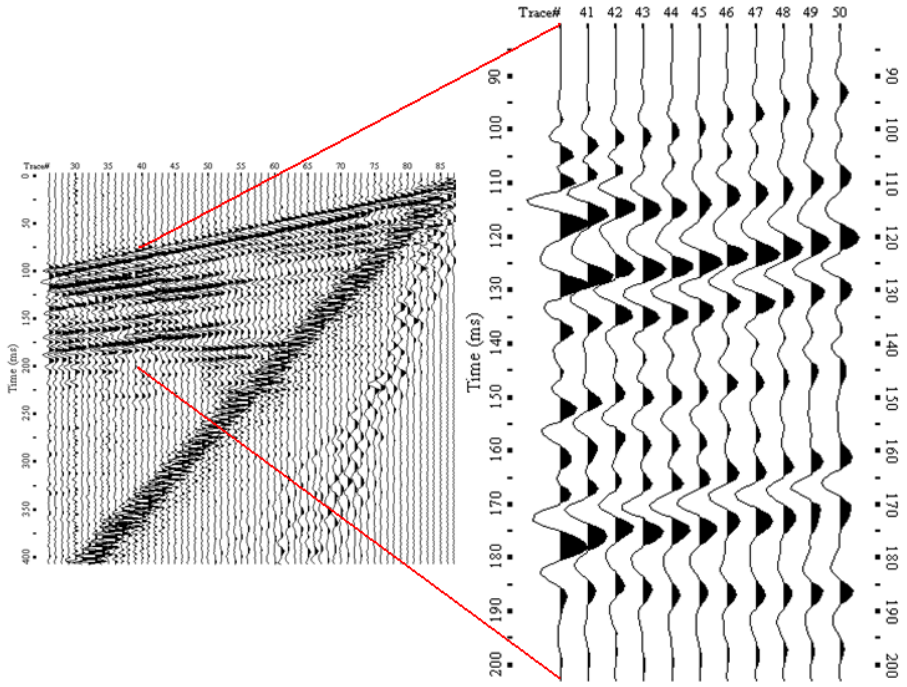

(A) Time section analyzed from the cross-correlation with the Synthetic Sweep (Shot 3901)

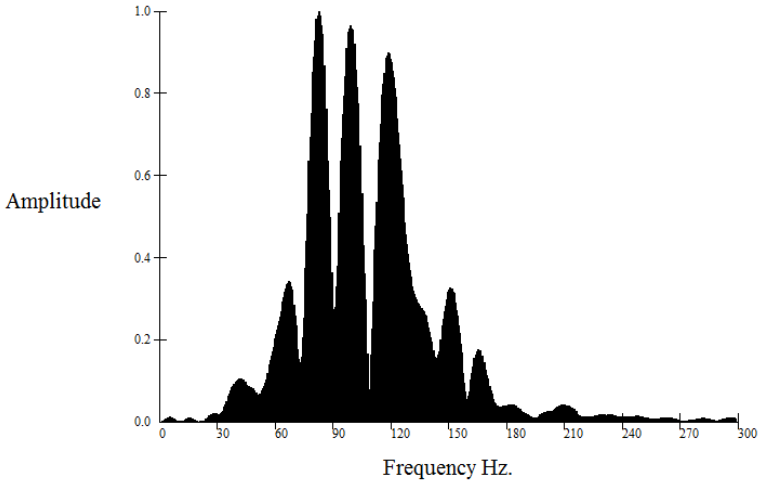

(B) Frequency vs Amplitude Spectra of the above time section

Figure 77. Cross-correlation with the synthetic sweep, Traces 40-50, ~80-200 ms.

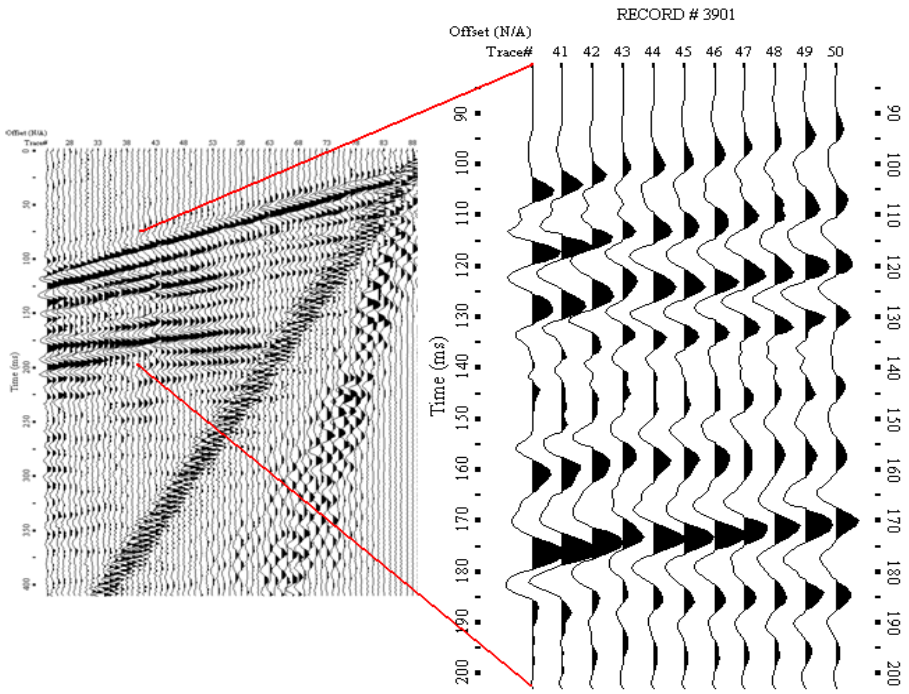

(A) Time section analyzed from the Deconvolution with the calculated Groundforce using the Dytran accelerometers (Shot 3901), filtered

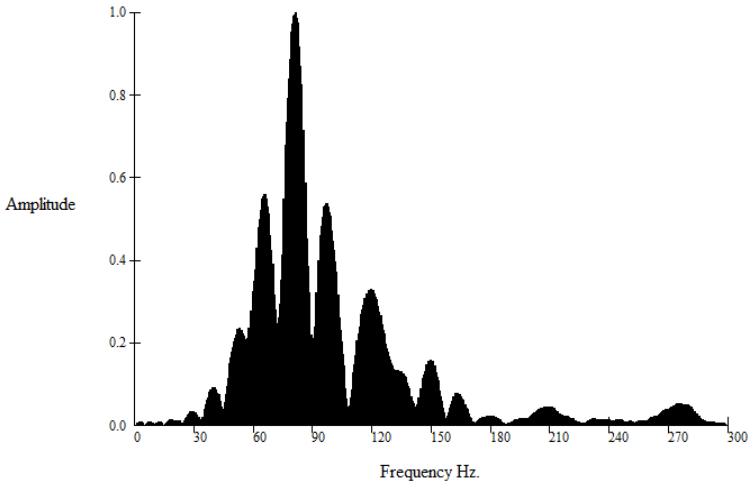

(B) Frequency vs Amplitude spectra of the above time section

Figure 78. Deconvolution with the calculated Groundforce using the Dytran accelerometers, Traces 40-50, ~80-200 ms.

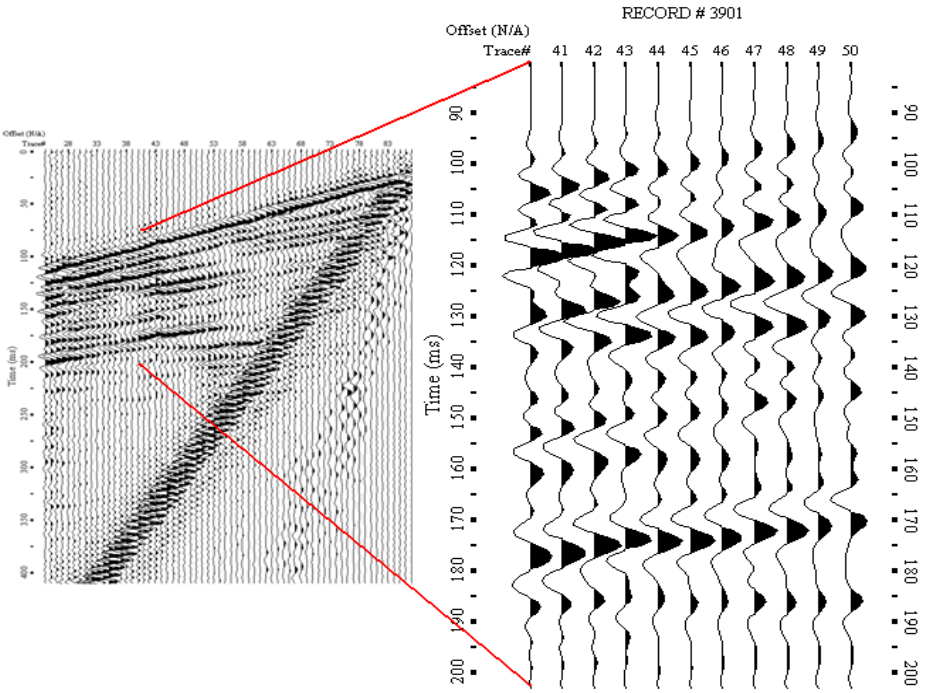

(A) Time section analyzed from the Deconvolution with the calculated Groundforce using the Endevco accelerometers (Shot 3901), filtered

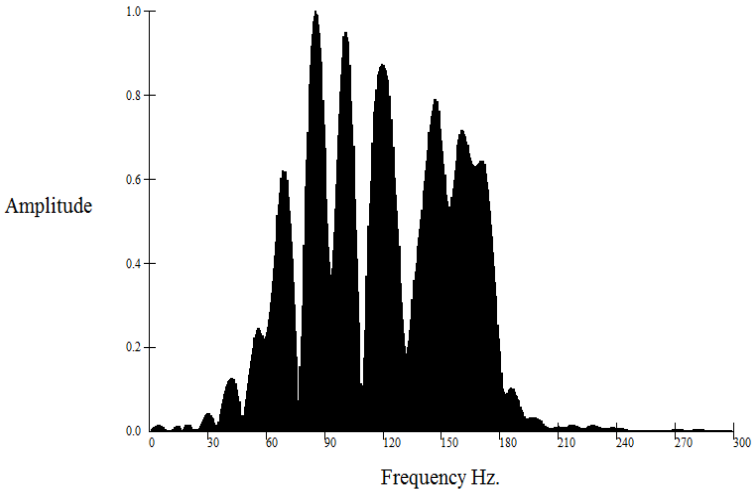

(B) Frequency vs. Amplitude spectra of the above time section

Figure 79. Deconvolution with the calculated Groundforce using the Endevco accelerometers, Traces 40-50, ~80-200ms.

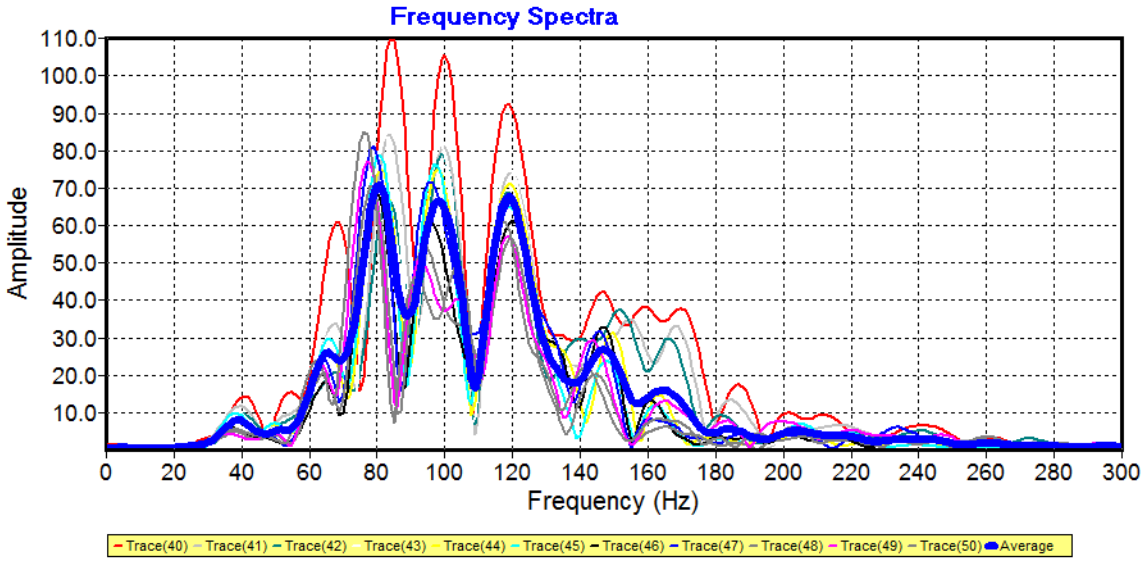

Figure 80. True amplitude spectra of traces 40-50 (80-200 ms) for cross-correlation with the synthetic sweep (Shot 3901).

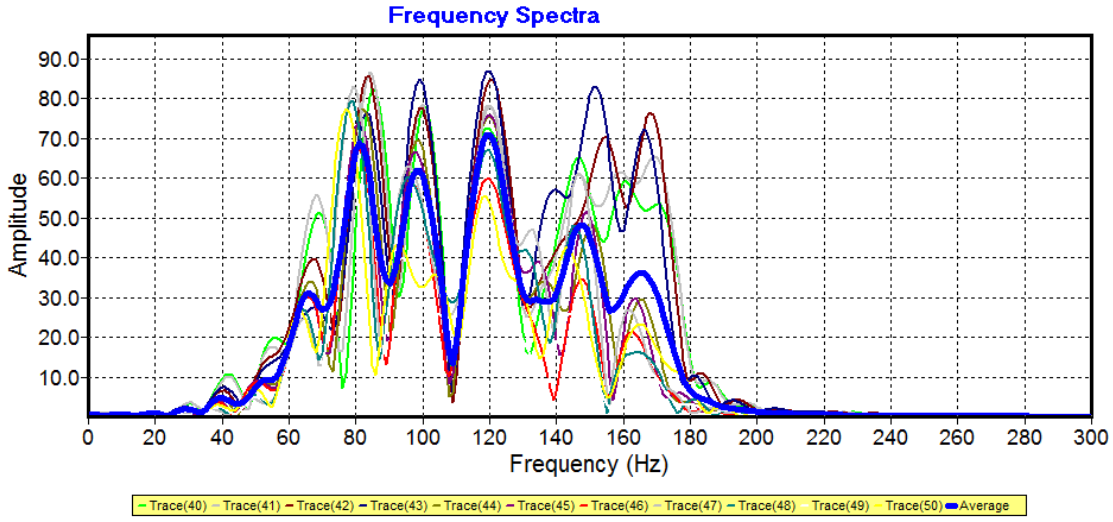

Figure 81. True amplitude spectra of traces 40-50 (80-200ms) for deconvolution using the calculated groundforce from the Endevco accelerometers (Shot 3901).

Discussion / Conclusion

Time-lapse high-resolution seismic was attempted to image a structure that can change horizontally and vertically within a few meters. In order for time-lapse techniques to be effective at measuring change of this type, surveys targeting natural dissolution features must be within a specific offset of the original location. Both the subsurface size of the feature and resolution limits determines the maximum offset.

Horizontal resolution must be considered when determining a maximum distance in which seismic lines used for time-lapse studies can be separated. With a Fresnel Zone radius of 33 m at the Hutchinson salt contact (approximately 120 m deep), structures 33 m or larger can be uniquely imaged. Horizontal changes occurring within 10 to 15 m can be identified on the seismic data. As evident from this study, a 15 m offset between survey lines was enough to image two completely different portions of the paleosinkhole. Surface elevation data collected from 1998 to 2000 illustrate the vertical changes associated with this feature. The northern edge of Hwy 50 dropped almost twice as much as the southern edge. This vertical change occurred within a surface distance of less than 7 m. Significant changes occurring within 10 m in the subsurface can be observed on the 2001 (CMPs 2350 to 2360 and 2450 to 2460) and 2008 data sets (CMPs 17255 to 17265). These factors lead to the conclusion that a maximum offset of 5 m, or 15 % of the Fresnel Zone radius, must be observed when attempting to use time-lapse techniques to study natural dissolution features.

Time-lapse seismic studies of natural dissolution features entail acquiring as identical 2-D slices as possible. Anthropogenic dissolution features require less accuracy in line placement. Anthropogenic subsidence features are caused by a single event and occur over decades. These features are often symmetric and well defined. Natural dissolution features form over millions of years with extended periods of activity and dormancy. This creates a feature that is irregular and unpredictable in shape. Periods of activity and dormancy creates lateral variability by different areas of the feature experiencing various growth rates.

Using groundforce calculated from ultra quite Endevco accelerometers located on the reaction mass and baseplate of the IVI Minivib for band-limited deconvolution provides a preferred method to processing high-frequency vibroseis data. Results comparable to cross-correlating the vibroseis traces with a synthetic sweep were produced. Absolute amplitude analysis revealed deconvolution produced higher reflection amplitudes than cross-correlation. Amplitudes of frequencies above 140 Hz (higher frequencies relate to higher resolution) from deconvolution are almost double those from cross-correlation.

The fact that the use of the Endevco accelerometers was successful in producing comparable results demonstrates that improvements are being made in accurately calculating true groundforce. Visual and amplitude comparisons illustrate that Endevco accelerometers produce a groundforce that better represents a combination of reaction mass and baseplate measurements. Results from deconvolution using the groundforce calculated from the Dytran accelerometers

showed lower resolution, higher noise data. The improved accelerometers have improved data quality.

References

Abelson, M., et al., 2003, Collapse-sinkholes and radar inferferometry reveals neotectonics concealed within the Dead Sea basin: *Geophysical Research Letters*, v. 30, p. 1545.

Anderson, N.L., R.W. Knapp, D.W. Steeples, and R.D. Miller, 1995, Plastic deformation and dissolution of the Hutchinson Salt Member in Kansas: *Kansas Geological Survey Bulletin* 237, p. 66-70.

Anstey, N.A., 1966. Correlation Techniques-A review. *Journal of the Canadian Society of Exploration Geophysics*, 2, p.55-86.

Aritman, Bibi C., 2001. Repeatability study of seismic source signatures. *Geophysics*, 66, no. 6, p. 1811-1817.

Baker, Gregory S., Don W. Steeples and Matt Drake, 1998. Muting the noise cone in near-surface reflection data: An example from southeastern Kansas. *Geophysics* 63, p. 1332.

Bauer, Andreas, Christian Lehr, Frans Korndorffer, Arjan van der Linden, John Dudley, Tony Addis, Keith Love, and Michael Myers, 2008. Stress and pore-pressure dependence of sound velocities in shales: Poroelastic effects in time-lapse seismic. *SEG Expanded Abstracts* 27, p. 1630.

Bayne, C.K., 1956. Geology and ground-water resources of Reno County, Kansas. *Kansas Geological Survey Bulletin 120*.

Bekara, Maiza, and Mirko van der Baan, 2008. Random and coherent noise attenuation by empirical mode decomposition. *SEG Expanded Abstracts*, p. 2591.

Bertrand, Alexandre and Jeremie Thiebaud, 2008, Detectability and time-shift estimation with high-resolution, time-lapse seismic. *The Leading Edge* 27, p. 636.

Bickel, S.H., 1982. The effects of noise on minimum-phase Vibroseis deconvolution. *Geophysics*, 47, p.1174-1184.

Bisshop, Thomas N., 1994, Correction amplitude, time, and phase mis-ties in seismic data. *Geophysics*, 59, no. 6, p. 946.

Black, R. and D.W. Steeples, 1994. Migration of Shallow Reflection Data. *SEG Expanded Abstracts* 12, p. 520.

Brittle K.F., L.R. Lines, and A.K. Dey, 2001. Vibroseis deconvolution: a comparison of cross-correlation and frequency-domain sweep deconvolution. *Geophysical Prospecting*, 49, p. 675-686.

Brook, Robert A, and Gary A. Crews, 1991. Experimental Analysis of Vibrator Baseplate Dynamics. *SEG Expanded Abstracts* 10, p. 743.

Coruh, Cahit, and John K. Costain. 1983. Noise attenuation by Vibroseis whitening (VSW) processing. *Geophysics*, 48, p. 543.

Cunningham, Allen B., 1979. Some alternative vibrator signals, *Geophysics* 44, p. 1901.

Doll, William E. and Cahit Coruh, 1995. Spectral whitening of impulsive and swept-source shallow seismic data. *SEG Expanded Abstracts 14*, p. 398.

Edelman, H.A.K., and H. Werner, 1982. The encoded sweep technique for Vibroseis. *Geophysics*, 47, p.809-818.

Frei, Walter, 1995. Refined field static corrections in near-surface reflection profiling across rugged terrain. *The Leading Edge* 14, p. 259.

Ghaderi, Amir, and Martin Landro, 2009, Estimation of thickness and velocity changes of injected carbon dioxide layers from prestack time-lapse seismic data. *Geophysics*, 74, no. 2, p. 17-28.

Ghose, Ranajit, 2002. High-frequency shear wave reflections from shallow subsoil layers using a vibrator source: sweep cross-correlation versus deconvolution with groundforce derivative. *SEG Int'l Exposition and 72nd Annual Meeting*.

Gogel, Tony., 1981. Discharge of Saltwater from Permian Rocks to Major Stream-aquifer Systems in Central Kansas. *Kansas Geological Survey Chemical Quality Series 9*.

Goupillaud, P.L., 1976. Signal design in the 'Vibroseis technique'. *Geophysics*, 41 no. 6, p. 1291-1304.

Hoeber, H. D. Lecerf, and D. Whitcombe, 2007, Matching of multiple time-lapse data using multi-coherence analysis. *SEG Expanded Abstracts* 24, p. 2418.

Huang, Xuri, Laurent Meister and Rick Workman, 1998, Improving production history matching using time-lapse seismic data. *The Leading Ed*ge 17, p. 1430.

Jefferson, Robert D. and Don W. Steeples, 1995. Effects of short-term variations in near-surface moisture content on shallow seismic data. *SEG Expanded Abstracts* 14, p. 419.

Jefferson, R. D., D.W. Steeples, R.A. Black and T. Carr, 1998, Effects of soil-moisture content on shallow-seismic data: *Geophysics*, 63, p. 1357-1362.

Klemperer, S.L., 1987, Seismic noise-reduction techniques for use with vertical stacking: An empirical comparison. *Geophysics*, 52 no. 3, p. 322-334.

Lambrecht, Jamie L., Rick Miller and Theresa Rademacker., 2004. Advantages and disadvantages of pre-correlation, pre-vertical stack processing on near-surface, high-resolution Vibroseis data. *SEG Expanded Abstracts 23*, p. 1425.

Lambrecht, Jamie L., 2006. Time-lapse high-resolution seismic imaging of a catastrophic salt-dissolution sinkhole in central Kansas. *Kansas Geological Survey Open-file Report No. 2006-23*.

Lebedev, Andrey V. and Igor A. Beresnev, 2004. Nonlinear distortion of signals radiated by vibroseis sources, *Geophysics* 69, p. 968.

Li, Z., W. Lynn, R. Chambers, Ken Larner, and Ray Abma, 1991. Enhancements to prestack frequency-wavenumber (f-k) migration. *Geophysics* 56, p. 27.

Li, Xiao-Ping, 1996. Ghost noise in vibroseis data and the elimination by deconvolution. *SEG Expanded Abstracts* 15 , p. 1607.

Luo, Yi, Krish P. Gunaratnam, Andrew H. Wu and Mohammed Alfarai, 2001. Histogram equalization and its application in seismic exploration. *SEG Expanded Abstracts* 20, p. 1835.

Margrave, Gary F., 2001. Direct Fourier migration for vertical velocity variations. *Geophysics* 66, p. 1504.

Merriam, Daniel., 1963. The Geologic History of Kansas. *Kansas Geological Survey Bulletin 162*.

Miller, R. D., 2002. High resolution seismic reflection investigation of the subsidence feature on U.S. Highway 50 at Victory Road near Hutchinson, Kansas. *Kansas Geological Survey Open-file Report No. 2002-17*, p. 1- 27.

Miller, Richard D. and Don W. Steeples, 2008, High-resolution Seismic-reflection Imaging of I-70 Sinkholes, Russell County, Kansas. *Kansas Geological Survey Open-file Report* 2008-18.

Miller, R.D., D.W. Steeples, J.L. Lambrecht, and N. Croxton, 2006, High-resolution seismic-reflection imaging 25 years of change in I-70 sinkhole, Russell, County, Kansas *SEG Expanded Abstracts*, p. 1411-1414.

Miller, R.D., D.W. Steeples, L. Schulte and J. Davenport, 1993, Shallow seismic-reflection feasibility study of the salt dissolution well field at North American Salt Company's Hutchinson, Kansas, facility: *Mining Engineering,* October, p. 1291-1296.

Miller, R.D., A. Villella, J. Xia, and D.W. Steeples, 2005, Seismic investigation of a salt dissolution feature in Kansas: Soc. Explor. Geophys., Investigations in Geophysics no. 13, Dwain K. Butler, ed., *Near-Surface Geophysics*, p. 681-694.

Neal, J.T., 1995, Supai salt karst features: Holbrook basin, Arizona. *Conference: 5. multidisciplinary conference on sinkholes and the engineering and environmental impacts of Karst,Gatlinburg, TN*,1-5 Apr 1995

Nissen, Susan E. and Jianghai Xia, 2002. Detecting shallow natural gas beneath Hutchinson, Kansas, using high-resolution seismic reflection. *Kansas Geological Open-file Report 2002-37*.

Porter-Hirsche, Jan and Keith Hirsche, 1998, Repeatability study of land data acquisition and processing for time lapse seismic. *SEG Expanded Abstracts* 17, p. 9.

Rademacker, Theresea, 2006. Optimizing High-Frequency Vibroseis Data. *University of Kansas*.

Radermacker, Theresea, Richard Miller, Jianghai Xia, Ross Black, and George Tsoflias, 2005. Enhancing the vibroseis technique through equipment noise reduction and optimizing the weighted sum signal. *SEG Expanded Abstracts* 24, p. 33.

Raef, Abdelmoneam E., Richard D. Miller, Alan P. Byrnes, and William E. Harrison, 2004. 4D seismic monitoring of the miscible CO2 flood of Hall-Gurney Field, Kansas. *The Leading Edge* 23, p. 1117.

Rickett, J.E. and D.E. Lumley, 2001. Cross-equalization data processing for time-lapse seismic reservoir monitoring: A case study from the Gulf of Mexico. *Geophysics* 66, p. 1015.

Robinson, E.A., and M. Sagaaf, 2001. Klauder wavelet removal before vibroseis deconvolution. *Geophysical Prospecting*, 49, p.335-340.

Routh, Partha S., and Phil D. Anno, 2008. Time-Lapse Noise Characterization by Inversion. *SEG Expanded Abstracts* 27, p. 3143.

Sallas, J.J., 1984. Seismic vibrator control and the downgoing P-wave. *Geophysics*, 49, p.732-740.

Sawin, Robert S. and Rex C. Buchana, 2002. Salt in Kansas. *Kansas Geological Survey, Public Information Circular (PIC) 21*.

Schrodt, Joseph K., 1987. Techniques for improving Vibroseis data. *Geophysics*, 52, p. 469-482.

Sheriff, Robert E., 2002, Encyclopedic Dictionary of Applied Geophysics 4th ed. *Geophysical Reference Series* 13.

Sherlock, Donald H. and Brian J. Evans, 1999, Time-lapse 3-D seismic with analogue sandbox models. *SEG Expanded Abstracts* 18, p. 1683.

Steeples, Don W. and Richard D. Miller, 1994. Pitfalls in Shallow Seismic Reflection. *SAGEEP* 7 , p. 9

Steeples, D. W., R.D. Miller, and R.A.Black, 1990. Static corrections from shallow-reflection surveys. *Geophysics* 55, p. 769.

Steeples, D.W., R.W. Knapp, and C.D. McElwee, 1986, Seismic reflection investigations of sinkholes beneath interstate 70 in Kansas: *Geophysics*, v. 51, p. 295-301

.

van der Baan, Mirko and Dinh-Tuan Pham., 2008. Robust wavelet estimation and blind deconvolution of noisy surface seismics. *Geophysics* 73 v. 37.

van der Veen, Michiel, Jan Brouwer, and Klaus Helbig, 1999. Weighted sum method for calculating ground force: an evaluation by using a portable vibrator system. *Geophysical Prospecting*, 47, p. 251-267.

Vossen, Robbert van, Jeannot Trampert, Andrew Curtis, and Andreas Leake, 2005, Source and receiver amplitude equalization using reciprocity – application to land seismic data. *SEG Expanded Abstracts 24*, p. 2177.

Walters, R. F., 1978, Land subsidence in central Kansas related to salt dissolution, *Kansas Geological Survey Bulletin 214*.

Wang, Zhijing, 1997. Feasibility of time-lapse seismic reservoir monitoring: The physical basis. *The Leading Edge* 16, p. 1327.

Watney, W.L., J.A. Berg, and Paul, S.[E.], 1988, Origin and distribution of the Hutchinson Salt (lower Leonardian) in Kansas, pp. 113-135, in: Morgan, W.A.; and Babcock, J.A., eds., Permian Rocks of the Midcontinent, Society of Economic Paleontologists and Mineralogists, Midcontinent Section, Special Publication, no. 1, 224 pages.

Watney, Lynn W and Susan E. Nissen, 2003. Detailed mapping of the Upper Hutchinson Salt and Overlying Permian strata beneath Hutchinson, Kansas. *Kansas Geological Survey Open-file Report No. 2003-66*.

Wei, Zhouhong, Sallas, John J., Crowell, John M. and James E. Teske, 2007. Harmonic distortion reduction on vibrators – Supressing the supply pressure ripples. *SEG Expanded Abstracts* 26, 51.

Williamson, Willow., 2008. Getting that Sinking Feeling. *The Hutchinson News*.

Yilmaz, Oz, 2001. *Seismic Data Analysis*. Society of Exploration Geophysics, 2nd Edition.

Yun, Ling, Huang Xuri, Gao Jun, Sun Deshen, and Lin Jixiang, 2007. Land time-lapse seismic processing techniques with nonrepeatability factors. *SEG Expanded Abstracts* 26, p. 2999.